

Roll Damping Prediction Method

To determine linear and non-linear roll damping coefficients based on multiple 2D CFD simulations

S. A. W. Smaal

Roll Damping Prediction Method

To determine linear and non-linear roll damping coefficients based on multiple 2D CFD simulations

by

S. A. W. Smaal

to obtain the degree of Master of Science in Marine Technology
at the Delft University of Technology,
to be defended publicly on Thursday August 1, 2019 at 02:00 PM.

Student number:	4224418
Project duration:	November 19, 2018 – August 1, 2019
Thesis committee:	Prof. dr. ir. J. Westerweel, TU Delft, Chairman
	Dr. ir. I. Akkerman, TU Delft, Supervisor
	Ir. D. Scheltens, Van Oord, Supervisor
	Ir. K. Visser, TU Delft

An electronic version of this thesis is available at <http://repository.tudelft.nl/>.

Preface

This thesis is written to obtain the degree of Master of Science in Marine Technology with the specialisation Hydromechanics at the Delft University of Technology. This research was conducted in cooperation with Van Oord.

Without the help of others I would not have been able to complete this research. I would like to thank my graduation committee for their supervision and guidance. I would like to thank Ido Akkerman for his supervision during my research. His insights and notes during meetings made that I kept looking critically at the work I was doing. Furthermore, I would like to thank Ido for helping me assemble a graduation committee.

I am particularly grateful to Daan Scheltens, my daily supervisor at Van Oord. His efforts relating hardware and software problems have made it possible to conduct the research in a convenient way. Furthermore, I would like to thank Daan for his useful remarks and help during our weekly meetings. I would very much like to thank him for his enthusiasm and positive attitude. This has encouraged me to keep working hard and obtaining the best results possible.

I would like to thank Van Oord for the opportunity they gave me. It has been a very pleasant experience working in a nice work environment with interested and helpful colleagues.

Finally, I would like to thank my family and friends. I would like to thank Sophie for supporting me throughout my thesis. I would like to thank my mother and brother. Finally, I would like to thank my fellow graduates at Van Oord for taking the time to discuss my research during our fun coffee breaks.

*S. A. W. Smaal
Delft, July 2019*

Abstract

Accurately predicting the ship motions, is essential knowledge when operating in water. To predict the ship motions, multiple ship characteristics have to be known. For the roll motion, one of these characteristics is the roll damping coefficient. Nowadays the industry standard to determine the roll damping coefficient of a ship is by performing model tests or using empirical formulas created in the late '70s. In recent years computational power has increased significantly. This increase makes it possible to start using computational fluid dynamics (CFD) for practical purposes instead of solely scientific research. The roll damping coefficient is a very interesting parameter to examine with viscous flow solvers as the roll motion is heavily influenced by the viscosity of the water. Multiple studies have been performed with 3D and 2D CFD simulations. By simplifying the simulation to 2D, calculation time is reduced drastically. This simplification is performed by only simulating one cross-section of the midship. Only simulating one cross-section causes a loss of accuracy in how well the roll damping coefficients can be determined as the damping effects of the bow and stern are not taken into account, or are roughly estimated.

During this research, a method to accurately determine the roll damping coefficients of a ship, while maintaining low computation time, is investigated. This method is based on performing multiple 2D CFD simulations of different cross-sections and combining the results to capture the behaviour of the entire ship. With this approach, the high accuracy of 3D simulations and the low computation time of 2D simulations are combined. The accuracy of this 2D section method is determined by comparing the results with experimental data.

The experimental data is obtained through free roll decay tests of a ship from Van Oord on model scale. A 3D CFD model, which simulates a free roll decay test, is created using OpenFOAM. The results of this simulation are compared to the experimental data to determine how well a 3D simulation can predict the roll damping coefficients. Next, a 2D CFD model is created using OpenFOAM which is validated using experimental data of a structure which has a uniform cross-section along the entire length. Lastly, the validated 2D CFD model is used for the 2D section method. Multiple cross-sections of the same ship from which the experimental data is obtained and with which the 3D CFD simulation is performed, are simulated. The results of the 2D section method are compared to the experimental results in order to determine how well this method can determine the roll damping coefficient of a ship.

The simulation of the 3D free roll decay test underestimated the linear damping. The non-linear damping was within the margins of the experimental data. The 2D forced oscillation simulations showed an excellent agreement in linear and non-linear damping with both the experimental data as with a comparable CFD simulation. The 2D section method slightly overestimates both the linear and non-linear damping of an entire ship but overall this method shows promising results. However, more research should be done to optimise the method further.

Contents

Preface	iii
Abstract	v
List of Figures	ix
List of Tables	xi
1 Introduction	1
1.1 Importance of Roll Damping	1
1.2 Literature review	1
1.3 Purpose of the research	3
1.4 Research question	3
1.5 Method	4
1.6 Document Structure	4
2 Roll Damping	5
2.1 Physics of the roll motion	5
2.2 Physics of roll damping	7
2.3 Estimating the roll damping	8
2.3.1 Empirical models	8
2.3.2 Model tests.	8
2.3.3 Computational fluid Dynamics	9
3 Governing equations behind the models	11
3.1 Navier-Stokes equations	11
3.2 Reynolds Averaged Navier-Stokes Turbulence Models.	11
3.2.1 $k - \omega$ SST turbulence model	12
3.2.2 $k - kl - \omega$ turbulence model	12
3.3 Multi-phase flow	12
3.4 Solution algorithm	12
3.4.1 The SIMPLE algorithm.	13
3.4.2 The PISO algorithm	13
3.4.3 The PIMPLE algorithm.	14
3.5 Mesh Methods	14
3.5.1 SnappyHexMesh.	14
3.5.2 Dynamic Mesh Method	14
3.5.3 Deforming Mesh Method	14
3.5.4 Overset Mesh Method	14
3.5.5 Deforming mesh method compared to overset mesh method	19
3.5.6 Complete mesh movement	19
3.6 Boundary Conditions	19
3.6.1 Boundary conditions 3D simulation	19
3.6.2 Boundary conditions 2D simulation	19
3.7 Initial conditions	19
4 3D free roll decay CFD simulation	21
4.1 Set-up of the simulation	21
4.2 Effect of the width of the domain	21
4.3 Effect of initial turbulence conditions.	23
4.4 Mesh convergence	23
4.5 Validation Approach	25

4.6	Comparison of free decay curves from Marin and OpenFOAM	25
4.7	Determining the damping coefficients	25
4.8	Comparing the damping coefficients with experimental data	28
4.9	Possible causes for deviations	30
4.9.1	Model tests	30
4.9.2	Simulation	30
4.9.3	Conclusion on deviations in results	30
4.10	Conclusion	30
5	2D forced oscillation CFD simulation	31
5.1	Validation Approach	31
5.2	Geometry of the hull shape	31
5.3	Numerical domain	32
5.4	Mesh Convergence Study	32
5.5	Damping extraction methods	33
5.5.1	Linearised equivalent damping	33
5.5.2	Non-linear damping	33
5.6	Results of the fully submerged simulations	36
5.7	Results of the simulations with free water surface	36
5.8	Conclusion	40
6	2D CFD section method	41
6.1	Method to combine multiple 2D results	41
6.2	Results of the fully submerged simulations	42
6.3	Results of the simulations with free water surface	46
6.4	Conclusion	48
7	Conclusion & Recommendations	51
7.1	Conclusion	51
7.2	Recommendations	52
A	Boundary and initial conditions	55
A.1	Boundary conditions	55
A.1.1	3D boundary conditions	55
A.1.2	2D boundary conditions	55
A.2	Initial conditions	57
A.2.1	Initial conditions of the 3D simulations	57
A.2.2	Initial conditions of the 2D simulations	57
B	Numerical schemes	59
B.1	Numerical schemes 3D	59
B.2	Numerical schemes 2D	59
C	Ship details	61
D	Details of the high-performance cluster	63
	Bibliography	65

List of Figures

2.1	Definition of ship motion	6
2.2	Explanation of roll motion	6
2.3	Typical roll decay curve	9
3.1	Visualisation of the water-air transition	13
3.2	Working principle of SnappyHexMesh	15
3.3	Deforming Mesh	16
3.4	The two meshes which are combined in the overset mesh method	17
3.5	Different cell types of overset mesh	18
4.1	Impact on free decay curve of different domain widths	22
4.2	Comparison of pressure waves in the domain	22
4.3	Impact on free decay curve of different initial turbulent values	23
4.4	Five different refinement levels for the mesh	24
4.5	Comparison between OpenFOAM and Marin	25
4.6	Comparison between OpenFOAM and Marin corrected	26
4.7	Typical decay curve	26
4.8	Typical p - q analysis	28
4.9	p - q analysis of model test 1 performed by Marin	29
4.10	p - q analysis of the OpenFOAM simulation	29
5.1	2D hull section	32
5.2	Circular domain for 2D simulations	32
5.3	Three different refinement levels for the mesh	34
5.4	Difference in reaction moment between the three different refinement levels for the mesh and close-up	35
5.5	Vorticity comparison between the results from Jaouen et al. and OpenFOAM	37
5.6	Pressure distribution comparison between the results from Jaouen et al. and OpenFOAM	37
5.7	Vorticity comparison between the results Jaouen et al. and OpenFOAM with $k - \omega$ SST turbulence model	38
5.8	Damping compared to experimental data from Ikeda et al.	38
5.9	Damping compared to experimental data from Ikeda et al. with free water surface	39
5.10	Vorticity at the 13th oscillation for free water surface simulation in OpenFOAM	40
6.1	Side view of the ship under consideration	41
6.2	Side view of the different ship sections	41
6.3	Cross-sections of the back-, mid- and frontsection	42
6.4	Mirrored cross-sections of the back-, mid- and frontsection	43
6.5	Meshes of the cross-sections	43
6.6	Viscous damping moment as calculated by OpenFOAM on 2D simulations	44
6.7	Vorticity at the three cross-sections at 13th oscillation	44
6.8	Viscous damping moment amplitude per section	45
6.9	Damping moment amplitude of experimental data and OpenFOAM	46
6.10	Meshes of the three sections with free water surface	47
6.11	Damping moment as calculated by OpenFOAM on 2D simulations with free water surface	47
6.12	Damping moment amplitude per section with free water surface	48
6.13	Damping moment amplitude following of experimental data and OpenFOAM	49
6.14	Vorticity at the three cross-sections at 13th oscillation with free water surface	49

List of Tables

4.1	Overview of different mesh sizes	22
4.2	Overview of different mesh sizes	24
4.3	Results p - q analysis from the experimental data from Marin	28
5.1	Overview of different mesh sizes	33
5.2	Normalised damping coefficient measured by Ikeda et al. per category	37
5.3	Normalised viscous damping coefficient found by Jaouen et al. and OpenFOAM	38
5.4	Normalized equivalent damping coefficient calculated from OpenFOAM simulation	39
6.1	Length per longitudinal section and corresponding multiplication factor for the reaction moment based on a cross-section length of 0.05 meter	42
6.2	The summation of the different linear and quadratic damping coefficients into the total damping coefficients as determined by the 2D section method	45
6.3	The linear and quadratic damping coefficient per free decay test and the average result from Marin	45
6.4	The summation of the different linear and quadratic damping coefficients into the total damping coefficients as determined by the 2D section method with free water surface	48
A.1	Boundary conditions for the 3D simulation using the $k - kl - \omega$ turbulence model (part 1)	55
A.2	Boundary conditions for the 3D simulation using the $k - kl - \omega$ turbulence model (part 2)	55
A.3	Boundary conditions for the 2D simulation using the $k - kl - \omega$ turbulence model (part 1)	55
A.4	Boundary conditions for the 2D simulation using the $k - kl - \omega$ turbulence model (part 2)	56
A.5	Initial conditions of the 3D simulations	57
A.6	Initial conditions of the 2D simulations	57
B.1	Numerical schemes used for 3D simulations	59
B.2	Numerical schemes used for 2D simulations	59
D.1	Information about the computer which was used for the OpenFOAM simulations	63

Nomenclature

Constants

μ_{air}	Dynamic viscosity of air	$1.81 e^{-5} [Pa \cdot s]$
μ_{water}	Dynamic viscosity of water	$1.05 e^{-3} [Pa \cdot s]$
ρ_{air}	Density of air	$1.225 [kg/m^3]$
ρ_{water}	Density of water	$998 [kg/m^3]$
g	Gravitational constant	$9.81 [m/s^2]$

Abbreviations

2D	Two dimensional
3D	Three dimensional
CFD	Computational Fluid Dynamics
CoG	Centre of Gravity
FAVOR	Fractional Area/Volume Obstacle Representation
PIV	Particle Image Velocimetry
RANS	Reynolds Averaged Navier-Stokes
URANS	Unsteady Reynolds Averaged Navier-Stokes
VoF	Volume of Fluid

Other Symbols

α	Phase volume fraction	$[-]$
$\ddot{\phi}$	Roll acceleration	$[rad/s^2]$
Δt	Time-step	$[s]$
Δx	Cell length in x-direction	$[m]$
$\dot{\phi}$	Roll velocity	$[rad/s]$
μ	Dynamic viscosity	$[Pa \cdot s]$
ω	Angular frequency	$[rad/s]$
ω_i	Weight coefficient	$[-]$
$\bar{\tau}$	Shear stress	$[N/m^2]$
\bar{u}	Average flow velocity	$[m/s]$
ϕ	Roll angle	$[rad]$
ϕ_a	Amplitude of forced oscillation	$[rad]$
ϕ_F	Cell value on overset mesh	depending on value

ϕ_{Fi}	Donor cell value	depending on value
ρ	Density	$[kg/m^3]$
$\hat{\mathbf{n}}$	Unit normal vector	$[-]$
\mathbf{r}	arm	$[m]$
ε	Phase shift	$[rad]$
a	Acceleration	$[m/s^2]$
B	Breadth	$[m]$
b	Damping coefficient	$[Nm/(rad/s)]$
b'	Normalised damping coefficient	$[-]$
b_1	First order damping coefficient	$[Nm/(rad/s)]$
b_2	Second order damping coefficient	$[Nm/(rad/s^2)]$
b_3	Third order damping coefficient	$[Nm/(rad/s^3)]$
b_e	Eddy damping coefficient	$[Nm/(rad/s)]$
b_f	Friction damping coefficient	$[Nm/(rad/s)]$
b_L	Lift damping coefficient	$[Nm/(rad/s)]$
b_l	Linear damping coefficient	$[Nm/(^\circ/s)]$
b_q	Quadratic damping coefficient	$[Nm/(^\circ/s^2)]$
b_w	Wave damping coefficient	$[Nm/(rad/s)]$
b_{bk}	Bilge keel damping coefficient	$[Nm/(rad/s)]$
b_{eq}	Equivalent linearised damping coefficient	$[Nm/(rad/s)]$
c	Restoring coefficient	$[Nm/rad]$
Co	Courant number	$[-]$
D	Depth	$[m]$
F	Force	$[N]$
F_b	Buoyancy force	$[N]$
F_f	Viscous force	$[N]$
F_p	Pressure force	$[N]$
I	Inertia matrix	$[m^4]$
m	Mass	$[kg]$
M_0	Amplitude of hydrodynamic moment	$[Nm]$
M_ϕ	Roll moment	$[Nm]$
M_a	Moment due to added mass	$[Nm]$
m_a	Added mass coefficient	$[Nm \cdot s^2/rad]$
M_b	Moment due to added damping	$[Nm]$

M_h	Hydrodynamic moment	[Nm]
M_{ext}	External moment	[Nm]
M_{tot}	Total moment	[Nm]
p	Hydrodynamic pressure	[Pa]
S	Surface	[m ²]
T	Roll period	[s]
t	Time	[s]
u	Flow velocity	[m/s]
u'	Fluctuating part of the flow velocity	[m/s]



Introduction

1.1. Importance of Roll Damping

The ability to accurately predict the ship motions has always been seen as desired knowledge. Even more so today when more and more complex operations are carried out at sea.

Ships move in six degrees of freedom; surge, sway, heave, pitch, roll and yaw. Out of these six motions, five consist out of a strong linear component and a less profound non-linear component. The roll motion, however, has a non-linear component which is in the same order of magnitude as the linear component. This strong non-linear behaviour makes it impossible to calculate the roll motion analytically to a satisfactory level of accuracy. The most important parameter to predict the roll motion is the roll damping. From 1976 to 1978 Ikeda et al. [14] did an extensive study on roll damping. They conducted a series of experiments and with the results they produced semi-empirical formulas to calculate the roll damping. These formulas proved to predict the roll damping well for typical ships of that time. In the years that followed many corrections and additions to these formulas of Ikeda et al. [14] were made to make them applicable to ships with characteristics which were different from the ones tested by Ikeda et al. [14]. Kawahara et al. [24], for example, did a study on how to improve the formulas for ships with a high centre of gravity. However, the best way to determine the roll damping today is through expensive and time-consuming model tests.

The method provided by Ikeda et al. [14] works satisfactory for conventional ship types and because it is unfeasible to do model tests for every ship, this method is given by the International Towing Tank Conference (ITTC) as practical option to calculate the roll damping coefficient. However, as computational power is increasing and its costs are dropping, it is tempting to look at other options to determine the roll damping coefficient. One of the options is computational fluid dynamics (CFD). CFD is a method to numerically simulate the flow around a ship which leads to the motions of the ship. CFD could thus be used to simulate the experiments, which are currently carried out in towing tanks with ship models. These CFD simulations could give accurate results without the high costs of model tests. CFD is used to calculate roll damping since as early as 1997 (Falzarano et al. [3]), but these CFD tests were solely done to find new coefficients for semi-empirical formulas. Due to the current development in computational power, it is now possible to use CFD to calculate the roll damping for ships directly without using the empirical formulas at all.

Therefore a CFD model, which has been verified and validated, is desirable to be able to calculate the roll damping in as little time as possible and which is applicable on multiple ship types in multiple conditions.

1.2. Literature review

In recent years, several studies on roll damping using CFD have been performed. Because of the increase in computational power, it is becoming more feasible to use CFD not only for research purposes but also for practical use. CFD, or viscous flow simulations, have three main advantages over model testing. It has relatively low costs, is flexible and gives accurate results. However, it is quite challenging to correctly set-up the simulation, as it is sensitive to chosen numerical schemes and turbulence models. The simulation should be validated with experimental data in order to check whether it gives reliable results.

CFD has been used to calculate roll damping as early as 1997 by Falzarano et al. [3]. However, only in recent years, extensive research has been done in this field.

Jaouen et al. [18] predicted the roll added mass and damping coefficient using a 2D unsteady Reynolds averaged Navier-Stokes (URANS) CFD code named ReFRESKO without taking wave-making damping into account. This wave-making damping is subtracted using potential flow theory by assuming the separate damping components can be linearised as stated by Ikeda et al. [14]. The results show good agreement with the test data of Ikeda et al. [14].

Jaouen et al. [19] continued their research and found that the viscous damping coefficient scales linearly with the roll amplitude for low dimensionless frequencies. Just as in their previous research, the wave-making effect is not taken into account. They achieved this by mirroring the hull section at the water plane. Jaouen et al. [19] also researched the viscous scale effect. The difference between the viscous damping coefficient between the model scale and full scale turns out to be 1.85%. One side note regarding this is that for the model scale tests, no wall models were used, where, in the full-scale tests, wall models were used which decrease the accuracy of the model.

Irkal et al. [17] did a free roll decay test in a tank to obtain experimental data which was then compared to results from their CFD tests to validate this CFD method. They tested hulls with different bilge keel layouts and the same hulls without bilge keels. For the CFD set-up, a Fractional Area/Volume Obstacle Representation (FAVOR) technique is used combined with a volume of fluid (VoF) method. This FAVOR method represents the body by calculating open area fractions on cell faces and open volume fractions in rectangular structured cells and distributing the solid and fluid portions in the cell. The medium above the water level is defined as void, i.e. with no density ($\rho = 0 [kg/m^3]$). Results are in good agreement with the tank test. However, they reported that the results of the CFD simulation are no longer reliable after ca. 10 oscillations. Furthermore, they also compared vorticity using particle image velocimetry (PIV) measurements. The vorticity from CFD and PIV has a good resemblance both in strength and location. Irkal et al. [17] also mention that scale effects are noticeable when there is a transition from laminar to turbulent flow or vice versa when going from model scale to full scale. Therefore, there are hardly any scale effects with bilge keels or sharp bilges, but there are scale effects with rounded bilges without bilge keels.

Yildiz et al. [32] did a URANS 2D simulation of a forced roll test in shallow draft with bilge keels. In shallow drafts, stronger non-linear effects occur due to the fact that the vortices generated by the bilge keels are close to the free surface. Katayama et al. [23] also investigated this shallow-draft effect and compared CFD results to experimental data and the method provided by Ikeda et al. [14]. The overall results show good agreement but the method provided by Ikeda et al. [14] deviates for shallow draft. This deviation is because the bilge keels are less effective when in close proximity to the free surface. The method provided by Ikeda et al. [14] does not take this effect into account, this causes the results to deviate from the CFD and experimental data.

Bonfiglio et al. [1] performed a 2D CFD simulation on the sway, heave and roll characteristics. OpenFOAM was used for the CFD calculations. The CFD results are compared to Vugts tank test data and the results of this simulation show reasonably good agreement.

After performing CFD simulations, Kawahara et al. [24] state that a better prediction method is needed for ships with a high centre of gravity (CoG). They concluded that the method prescribed by Ikeda et al. [14] and Himeno [8] underestimates the roll damping in these situations.

Chen et al. [2] used OpenFOAM to study 2D roll motion of a ship section and compared the results to experimental data of a 3D model. Instead of performing a free decay or forced oscillation simulation, they used the regular wave input method. No turbulence model was used for the simulations. They did not model turbulence in order to reduce computation time. Their code predicted the natural frequency of the roll motion accurately, but the damping coefficient did not match with the experimental data. Chen et al. [2] think this is due to the 2D flow assumption and the frictional damping of the hinges used during the experiment.

Gu et al. [6] and Gu et al. [7] performed two consecutive studies on roll damping in 2D and 3D using CFD. Although their findings were better than results obtained with the method provided by Ikeda et al. [14], there is still a rather large error.

Yang et al. [30] did a free decay test with forward speed of the DTMB 5512 destroyer using 3D CFD simulation in Fluent. The free surface is simulated using the VoF method. The results are good compared to experimental data. For three different initial roll angles, the error in damping coefficient varies from 0.17% to 2.15%.

Gokce and Kinaci [5] did a numerical study on free roll decay on the benchmark ship DTMB 5415. A 3D RANS code of the software package Star CCM+. Instead of using an overset mesh or sliding interface mesh, they used a deforming mesh. This type of mesh is not re-meshed with the movement of the body but is deformed. This deforming causes problems when large deformations occur. Because of this, they simulated roll decay simulations with initial angles no larger than 10° . They accurately predicted the amplitude of the roll

motion, but the period was overestimated. Nonetheless, they used their model to calculate the different components which counteract the roll motion. Firstly, the benchmark case was calculated without any damping, i.e. solely the restoring moment was taken into account. Secondly, only wave and eddy damping were considered by making the fluid inviscid. Thirdly, the viscous effects are taken into account and lastly, the effect of forward speed is investigated. This was done in order to determine the impact of different components of the roll damping.

Yang et al. [31] did a 3D CFD simulation in Fluent of a roll decay test with and without forward speed. A deforming mesh is used, which is updated every time-step. Furthermore, the ship is restrained in all directions except for roll. The roll motion acts around the centre of gravity at rest. They used the $k - \omega$ SST turbulence model. The results from the simulations were compared to test data and empirical formulas of the DTMB 5512 and a series 60 ship. The roll damping results from the CFD simulations were in good agreement with the test data and predicted the damping more closely to the test data than empirical formulas.

Jiang et al. [21] performed a 3D CFD simulation of a free roll decay test in STAR CCM+ using an overset mesh method. After having compared the results to experimental data of the DTMB 5512 they concluded that the simulation data was in good agreement with the experimental data and that the model could be used for predicting the roll damping.

From these researches, a trend follows. 3D CFD simulations are more accurate than 2D simulations for complete ships. However, this comes at the cost of longer computation time and higher computational power.

1.3. Purpose of the research

As stated above, a CFD model, which has been verified and validated, is desired, to be able to calculate the roll damping. The goal of this research is to develop a model which gives satisfactory results within an acceptable simulation time. As 3D CFD simulations take lots of time, it is preferable to use 2D simulations. However, simplifying from 3D to 2D means a loss of information. For the case of a ship moving in water this means that the complex 3D geometry is simplified to one cross-section taken amidships. The results gathered from the simulation using this single cross-section will then be extrapolated over the length of the ship, although this cross-section is not representative for the entire ship. The stern and bow of the ship have a different geometry than the midsection and rapidly change in lengthwise direction. The opposed solution to this is to take multiple 2D cross-sections of the ship which account for different longitudinal sections of the ship, in this case, the stern the midsection and the bow. This approach is chosen in order to get more accurate results than a single 2D cross-section, but using less computation time than a 3D simulation.

1.4. Research question

To be able to use a model mentioned in Section 1.3 for practical purposes, it should first be investigated whether this is a valid method. This will be done by answering the following main research question:

Is it possible to determine the roll damping coefficients of a ship by combining the results of 2D OpenFOAM CFD simulations of multiple cross-sections of the ship?

In order to answer this main question, three sub-questions have to be answered:

1. Is OpenFOAM capable of simulating 3D free roll decay tests in order to calculate the roll damping coefficients, which are in accordance with experimental data?
2. Is OpenFOAM capable of simulating 2D forced oscillation tests in order to calculate the roll damping coefficients, which are in accordance with 2D experimental data?
3. Is it possible to combine the results of multiple 2D CFD simulations, to obtain roll damping coefficients, which are in accordance with 3D experimental data?

In this research, the roll damping will be calculated using the open-source CFD code OpenFOAM¹. With this software, free decay tests and forced oscillation tests are simulated. These simulations will be compared to experimental data. The experimental data to validate the 3D model is obtained through a free roll decay test of one of Van Oord's ships executed by Marin at their research institute. The 2D simulation will be validated using the experimental data from Ikeda et al. [14] and the CFD simulation data from Jaouen et al. [19]. By doing this, the sub-questions and, eventually, the main research question can be answered.

¹During this complete research OpenFOAM version 1812 is used. This software ran inside Docker on a virtual Linux machine

1.5. Method

At first, a free decay test will be simulated in 3D in OpenFOAM to answer the first sub-question. To achieve this, the type of settings which OpenFOAM needs, have to be determined. These settings are a.o. the solver, the numerical schemes and the turbulence model. The settings will be chosen based on the best possible option for this simulation.

Secondly, a mesh has to be built. A decision has to be made regarding the structure of the mesh. The choice between structured or unstructured has to be made. As the problem is one with a moving geometry, dynamic meshing has to be applied. There are multiple methods to make the mesh dynamic and the best suitable method has to be chosen for this situation. The type of dynamic meshing depends on multiple criteria, e.g. the amount and direction of movement in the system. After this has been determined, the mesh has to be built according to the needs for this type of simulation. With the mesh complete, a mesh convergence study has to be conducted to see to what extent the solution depends on the mesh size. After completing the mesh convergence study, a mesh size has to be chosen based on accuracy and calculation time, to be able to get accurate results within an acceptable amount of time.

After having determined what mesh size and which OpenFOAM settings will be used, the simulation will be run and results will be compared to experimental data.

After answering the first sub-question, the next sub-question can be answered. For this, the 3D simulation mentioned above will be down-scaled to a 2D simulation but changing as little as possible regarding the determined settings in order to do the same simulation but in 2D.

The validation of the 2D code will be done using experimental data provided by Ikeda et al. [14] and CFD simulations performed by Jaouen et al. [18]. This experiment was not a free roll decay test but a forced roll motion test. This will thus have to be adjusted in the 3D model used above. Also, because the geometry is different and because it is now a 2D simulation, a new mesh will have to be generated. The new mesh is generated in a similar manner as discussed above and it will have the same type of structure.

After completing the 2D simulation set-up and building the mesh, the simulation has to be verified and a new mesh convergence study has to be conducted. When these steps are taken, the simulation can be run and the results can be compared with the experimental data. After running these simulations the second sub-question can be answered.

Thereafter, the last sub-question has to be answered. This will be done by simulating three cross-sections of the ship which are located at the backsection, the midsection and the frontsection to capture the global geometry of the ship. The results of these 2D simulations will be combined by multiplying the resulting damping moments with their corresponding multiplication factor, in order to obtain the damping moments of the longitudinal sections, and adding these together. These combined results give the roll damping of the entire ship. This result will then be compared to the roll damping obtained by the experiments performed by Marin.

Finally, the main research question will be answered.

1.6. Document Structure

In the first chapter, the problem is introduced and the examined literature is summarised. The second chapter contains essential background knowledge about the roll motion and roll damping in order to provide a better understanding of the examined problem. The third chapter consists of governing equations which are used by the model presented in this research and other settings of the model. The fourth chapter describes the verification and validation of the 3D free decay simulation and presents a comparison between the 3D CFD simulation and the experimental results. The fifth chapter describes this for the 2D forced oscillation simulation. In the sixth chapter, the proposed 2D section method is explained and results gathered with this method are compared to experimental data. The final chapter presents the conclusion of this research and gives recommendations for future research.

2

Roll Damping

In this chapter, the physics behind the roll motion and roll damping will be explained.

2.1. Physics of the roll motion

To understand roll damping, it is first important to understand how a ship behaves free-floating. A ship moves in six degrees of freedom when free-floating. There are three translational motions:

- Surge, motion in the forward and backward direction, x-axis, positive forward
- Sway, motion in the sideways directions, y-axis, positive to port side
- Heave, motion in upward and downward direction, z-axis, positive upward

Apart from these three translational directions, the ship is also free to rotate around the translation axes. These three rotations are defined as:

- **Roll, rotation around the x-axis, positive right turning**
- Pitch, rotation around the y-axis, positive right turning
- Yaw, rotation around the z-axis, positive right turning

These movements are graphically shown in Figure 2.1. The roll motion is not fixed about the x-axis, other than Figure 2.1 suggests. The rotation axis is parallel to the x-axis and passes through the centre of buoyancy when the ship is rolling and full motion coupling is taken into account.

During the roll motion, the structure interacts with the fluid. The fluid acts on the structure with two types of forces; the pressure force, F_p , in normal direction and the viscous or friction force, F_f , in tangential direction as visualised in Figure 2.2. The integration of these forces over the structure surface generates a buoyancy force F_b and a restoring moment M_ϕ around a longitudinal-axis through the centre of rotation, which is defined by the centre of buoyancy and the centre of gravity. The centre of buoyancy and the centre of gravity are given in Figure 2.2 as the black dot at the beginning of the F_b vector and the black dot at the beginning of the F_g vector respectively.

With these forces and moments, the total hydrodynamic moment based on the total hydrodynamic force can be determined by multiplying each force with its corresponding lever arm. From this, Equation (2.1) follows.

$$M_h = \int_S \mathbf{r} \times \left(-p\mathbf{i} + \bar{\tau} \right) \hat{\mathbf{n}} dS \quad (2.1)$$

In Equation (2.1) M_h is the hydrodynamic moment around the roll axis, \mathbf{r} is the lever arm, p is the hydrodynamic pressure and $\bar{\tau}$ the shear stress, $\hat{\mathbf{n}}$ is the unit normal vector and S is the surface of the structure.

If one assumes that the structure is a rigid body, Newton's second law of motion, which is given in Equation (2.2), can be used to describe the motions of the structure. The equation of motion for the roll motion, which follows from Newton's law is given in Equation (2.3).

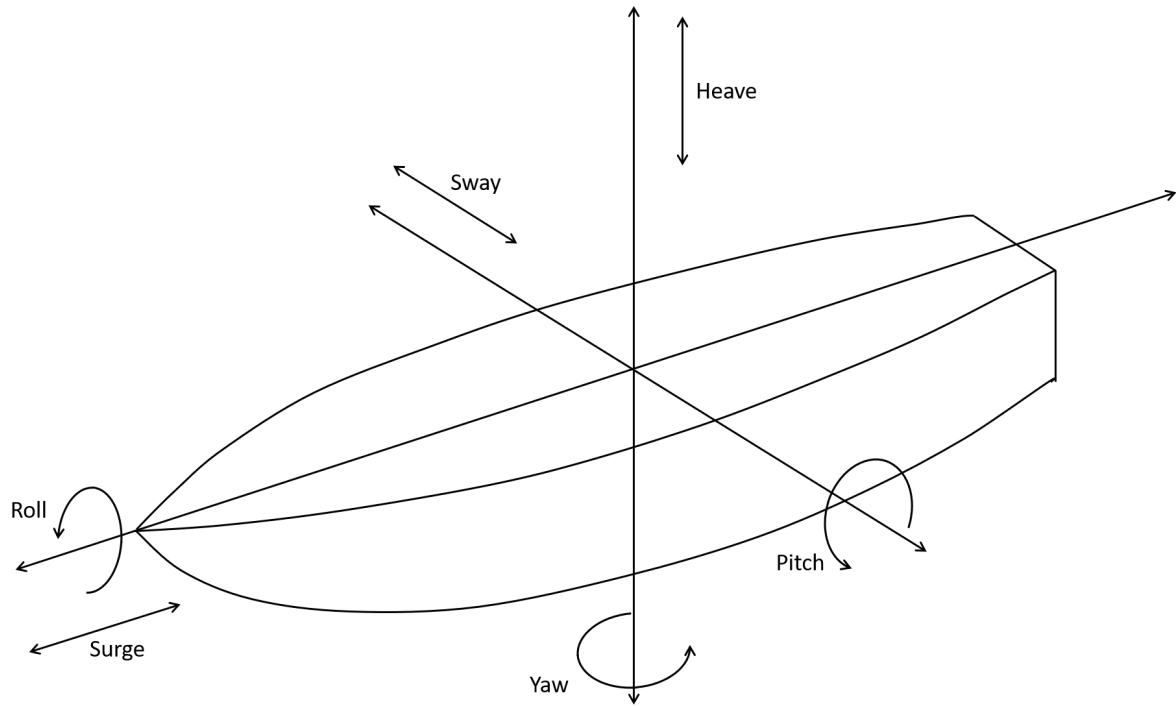


Figure 2.1: Definition of ship motion (Malara et al. [25])

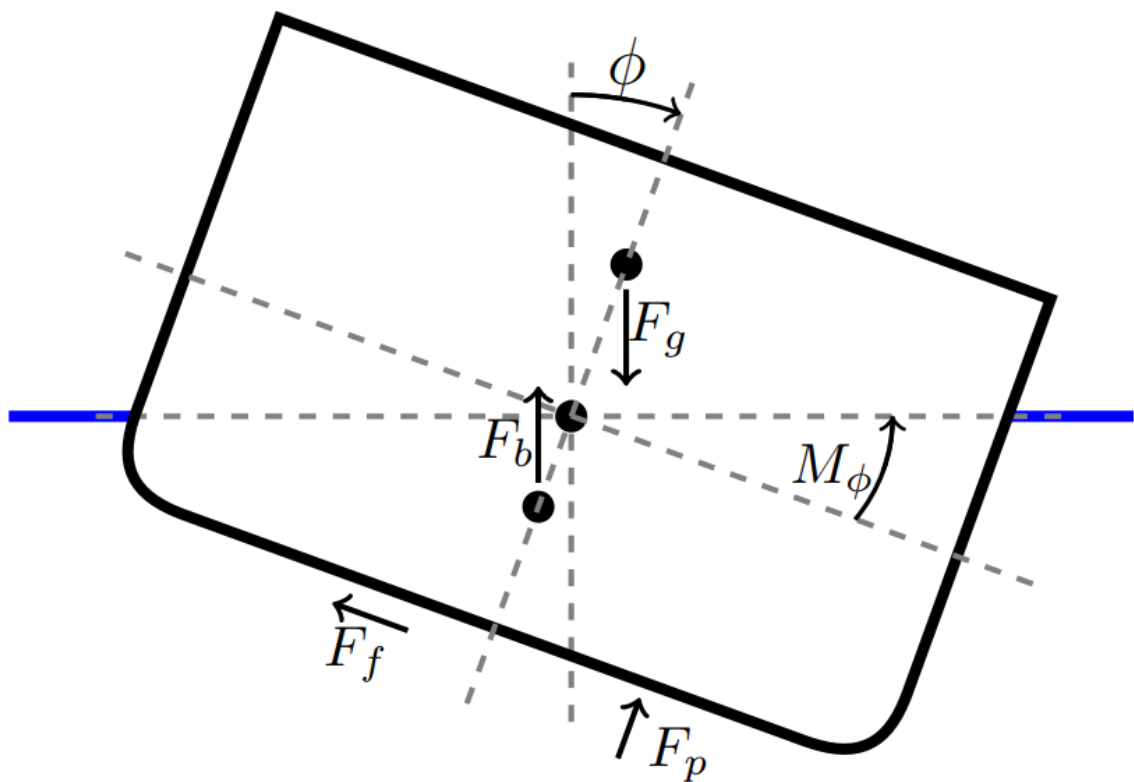


Figure 2.2: Explanation of roll motion

$$F = ma \quad (2.2)$$

$$M_{tot} = I\ddot{\phi} \quad (2.3)$$

Where F is the net force, m is the mass, a is the acceleration, M_{tot} is the total moment, I is the inertia and $\ddot{\phi}$ is the roll acceleration.

By splitting M_{tot} in an external moment M_{ext} and a moment due to the forces of the water M_h , Equation (2.4) is obtained.

$$M_{ext} - M_h = I\ddot{\phi} \quad (2.4)$$

Because M_h in Equation (2.4) accounts for all the forces acted on the structure by the water M_h can be expressed as:

$$M_h = M_a(\ddot{\phi}) + M_b(\dot{\phi}) + M_c(\phi) \quad (2.5)$$

Where M_a is the moment due to added mass as a function of the roll acceleration $\ddot{\phi}$, M_b is the added damping moment as a function of the roll velocity $\dot{\phi}$ and M_c is the restoring moment as a function of the roll angle ϕ . This equation only holds under the assumption that there is no coupling between the roll motion and other ship motions and that there is no dependency on both acceleration and velocity at the same time.

2.2. Physics of roll damping

According to Ikeda et al. [14], the total roll damping coefficient for a ship can be subdivided into four components:

- Friction damping
- Eddy damping
- Lift damping
- Wave damping
- Bilge keel damping

This last term can be divided into three components:

- Bilge keel normal force damping
- Hull pressure damping due to bilge keels
- Wave damping due to bilge keels

Friction damping is a result of the viscosity of water. Due to this viscosity, a thin layer of water, the boundary layer, is attached to the structure. When the structure moves through the water, a difference in velocity exists between the boundary layer and the water away from the body. This causes shear stress, which results in friction drag.

Eddy damping occurs when a structure moves through water and causes pressure differences due to the geometry of the structure. When a structure rolls in water, it creates high a pressure field at the forward moving part of a corner and a low pressure field around that corner. Because water flows from high to low-pressure regions, local flows around the corner arise. This causes separation of the boundary layer. The vortices created due to this separation are called eddies and are the source of eddy damping.

The pressure differences mentioned above also create a lift component. This is the lift damping.

The energy dissipation due to the presence of a free water surface is referred to as wave damping. In other words, the energy lost for the creation of waves causes wave damping.

If bilge keels are fitted to the structure this will increase the damping. The damping increases due to the normal forces acting on the bilge keels when moved through the water, the pressure differences at the front side and back side of the bilge keels and the increased wave damping due to eddies created at the bilge keels dissipating at the free water surface.

2.3. Estimating the roll damping

In order to determine this damping coefficient, several techniques have been developed. These can be divided into three main categories. Based on experiments, empirical models have been developed to estimate the roll damping. If a more accurate estimate is necessary, model tests for the ship in question can be performed. Multiple different model tests can be performed in order to determine the roll damping behaviour. The last category is based on the same techniques as used by model tests, but instead of performing actual tests, the tests are simulated using CFD, a numerical method to simulate viscous flow.

2.3.1. Empirical models

Between 1977 and 1981 Ikeda et al. [14] and Himeno [8] did extensive research regarding roll damping. This research was the basis for the development of empirical models regarding roll damping. According to Ikeda et al. [14] the roll damping could be divided into multiple components, as mentioned in Section 2.2, and that these separate components can be summed to get the total damping coefficient as given in Equation (2.6).

$$b = b_f + b_e + b_L + b_w + b_{bk} \quad (2.6)$$

Where b_f is the friction damping, b_e is the eddy damping, b_L is the lift damping, b_w is the wave damping and b_{bk} is the bilge keel damping. Ikeda et al. [14] validated this approach by extensive model testing. The empirical formulas for each of these components have been given by Ikeda et al. [11], Ikeda et al. [12], Ikeda et al. [13], Ikeda et al. [14] and Ikeda et al. [15]. Himeno [8] combined all these works and updated them. His work is still widely used by the industry. Obviously, more modifications have been made since to make it applicable to a wider variety of ships.

2.3.2. Model tests

There are four types of model tests to determine the roll damping. These are:

- Free roll decay tests
- Forced roll motion oscillation tests
- Excited roll motion oscillation tests
- Regular wave input tests

These four types of model tests will be explained below. For this research, data from a free decay test and forced roll motion oscillation test are used to determine the accuracy of the developed models. It is worth mentioning that these experimental methods are widely accepted and validated as methods to determine the roll damping. However, some errors remain as the tests are done at model scale. Because of this, scale effects are introduced, which cause an error. Another drawback of determining the roll damping through model tests are the inflexibility in adaptations to the models and high costs.

Free roll decay test

With a free roll decay test, a model of the ship is placed in a basin of water under an angle. Once the water is entirely calm and undisturbed, the model is released. As the model is released, the buoyancy forces will generate a restoring moment. This restoring moment results in a rolling motion back to the neutral position and beyond that point to the other side. The model continues with this rotation until the restoring moment reaches its maximum value and will then decrease as the model starts to roll back again. This process continues until the motion energy of the ship is lost due to damping effects. During this decay test, the roll angle is measured. This signal returns a decay curve. An example of such a decay curve is given in Figure 2.3.

Looking at this curve, it is clear that the system is damped. From this curve, the damping coefficients can be determined. How the damping coefficients will be determined from the decay curve will be explained in Section 4.7.

Forced roll motion oscillation test

As the name suggests, a forced roll motion test forces the ship to roll harmonically with a chosen period and amplitude. During these oscillations, the reaction moment is measured. In Section 5.5 a method to extract the damping coefficients from this experiment will be explained.

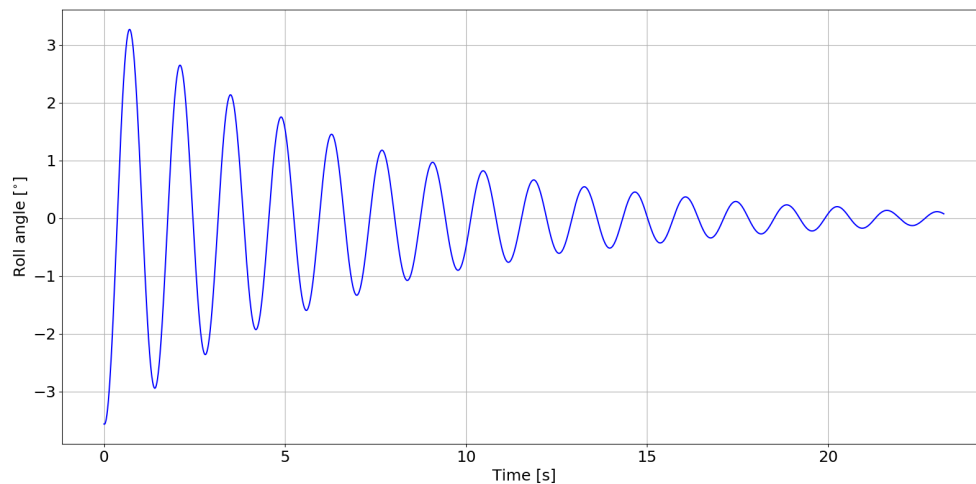


Figure 2.3: Typical roll decay curve

Excited roll motion oscillation test

An excited roll motion oscillation test is basically the same as the forced roll motion oscillation test. However, during an excited roll motion oscillation test, the moment is imposed and the motion is measured.

Regular wave input test

It is also possible to determine the roll damping using a known wave input. The wave input can be a regular or irregular wave, but the wave input needs to be known. This method may be the most realistic method to determine the roll damping but has many difficulties. Before using this type of experiment, it should first be validated as done by Irkal et al. [17].

2.3.3. Computational fluid Dynamics

With computational fluid dynamics, all the experiments mentioned above can be simulated numerically. Advantages of performing numerical simulations are that they are cheaper and faster than real-life experiments. Another significant advantage is the flexibility of numerical simulations. However, in order to be sure that the simulation is a good representation of reality, it should always be validated with experimental data.

3

Governing equations behind the models

In this chapter, the governing equations and settings for the simulations will be explained.

3.1. Navier-Stokes equations

During this research, OpenFOAM has been used to simulate viscous flows. To do so, OpenFOAM solves the conservative form of the incompressible Navier-Stokes equations, which consist of the momentum equation, as given in Equation (3.1), and the continuity equation, given in Equation (3.2).

$$\rho \left(\frac{\partial u_i}{\partial t} + u_j \frac{\partial u_i}{\partial x_j} \right) = - \frac{\partial p}{\partial x_i} + \frac{\partial}{\partial x_j} \left[\mu \left(\frac{\partial u_i}{\partial x_j} + \frac{\partial u_j}{\partial x_i} \right) \right] + \rho g_i \quad (3.1)$$

$$\frac{\partial u_i}{\partial x_i} = 0 \quad (3.2)$$

In which u is the velocity vector of the flow, μ is the dynamic viscosity of the fluid, g is the gravitational acceleration and ρ is the density of the fluid.

During this research, a Reynolds averaged Navier-Stokes model is used. This model decomposes the variables in a mean value and a fluctuating value, as is shown for the velocity in Equation (3.3).

$$u(x, t) = \bar{u}(x) + u'(x, t) \quad (3.3)$$

Where $u(x, t)$ is the total velocity in time and space, \bar{u} is the mean velocity, u' is the fluctuating velocity and (x) is the position vector in three dimensions.

Because the mean operator is a Reynolds operator, it has a set of properties. One of these properties is that the mean of the fluctuating part is equal to zero. If we apply this Reynolds averaging to the Navier-Stokes equations, Equations (3.1) and (3.2), the following set of equations is obtained.

$$\rho \left(\frac{\partial \bar{u}_i}{\partial t} + \bar{u}_j \frac{\partial \bar{u}_i}{\partial x_j} \right) = - \frac{\partial p}{\partial x_i} + \frac{\partial}{\partial x_j} \left[\mu \left(\frac{\partial \bar{u}_i}{\partial x_j} + \frac{\partial \bar{u}_j}{\partial x_i} \right) - \rho \overline{u'_i u'_j} \right] + \rho g_i \quad (3.4)$$

$$\frac{\partial \bar{u}_i}{\partial x_i} = 0 \quad (3.5)$$

By introducing a turbulence model, the added term $-\rho \overline{u'_i u'_j}$ in Equation (3.4) can be solved. Turbulence models will be further explained in Section 3.2.

3.2. Reynolds Averaged Navier-Stokes Turbulence Models

RANS turbulence models offer the most cost-effective approach for computing complex turbulent flows. Typical examples of such models are the $k - \epsilon$ or the $k - \omega$ models in their different forms. These models simplify the problem to the solution of two additional transport equations and introduce an Eddy-Viscosity to compute the Reynolds Stresses. RANS turbulence models are suitable for many applications and typically provide

the level of accuracy required. As none of the models is applicable to every possible situation, a model suitable for the problem at hand should be chosen.

Flow separation and vortex shedding have a significant impact on the roll motion and more specifically on the damping. These phenomena can be captured using turbulence modelling. Therefore two turbulence models have been investigated during this research, namely the $k - \omega$ SST model and the $k - kl - \omega$ model. On these two models will be elaborated in the sections below.

3.2.1. $k - \omega$ SST turbulence model

The $k - \omega$ SST model is based on the $k - \epsilon$ model and the simple $k - \omega$ model. It combines the positive aspect of these two models. To be more precise, at the boundary layer the $k - \omega$ SST model behaves the same as the simple $k - \omega$ model. Because of this, no wall functions, approximations close to the wall, have to be implemented. Outside this boundary layer, the $k - \omega$ SST model behaves like the $k - \epsilon$ model which makes it more robust than the simple $k - \omega$ model. For more information on these two models is referred to Wilcox [29].

3.2.2. $k - kl - \omega$ turbulence model

The $k - kl - \omega$ model is a turbulence model for low Reynolds number turbulent flows and transitional flows (Fürst [4]). The $k - kl - \omega$ model is a three equation model based on the two equation $k - \omega$ model. In the $k - kl - \omega$ model, the equation for k is divided into a laminar and a turbulent part. Another benefit is that the initial conditions can be set to zero, which is not the case with the two above-mentioned models. The effect of initial conditions will be discussed in Section 4.3.

3.3. Multi-phase flow

To model a free water surface, OpenFOAM uses the Volume of Fluid method (Hirt and Nichols [9], Jasak [20]). To control the amount of the two different fluids in a control volume, a scalar α is added. During this research the two fluids are water and air. α has a value between 0 and 1 with a value of 1 corresponding to a control volume filled with water and a value of 0 corresponding to a control volume filled with air. Control volumes exist at the free water surface which are partly filled with water and partly filled with air. As the fluid in a certain control volume can only have one density value and one viscosity value, an interpolation is made as given in Equations (3.6) and (3.7).

$$\rho(x, t) = \rho_{water}\alpha + \rho_{air}(1 - \alpha) \quad (3.6)$$

$$\mu(x, t) = \mu_{water}\alpha + \mu_{air}(1 - \alpha) \quad (3.7)$$

The behaviour through time and space is determined by the transport equation given in Equation (3.8).

$$\frac{\partial \alpha}{\partial t} + \overline{u_i} \frac{\partial \alpha}{\partial x_i} = 0 \quad (3.8)$$

In Figure 3.1, the transition between water and air is visualised. Herein the blue, corresponding to $\alpha = 0$, indicates the control volumes filled with air and the red, corresponding to $\alpha = 1$, indicates the control volumes filled with water. At the free water surface the transition region can be seen with $0 < \alpha < 1$.

3.4. Solution algorithm

To solve the Navier-Stokes equations, numerical techniques for coupling the continuity and momentum quantities are needed. The SIMPLE, PISO and PIMPLE algorithm do this within OpenFOAM. These numerical methods are needed because the momentum equations, given in Equation (3.1), in x , y and z , have four unknowns for three equations. To still be able to solve this, the continuity equation (Equation (3.2)) can be used. However, the continuity equation does not contain the pressure term. This is where the numerical techniques come in. This problem is also known as the pressure-momentum coupling problem.

By doing a semi-discretisation on the momentum equation, which means discretising the time derivative while keeping the space derivative in partial differential form, the continuity equation can be used to eliminate the velocity and get to the well known Poisson equation for the pressure.

Now an equation for momentum and pressure is obtained. These equations are solved sequentially while keeping all other variables constant. By an iterative process, the solution, which is in agreement with all constraints, is found for the next time-step (Holzmann [10]).

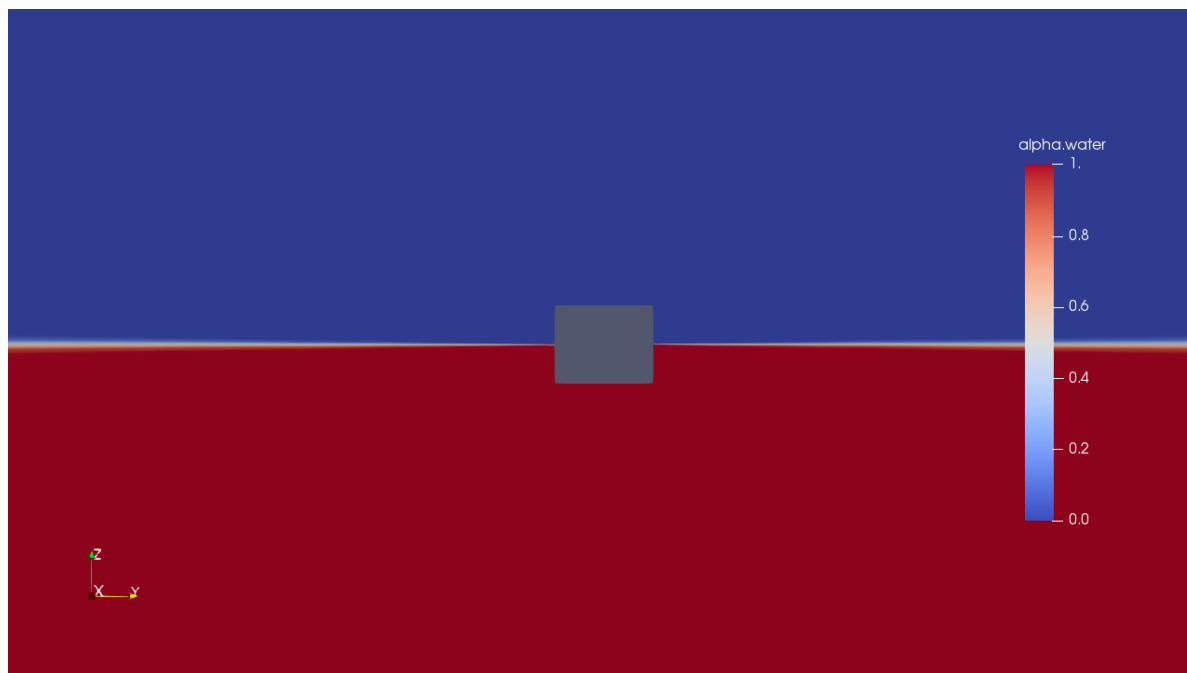


Figure 3.1: Visualisation of the water-air transition

The solution algorithm used during this research is the PIMPLE algorithm. The PIMPLE algorithm is a combination of the steady-state solution algorithm SIMPLE and the transient solution algorithm PISO. These two algorithms will be briefly described below, before further elaborating on the PIMPLE algorithm.

3.4.1. The SIMPLE algorithm

The SIMPLE algorithm in OpenFOAM has no time derivation. This means that the SIMPLE algorithm can only be used for steady-state behaviour. Furthermore, as there is no time derivation and thus a missing term in the equations which need to be solved, the algorithm is inconsistent. To prevent the solution from diverging and maintain stability, the equations are under-relaxed. This means that the initial guess, e.g. for u , for the next iteration is multiplied by a factor between 0 and 1. It is crucial to choose this value carefully as it will make the simulation unstable when a too large value is chosen and very time consuming when a too small value is chosen. The solution is eventually found when it is converged to a certain chosen level of accuracy.

3.4.2. The PISO algorithm

The PISO algorithm differs from the SIMPLE algorithm in the way that it does have the time derivation incorporated. Because of this, the algorithm is consistent and does not need any under-relaxation. However, based on the simulation type, it does require the Courant number not to exceed 1. In Equation (3.9) the formula to calculate the Courant number is given.

$$Co = \frac{u\Delta t}{\Delta x} \quad (3.9)$$

Where Co is the Courant number, u is the local flow velocity in the cell, Δt the time-step size and Δx the length of the cell in x -direction.

To get a better understanding of what this Courant number represents, imagine the following. When the Courant number is smaller than 1, the information from one cell can only reach the neighbour cell within one time-step. If the Courant number would be larger than 1, the information could influence cells which are not neighbouring the subject cell.

From Equation (3.9) we learn that a higher flow velocity requires a smaller time-step and a smaller cell length also requires a smaller time-step. This results in rapidly increasing simulation times with finer meshes.

As it is a transient solver, the solution is reached when the last time-step has been calculated. In other words when adding another time-step, which exceeds the preset end time, the simulation is stopped.

3.4.3. The PIMPLE algorithm

The PIMPLE algorithm, as mentioned before, combines the SIMPLE and PISO algorithm. The PIMPLE algorithm has many input parameters to control the different iterative processes within the procedure of solving the continuity and momentum equations. The two most important parameters are:

- `nCorrectors`: This parameter determines the number of times the PIMPLE algorithm solves the continuity equation and momentum corrector in each time-step.
- `nOuterCorrectors`: This parameter sets the total number of times the algorithm loops over the entire system of equations within one time-step.

The solution is truly implicit when both these parameters are higher or equal to one. The fact that the solution is implicit makes it possible to use a Courant number which is larger than 1.

3.5. Mesh Methods

Three types of meshes exist: structured meshes, unstructured meshes and a combination of the two. Structured meshes consist of solely hexahedral cells where, in an unstructured mesh, the cells can take different forms. During this research, almost entirely structured meshes are used. The meshes are not fully structured due to the usage of SnappyHexMesh. SnappyHexMesh is a tool to mesh complex geometries and is described in Section 3.5.1.

3.5.1. SnappyHexMesh

The ship hull needs to be meshed within the domain. For such complex geometries OpenFOAM uses a tool called SnappyHexMesh (SHM). How this tool works is visualised in Figure 3.2 and will be explained below.

SHM takes an STL file as input and snaps this in a mesh which consists of purely hexahedral cells (Figures 3.2a and 3.2b). This is done by halving the cells close to the boundary of the structure until the surface is captured up until a given refinement level (Figures 3.2c and 3.2d). Hereafter, the cells within the STL surface are removed and the uncut cells are 'snapped' to the STL surface (Figures 3.2e and 3.2f). Lastly, layers can be added perpendicular to the STL surface to capture the boundary layer correctly (Figure 3.2g). The snapping process makes that not all cells in the mesh remain hexahedral.

3.5.2. Dynamic Mesh Method

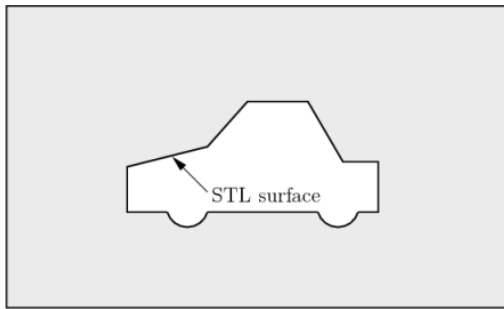
A free decay test was simulated in 3D and a forced oscillation was simulated in 2D during this research. As these two simulations both require the structure to move in the domain, dynamic mesh methods had to be used. Two types of dynamic mesh methods have been investigated both for the 3D case for the 2D case. For the 3D case, these are the deforming mesh method and the overset mesh method. For the 2D case, these were the deforming mesh method and a method in which the complete domain moves.

3.5.3. Deforming Mesh Method

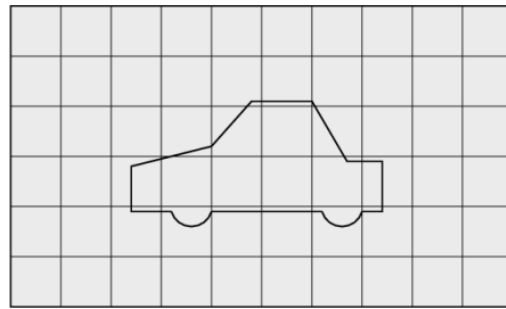
The deforming mesh method, as the name suggests, deforms the cells within the mesh in order to make the motion of the structure possible. In Figure 3.3, the way this works is visualised. One might notice some strange lines. These lines are a result of SnappyHexMesh in combination with the fact that this is a slice of a 3D mesh. Figure 3.3a shows the initial mesh and Figure 3.3b shows the mesh at its ultimate deformation. If the motions are not too severe, i.e. roll angles below 10° , as is the case during this research, this should be a suitable approach. However, when tested, this approach caused cells to deform too much, which resulted in cells with negative volumes and/or very skew orientations.

3.5.4. Overset Mesh Method

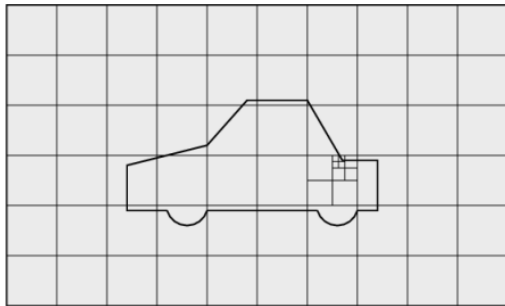
The overset mesh method uses two meshes, a background mesh and an overset mesh. The background mesh is fixed while the overset mesh is free to move in six degrees of freedom. Using SnappyHexMesh, the ship is meshed in the overset mesh. Because this overset mesh is a different mesh, there is no need to mesh the ship under an angle. The overset mesh can later be rotated and placed in the background mesh to create the initial roll angle, as seen in Figure 3.4a as well. SnappyHexMesh works better with symmetrical shapes and due to the fact that the ship is meshed in the upright position, the mesh around the ship will be better than is the case with the deforming mesh. This can be clearly seen in Figure 3.4a.



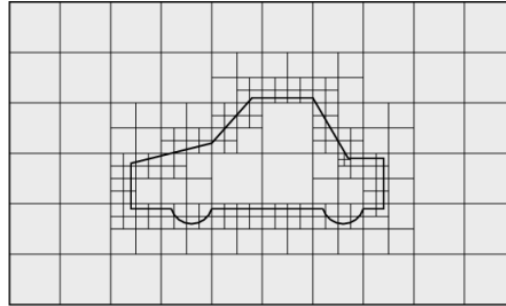
(a) Step 1: Import the STL-file with the structure



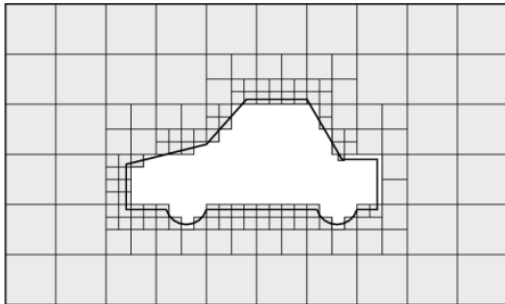
(b) Step 2: Place the structure in the hexahedral mesh



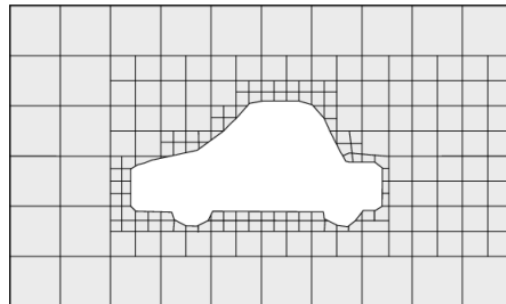
(c) Step 3: Refine at the surface of the structure



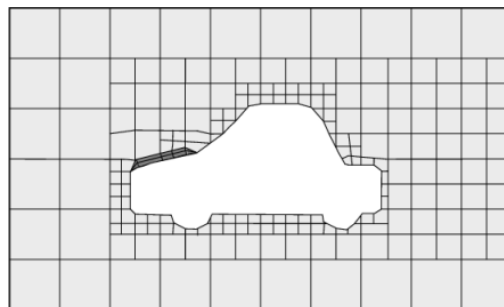
(d) Step 4: Refine complete structure at the surface



(e) Step 5: Delete cells inside the structure

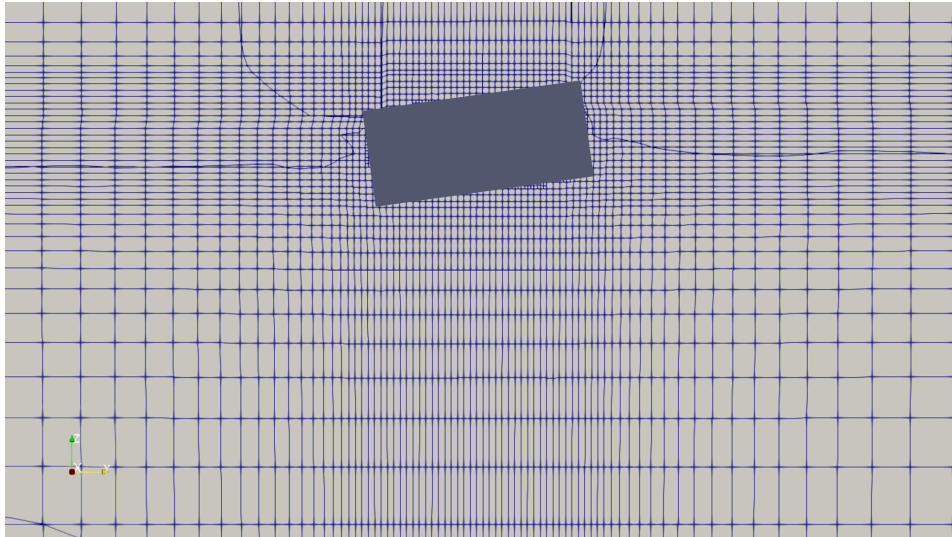


(f) Step 6: Snap cells to the structure

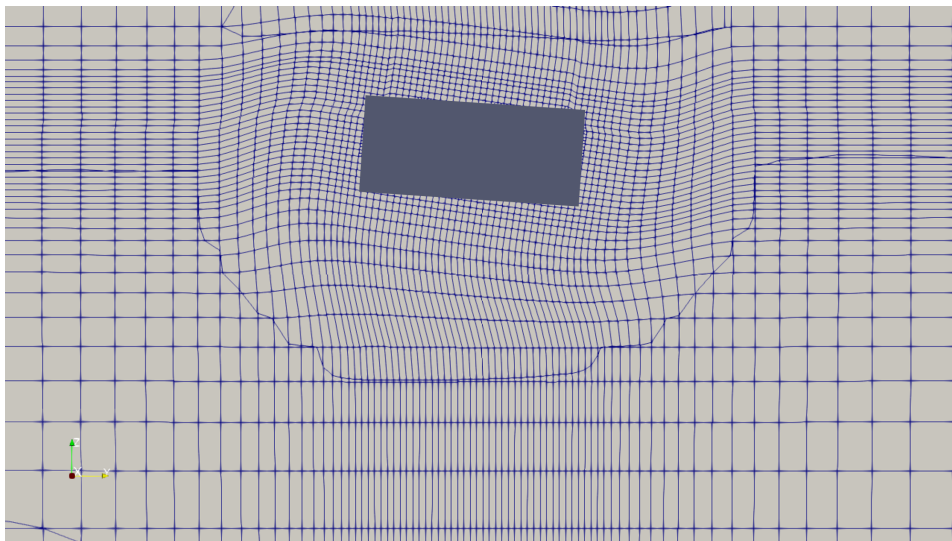


(g) Step 7: Add layers perpendicular to the structure

Figure 3.2: Working principle of SnappyHexMesh (The OpenFOAM Foundation [28])

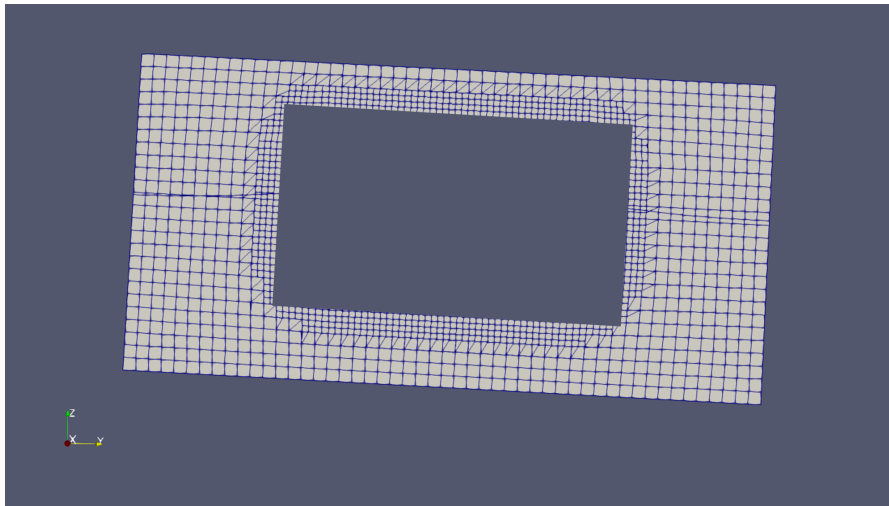


(a) Initial position; no deformation

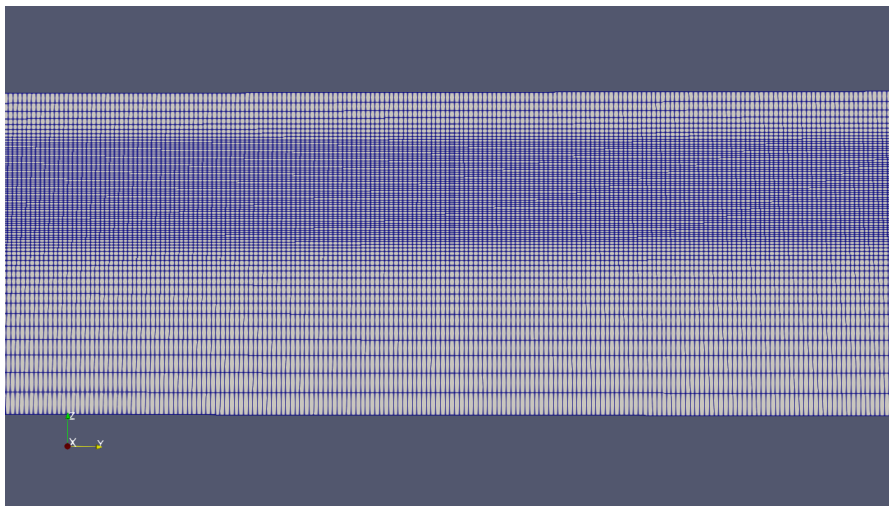


(b) Maximum deformation

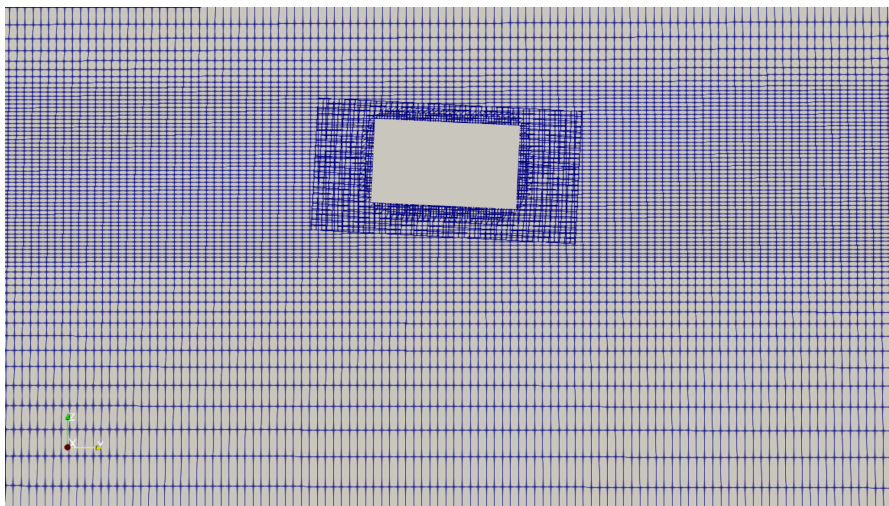
Figure 3.3: Deforming Mesh. The hull is replaced by a rectangle because of confidentiality.



(a) Overset mesh



(b) Background mesh



(c) Combined mesh

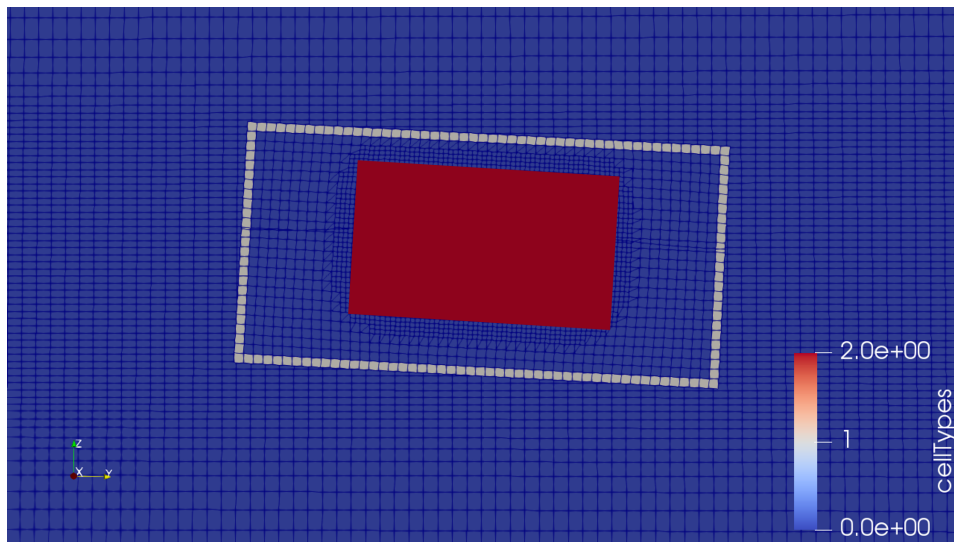
Figure 3.4: The two meshes which are combined in the overset mesh method. The hull is replaced by a rectangle because of confidentiality.

As can be seen in Figure 3.4b, the background mesh exists purely out of hexahedrons. Around the free water surface, the mesh is refined to capture the free water surface more accurately. The figures shown in Figures 3.4a and 3.4b are not shown on the same scale. The exact dimensions of the domain will be given in Section 4.2 In Figure 3.4c, the two meshes combined are shown as they are used during the simulation.

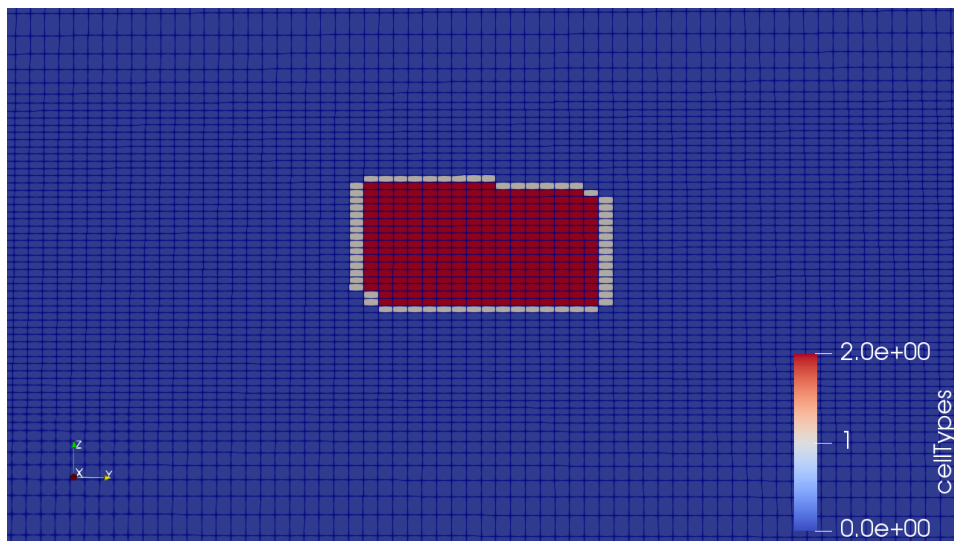
Different cell types are shown in Figure 3.5. The blue cells are the cells in which the system of equations is solved, the grey cells are interpolation cells and the red cells are hole cells. The blue cells are no different from cells in the deforming mesh method. In these cells, the system of equations is solved. The interpolation cells on the overset mesh copy the value of the cell from the background mesh with which they coincide. If the interpolation cells coincide with multiple cells, the values of these cells are calculated according to Equation (3.10) as explained by Shen et al. [27].

$$\phi_F = \sum_{i=1}^n \omega_i \cdot \phi_{Fi} \quad (3.10)$$

Where ϕ_F is the value of the interpolation cell on the overset mesh, ω_i is the weight coefficient and ϕ_{Fi} is the donor cell value of the background mesh. The hole cells are cells are ignored during solving. More specifically, these cells have no values.



(a) Overset mesh showing different cell types



(b) Background mesh showing different cell types. The hull is replaced by a rectangle because of confidentiality.

Figure 3.5

3.5.5. Deforming mesh method compared to overset mesh method

For the 3D free roll decay simulations, the overset mesh technology is chosen. The slight increase in number of cells is not a big problem with regard to computation time. The deformation of cells in the deforming mesh makes the Courant number increase and thus, the time-step decrease. This increases the computation time which is the main reason why the overset mesh method is chosen.

3.5.6. Complete mesh movement

For the 2D simulations, another dynamic mesh method is chosen. The 2D simulations are forced motion oscillation simulations. The deformation of cells is undesirable as described in Section 3.5.5. OpenFOAM has the option to move the complete mesh. For the 2D simulations, this method is chosen as it requires less computation time than the overset mesh method and the mesh quality is excellent with the moving mesh.

In order to keep the water at rest far away from the structure, a circular domain is used with free-slip boundary conditions as will be explained in Section 3.6.

3.6. Boundary Conditions

The CFD problem at hand is defined under the limits of boundary conditions. These boundary conditions are constraints to the incompressible Navier-Stokes equations and the Volume of Fluid method.

A brief description of the different boundary conditions per case is given below. The exact boundary conditions used per case are given in Appendix A.1.

3.6.1. Boundary conditions 3D simulation

There are multiple boundaries in the 3D domain. The domain is enclosed by four stationary walls, a bottom, a topside and the ship which is a moving wall. For every variable solved during the simulation, a boundary condition has to be set for each boundary. As the stationary walls and the bottom have the same boundary condition for every variable, they are grouped together.

The boundary condition for the velocity at the walls and bottom is a no-slip boundary condition. This means that at the wall, the tangential and normal velocity is zero at all times. For the ship, which is a moving wall, a special moving wall condition is chosen. This condition does not allow for any normal velocity. The tangential velocity is the same as the velocity in the cell directly adjacent to the wall. The top side has an inlet-outlet boundary condition. For the outflow, the velocity is fixed at zero for the tangential and normal component. For the inflow, the normal velocity is calculated and the tangential velocity is fixed at zero.

For the pressure, no conditions should have to be specified because the pressure values at the boundaries follow from solving the Navier-Stokes equations in combination with the velocity boundary conditions. However, OpenFOAM requires boundary conditions for the pressure as well. The pressure boundary conditions are chosen in such a way that the values are the same as when the Navier-Stokes equations would have been solved, using the velocity boundary conditions.

The phase fraction α also requires boundary conditions. This boundary condition is one which gives the value for α at the wall the same value as the cell adjacent to it.

3.6.2. Boundary conditions 2D simulation

There are also multiple boundaries in the 2D domain. The 2D case is a circular domain with the ship at the centre of it. This, in combination with the fact that it is a 2D simulation, makes that there are only two walls, the circular wall at the end of the domain and the ship in the centre. The circular wall is interrupted at the top to allow for an inlet-outlet condition. The ship has the same boundary condition as with the 3D case: a moving wall velocity. The circular wall has a free slip condition assigned to it. This is because of the rotating motion of the complete domain. This free slip condition allows for tangential velocities at the boundary but not for normal velocity.

For the pressure and phase fraction, the same holds as for the 3D boundary conditions.

3.7. Initial conditions

For the calculation of the first time-step, field values of the previous time-step are necessary. These values are called the initial conditions. These parameters are the velocity, the pressure and the turbulence values. At the start of the simulation, the velocity in the water is zero as is the pressure field. The initial turbulence values are also zero. An overview of these parameters is given in Appendix A.2.

4

3D free roll decay CFD simulation

In this chapter, the validation of the 3D free decay model is reported. The validation process was done using experimental data. Multiple studies have been done to find the best turbulence model, initial turbulence values and domain size for the simulation. This is done in order to answer the first sub-question.

Is OpenFOAM capable of simulating 3D free roll decay tests in order to calculate the roll damping coefficients, which are in accordance with experimental data?

4.1. Set-up of the simulation

A free roll decay test is performed by placing a floating structure under an initial angle in a tank with water and releasing the structure, as mentioned in Section 2.3.2. When performing a CFD simulation, this set-up is no different. The ship is placed under an angle at the free water surface in such a way that the water displacement under initial roll angle is equal to the weight of the ship. When the simulation starts, the ship is free to move in six degrees of freedom. Because of the initial roll angle, it starts to roll and the typical decay curve is extracted from the simulation. With this decay curve, the linear and non-linear damping coefficients can be determined, as will be explained in Section 4.7. It is important to choose the size of the domain, in which the ship is placed, with care. If the domain is too small, the waves created due to the ship motion will reflect at the boundaries of the domain and will impair the results. However, if the domain is chosen too big, more cells are needed, which will increase the computation time. Another critical factor is the turbulence model. Apart from the turbulence model itself, the initial values of turbulence are just as important, as mentioned by Karagiannis et al. [22].

4.2. Effect of the width of the domain

As mentioned above, the chosen domain size is essential for obtaining valid results. For a free roll decay simulation, the width of the domain is of particular interest, as waves will propagate in this direction due to the roll motion. To determine the correct width of the domain, three domain sizes have been tested and the difference in decay curves has been compared to see whether waves will reflect at the boundaries and impair the results. The dimensions of these different domain sizes are given in Table 4.1. The domains vary only in width, B . For the depth, 3.5 meters is chosen, which corresponds to deep water conditions. This is chosen because the experimental data against which it will be compared is also obtained in deep water conditions. The length, L , of the domain is chosen in such a way that there is at least half a ship length in front of the ship and behind the ship. As the ship has no significant forward or backward motion this should be sufficient.

The free decay curves of the different domains are shown in Figure 4.1. From the disturbed decay curve of domains $B=L$ and $B=1.5 L$, shown in Figure 4.1, it can be concluded that the results are impaired. As the simulations only differ in width of the domain, this impairment is due to the reflection of the waves, generated by the ship, at the boundary. In Figure 4.2, the difference in wave propagation can be seen after 8 seconds of simulation time. Here it can be seen that in domain $B=L$ and $B=1.5 L$ the waves have already reached the boundary. For domain $B=2 L$, this is not the case. All simulations from this point on are done using the $B = 2 L$ domain dimensions.

Table 4.1: Overview of different mesh sizes

Mesh	Lenght [m]	Width [m]	Depth [m]
B = L	12	12	3.5
B = 1.5 L	12	18	3.5
B = 2 L	12	24	3.5

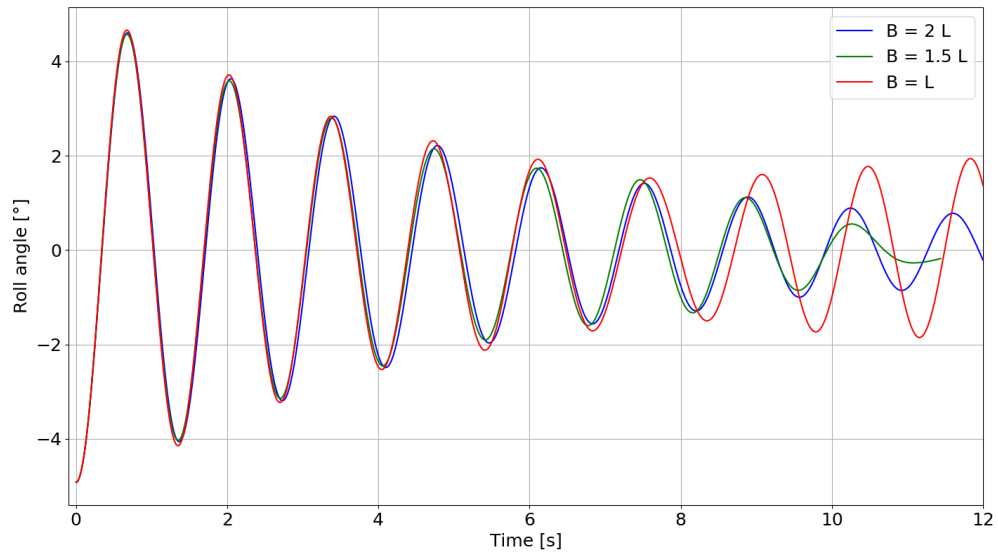
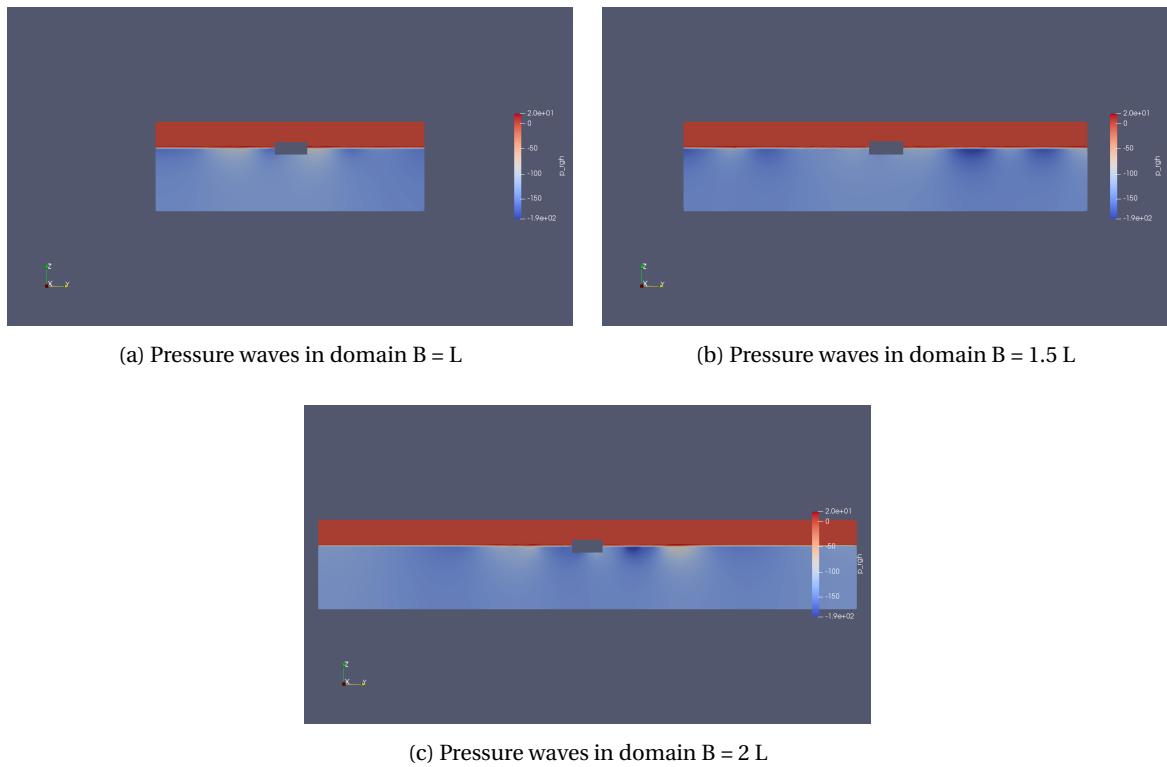


Figure 4.1: Impact on free decay curve of different domain widths

Figure 4.2: Comparison of pressure waves at $t=8s$ in the domain for three different widths, the hull is a square because of confidentiality

4.3. Effect of initial turbulence conditions

As mentioned by Karagiannis et al. [22], the initial turbulence conditions have a significant impact on the turbulence development during the simulation. Karagiannis et al. [22] simulated a swash flow which is different from a free roll decay test. To verify if initial conditions are of large impact for this type of simulation, a verification study has been done. The decay curves of three simulations, which only differ in initial turbulence conditions, are compared. The results are shown in Figure 4.3. The simulations use the $k-\omega$ SST turbulence model. The legend of the figure shows the different initial turbulence values. Because a big difference can be seen in the amount of damping in the system, it can be concluded that also for this type of simulations the initial values are of significant impact.

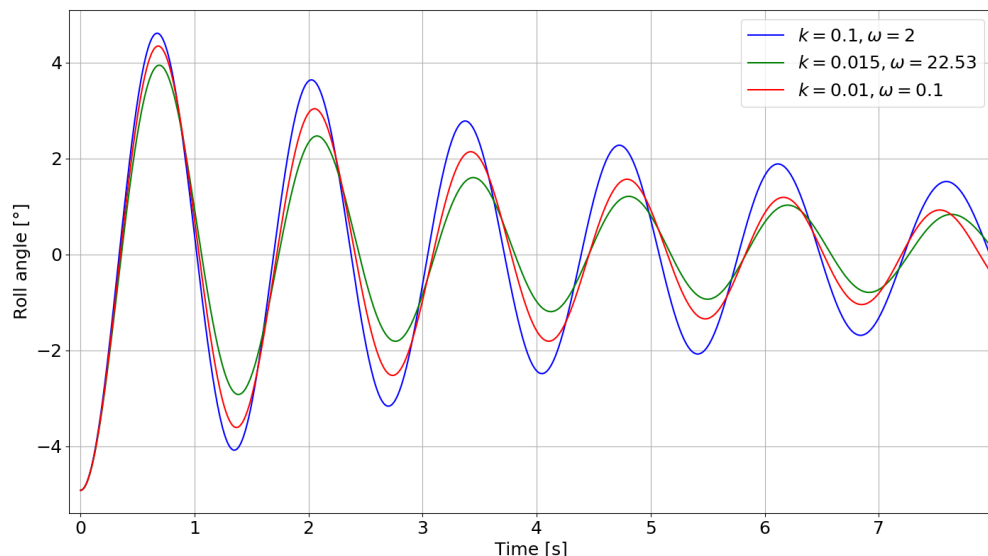


Figure 4.3: Impact on free decay curve of different initial turbulent values

Ideally, the model test with which the CFD results are compared, would have been performed in entirely still water without any turbulence already present. Unfortunately, this was not the case. If the turbulence values of the model test would have been known, the $k-\omega$ SST turbulence model was an excellent model to simulate a free roll decay according to Gu et al. [6, 7], Jaouen et al. [18] and Jiang et al. [21]. However, as the turbulence in the water at the time of the model test was not known, the $k-k_l-\omega$ turbulence model has been chosen. The $k-k_l-\omega$ turbulence model can have the initial turbulence values set to zero. Because the guidelines of the International Towing Tank Conference [16] state that there should be no initial turbulence, the $k-k_l-\omega$ turbulence model, with initial turbulence values set to zero, has been selected for the simulations.

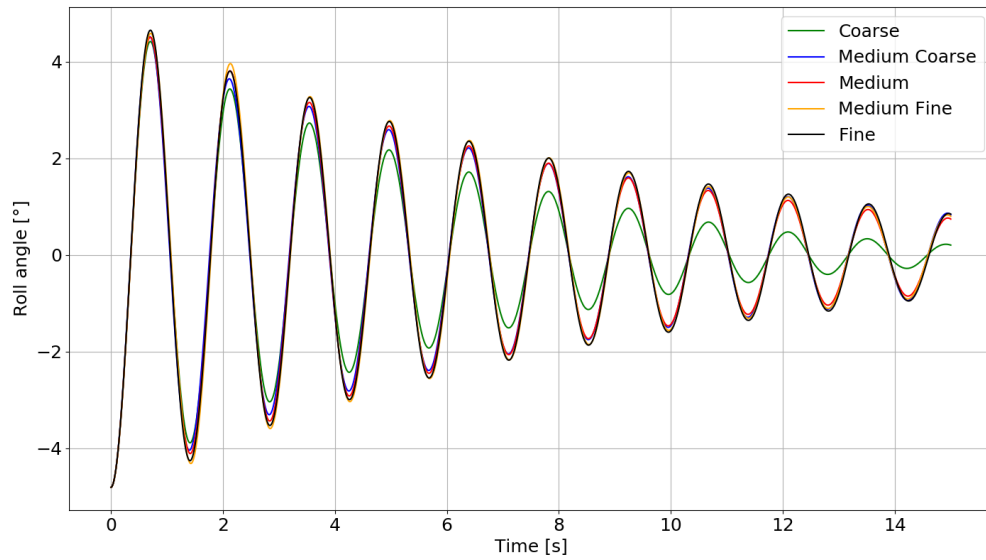
4.4. Mesh convergence

A mesh convergence study is performed to see when grid independence is reached. Five different levels of mesh refinement have been used in order to investigate this. The different mesh refinements and simulation times are given in Table 4.2. All of these simulations were performed on 30 cores on the high-performance cluster of which the details are given in Appendix D.

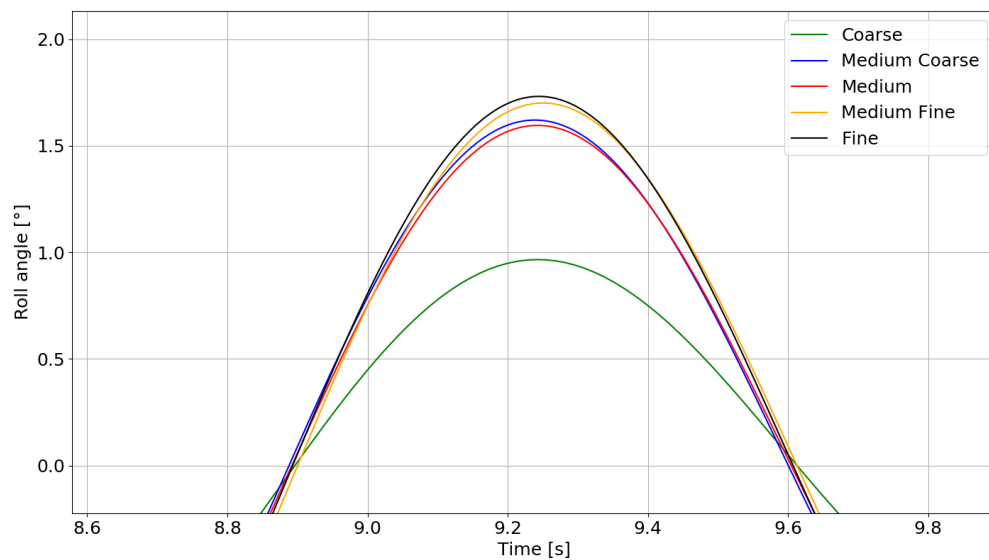
The free decay curves for the five different meshes are shown in Figure 4.4. It is clear that the Coarse mesh does not capture the motions correctly and thus does not capture the damping correctly. For the other four meshes, it is necessary to look at the close-up of the curves given in Figure 4.4b. Here, the differences between the finer meshes are more evident. It can be seen that with an increasing refinement level, the result converges. Although the Fine mesh and Medium Fine mesh still do not coincide, the results are regarded in enough agreement with each other to consider the Medium Fine mesh as converged. For simulations of the 3D free decay tests during this research, the Medium Fine mesh is used.

Table 4.2: Overview of different mesh sizes

Mesh	Total number of cells	Computation time [h]
Coarse	951.000	4
Medium Coarse	2.164.000	54
Medium	3.783.000	73
Medium Fine	4.989.000	137
Fine	6.292.000	239



(a) Complete time trace



(b) Close-up at 7th peak

Figure 4.4: Five different refinement levels for the mesh

4.5. Validation Approach

In order to check whether the CFD results obtained with OpenFOAM are reliable, they should be compared to experimental data. The data used in this research is provided by Van Oord. Marin has done free decay tests commissioned by Van Oord for a certain ship. These tests were performed on model scale. The CFD simulations performed in this research were done using the ship at the same scale, i.e. model scale. The characteristics of the ship at model scale are given in Appendix C. To validate the CFD simulation, the results should be compared to the experimental data of the model test from Marin. First, the free decay curves will be compared and secondly, the resulting damping coefficients will be compared.

4.6. Comparison of free decay curves from Marin and OpenFOAM

For comparison with the results of Marin, the Medium Fine mesh is used. The results are shown in Figure 4.5.

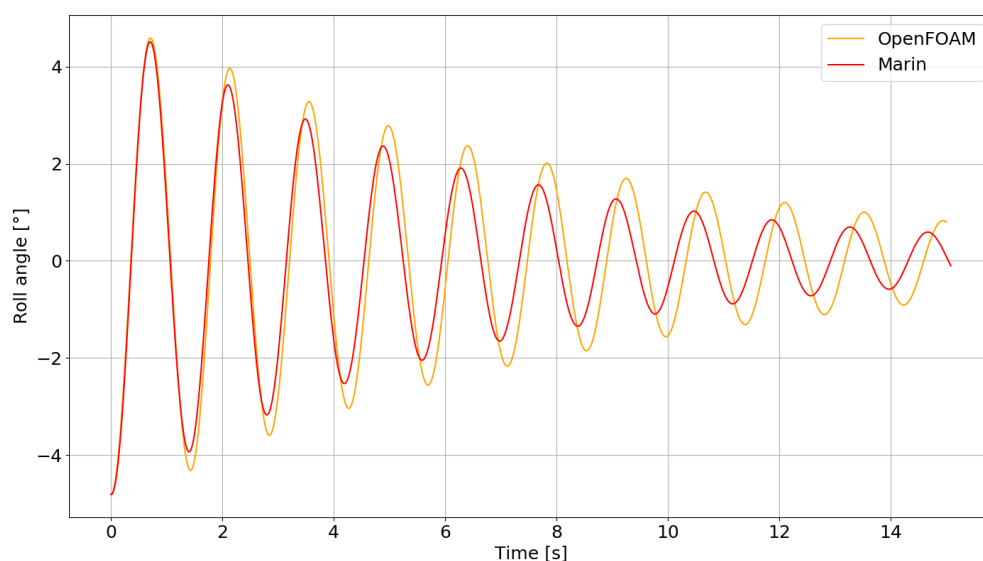


Figure 4.5: Comparison between OpenFOAM and Marin

It is clear that neither period nor amplitude is in perfect agreement. The time trace of the Marin test is enlarged by 1.98% in Figure 4.6. From this figure we can assume that the period of the simulation is off by 1.98%. Several aspects could have caused this. The ship was modelled as accurately as possible. After production, some moveable weights were placed to comply with the characteristics. However, when the model was placed in the water, it was found that the metacentric height was not correct. To correct for this, some weights were moved around which also had an impact on the radii of gyration and thus on the natural roll period. This could be a possible reason why the periods of the simulation and the test do not match. Other possible reasons are given in Section 4.9.

The amplitude differs as well. The maximum difference in amplitude is 15.32%. This does not seem like much, but it has quite a drastic impact on the damping coefficient as can be seen in Section 4.8. Possible reasons for this difference are given in Section 4.9.

4.7. Determining the damping coefficients

The linear and higher-order damping coefficients can be determined from the free decay curve. Only the second-order or quadratic damping coefficient will be determined, as higher-order damping coefficients are very small compared to the linear and second-order damping coefficient. The damping coefficients are determined in a similar way Marin determined them for the experimental data. The method is based on the comparison of energy loss and work done and will be explained below. The basis of this analysis is a mass-damper-spring system.

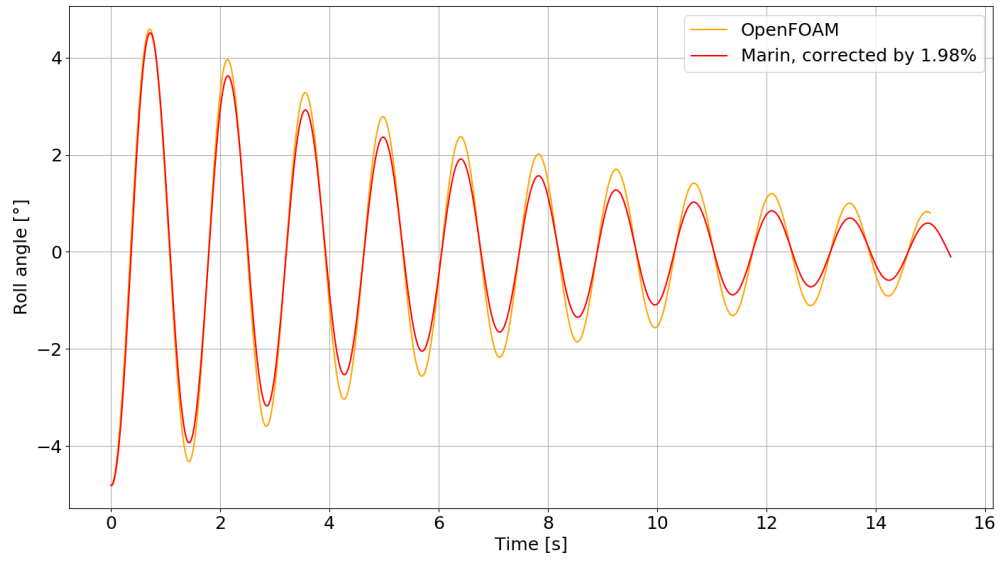


Figure 4.6: Comparison between OpenFOAM and Marin corrected by 1.98%

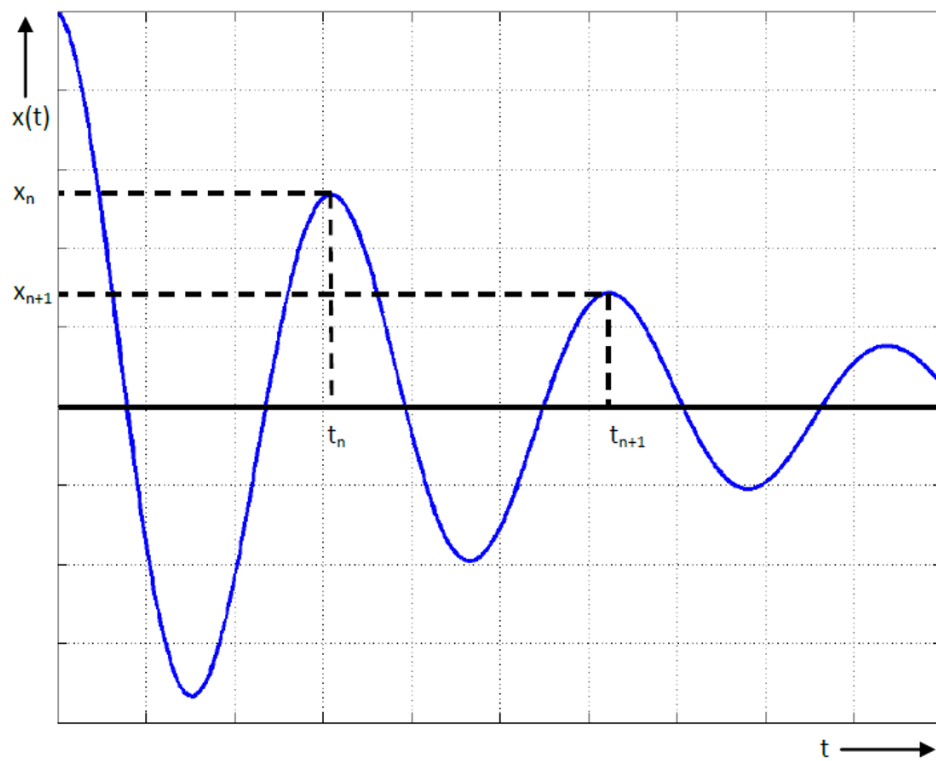


Figure 4.7: Typical decay curve

Figure 4.7 shows a typical decay curve. Within Figure 4.7, a peak and its successive peak are given by x_n and x_{n+1} at time t_n and t_{n+1} respectively. The loss of energy in this interval is given by Equation (4.1).

$$\Delta E_n = \Delta E_{\text{kin},n} + \Delta E_{\text{pot},n} = \frac{1}{2}m\dot{x}_n^2 - \frac{1}{2}m\dot{x}_{n+1}^2 + \frac{1}{2}cx_n^2 - \frac{1}{2}cx_{n+1}^2 \quad (4.1)$$

Where ΔE is the difference in total energy, ΔE_{kin} is the difference in kinetic energy, ΔE_{pot} is the difference in potential energy, m is the mass, \dot{x} is the velocity, c is the damping coefficient and n is a certain peak in the decay curve.

At the peaks the velocity is zero, this means that at time t_n and t_{n+1} , $\dot{x}_n = \dot{x}_{n+1} = 0$. If we apply this to Equation (4.1), eq. (4.2) is obtained:

$$\Delta E_n = \frac{1}{2}c(x_n^2 - x_{n+1}^2) = \frac{1}{2}c(x_n + x_{n+1})(x_n - x_{n+1}) = c\bar{x}_n\Delta x_n \quad (4.2)$$

Where \bar{x}_n and Δx_n are defined as:

$$\bar{x}_n \equiv \frac{1}{2}(x_n + x_{n+1}) \quad (4.3)$$

$$\Delta x_n \equiv x_n - x_{n+1} \quad (4.4)$$

From the general solution of a lightly (sub-critically) damped mass-damper-spring system, which a free roll decay test is, it follows that:

$$c \approx m\omega^2 \quad (4.5)$$

Using this and the definition of \bar{x}_n and Δx_n , Equation (4.2) can now be written as Equation (4.6):

$$\Delta E_n = m\omega^2\bar{x}_n\Delta x_n \quad (4.6)$$

The work done by the damping force at n is given by:

$$W_{\text{damp},n} = \int_{t_n}^{t_{n+1}} (b_l + b_q|\dot{x}(t)|)\dot{x}(t)\dot{x}(t)dt = b_l \int_{t_n}^{t_{n+1}} \dot{x}^2(t)dt + b_q \int_{t_n}^{t_{n+1}} |\dot{x}(t)|\dot{x}^2(t)dt \quad (4.7)$$

Where W_{damp} is the work done by the damping force, b_l is the linear damping coefficient and b_q is the quadratic damping coefficient.

It is assumed that, within the time interval between t_n and t_{n+1} the roll angle is approximated by:

$$x(t) = \bar{x}_n \cos \omega t \quad (4.8)$$

The corresponding roll velocity will then be:

$$\dot{x}(t) = -\omega\bar{x}_n \sin \omega t \quad (4.9)$$

Substituting this velocity in Equation (4.7) gives:

$$W_{\text{damp},n} = \omega^2\bar{x}_n^2 b_l \int_{t_n}^{t_{n+1}} \sin^2 \omega t dt + \omega^3\bar{x}_n^3 b_q \int_{t_n}^{t_{n+1}} |\sin \omega t| \sin^2 \omega t dt \quad (4.10)$$

Solving this gives the total work done by the damping force:

$$W_{\text{damp},n} = \pi\omega\bar{x}_n^2 b_l + \frac{8}{3}\omega^2\bar{x}_n^3 b_q \quad (4.11)$$

Assuming that all lost energy is due to the work done by the damping force, it can be stated that:

$$\Delta E_n = W_{\text{damp},n} \quad (4.12)$$

With Equations (4.6) and (4.11), Equation (4.13) is obtained:

$$m\omega^2\bar{x}_n\Delta x_n = \pi\omega\bar{x}_n^2 b_l + \frac{8}{3}\omega^2\bar{x}_n^3 b_q \quad (4.13)$$

Dividing Equation (4.13) by \bar{x}_n^2 and $m\omega^2$ gives Equation (4.14).

$$\frac{\Delta x_n}{\bar{x}_n} = \frac{\pi}{m\omega} b_l + \frac{8}{3m} b_q \bar{x}_n \quad (4.14)$$

This can be written as:

$$\frac{\Delta x_n}{\bar{x}_n} = p + q \bar{x}_n \quad (4.15)$$

Where

$$b_l = \frac{p}{2\pi} b_{\text{crit}} \quad , \quad b_q = \frac{3q}{16\omega} b_{\text{crit}} \quad (4.16)$$

Plotting the difference in succeeding peaks against the average values of those two peaks for the complete decay curve and fitting a linear function through these points makes it possible to determine the values of p and q . In Figure 4.8, an example of such a p - q analysis is given. In the legend of this figure, the linear function is shown. For this example $p = 0.1707$ and $q = 0.0006755$. With Equation (4.16), the linear and second-order damping component can be determined.

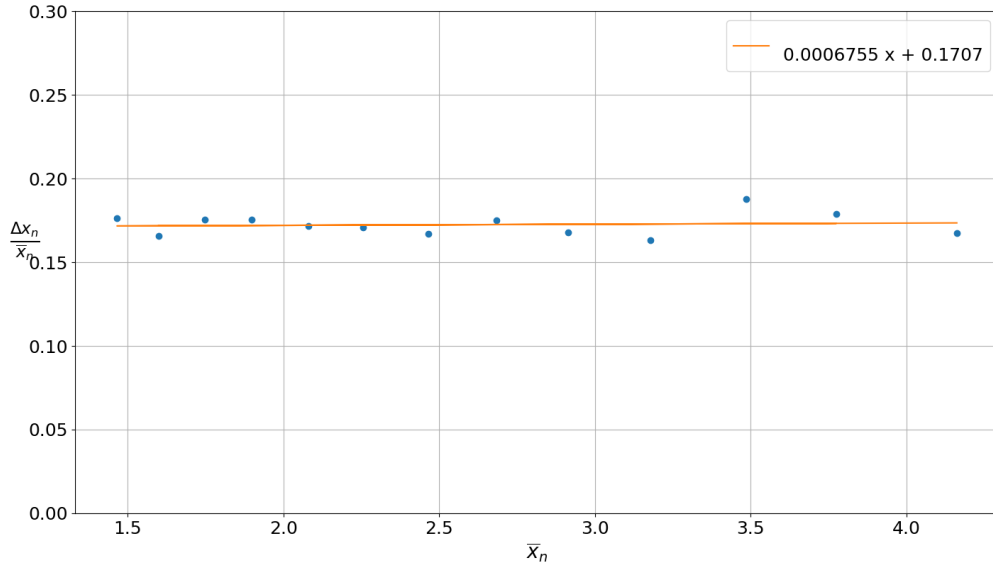


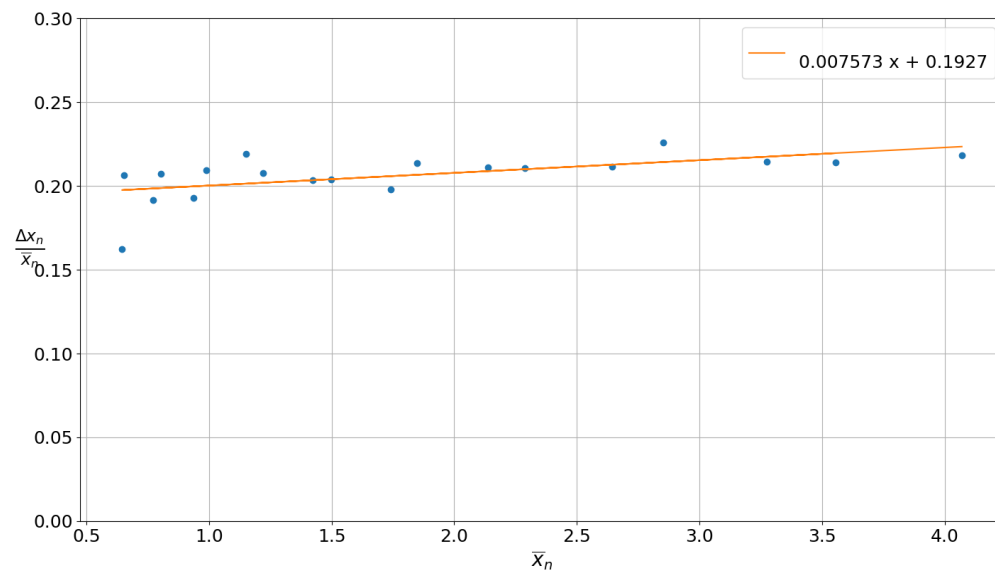
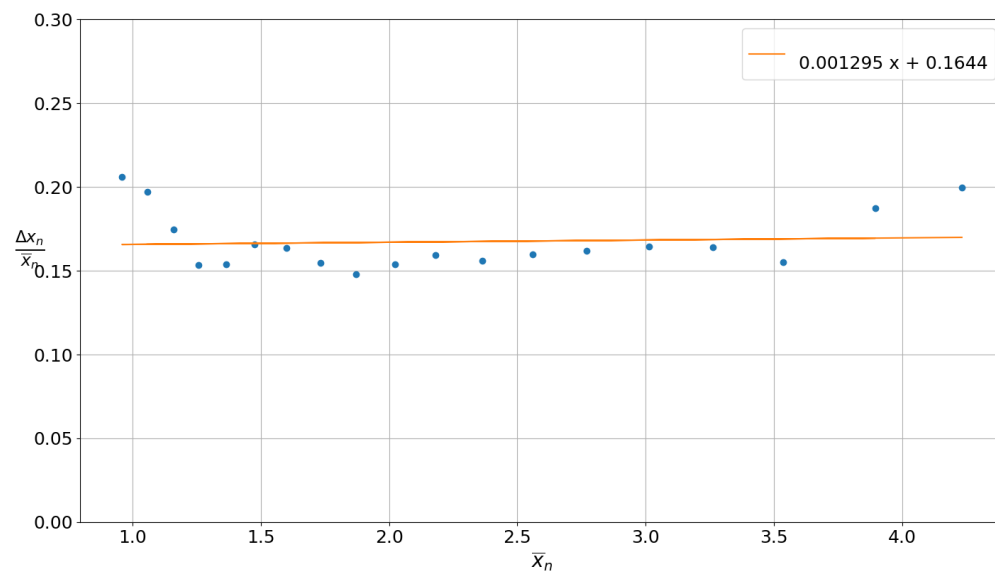
Figure 4.8: Typical p - q analysis

4.8. Comparing the damping coefficients with experimental data

The damping coefficients have been determined for the Marin and OpenFOAM results using the above-mentioned method. Marin did the free decay test three times and for all three tests, the p - q analysis is performed. To determine the damping coefficient of the OpenFOAM simulation, the results of the Medium Fine mesh have been used. The p - q analysis of the first Marin test and the OpenFOAM simulation are shown in Figures 4.9 and 4.10 respectively and an overview of the damping values is given in Table 4.3.

Table 4.3: Results p - q analysis from the experimental data from Marin

Test	p [-]	q [1/°]	b_l [Nm/(°/s)]	b_q [Nm/(°/s ²)]
Marin 1	0.1927	0.0076	34.065	0.3516
Marin 2	0.2002	0.0000	35.426	0.0000
Marin 3	0.2004	0.0023	35.532	0.1064
OpenFOAM	0.1644	0.0013	29.060	0.0599

Figure 4.9: p - q analysis of model test 1 performed by MarinFigure 4.10: p - q analysis of the OpenFOAM simulation

When comparing the different Marin model tests, it can be seen that the linear damping coefficient is reasonably constant through all three tests. The quadratic damping deviates quite a lot, but has very small absolute values.

When the Marin results are compared to the results from OpenFOAM, it can be seen that OpenFOAM underestimates the linear damping. The quadratic damping is also below the average value determined by Marin but is within the range of values found by Marin.

The fact that Marin repeated the test 3 times and found such a significant spread in quadratic damping raises the question whether this analysis approach is the correct one for a system with this little quadratic damping. The sensitivity regarding quadratic damping originates in the selection of the number of peaks taking into account for the p - q analysis.

4.9. Possible causes for deviations

Multiple factors can be the cause of the difference in results. These can result from the tests or the simulation.

4.9.1. Model tests

With the model tests at Marin, not all factors could be controlled as well as within a numerical simulation. In ideal circumstances, the water in the tank would have been completely still, i.e. no turbulence present at the beginning of the test. Unfortunately, this was not the case.

Another difference between the model tests and the simulation was how they were initialised. Within the numerical simulation, the ship was fixed at its initial roll angle and placed in entirely still water. At the start of the simulation, the ship was released from this angle and started to roll. This is the method recommended by the International Towing Tank Conference [16]. Before initialising the test at Marin, the ship was free-floating. To start the test, a stick was used to start the rolling motion by applying a non-measured force to the ship. With this stick, the roll motion was started with several oscillations of applied force through the stick. As the size of the force and direction of the applied force have not been measured it was impossible to simulate this within the numerical simulation.

Another disadvantage of this method is that with these applied forces, the water around the ship is set in motion and causes turbulence. Because the amount of turbulence was also not measured, it was impossible to account for this within the simulation.

4.9.2. Simulation

The deviation in results could also originate from the simulation. In Chapter 5 it will be shown that the presence of a free water surface can cause unrealistic turbulence at the free water surface.

Another cause could be the turbulence model or its initial values. As mentioned before the initial turbulence values at the start of the model test were not known. A study to determine these initial values fell outside the scope of this research.

4.9.3. Conclusion on deviations in results

The differences in results could thus be explained by the sub-optimal conditions during the model tests regarding the reproducibility. However, this can not be stated with complete certainty as the numerical simulation could also be lacking in a certain way.

Within the scope of this research, there was no room to use different experimental data to validate the simulation.

4.10. Conclusion

The 3D free decay simulation was not successfully validated. This could have been caused by the simulation or due to the fact that the data, which was used for the validation, was not reproducible. Due to this no clear answer on the first sub-question can be given.

5

2D forced oscillation CFD simulation

In this chapter, the validation process of the 2D forced oscillation model is reported in order to answer the second sub-question.

Is OpenFOAM capable of simulating 2D forced oscillation tests in order to calculate the roll damping coefficients, which are in accordance with 2D experimental data?

5.1. Validation Approach

The eventual goal is to check whether the combined results of multiple 2D sections can predict the damping behaviour of a ship. During a free decay test, the ship will oscillate in its natural period. However, the 2D sections have different geometries and weights and thus they will have different natural periods. Because of this, a free decay test is not feasible for the 2D model. In order to combine the different sections, all sections should oscillate in the same period. As the resulting damping coefficients should be compared to the damping coefficients resulting from Marin's experiments, the oscillation period should be the same as the natural period of the complete ship. To ensure the same period a forced oscillation test is chosen. The damping will be determined with the results of these forced oscillation simulations.

To validate the 2D model, the results from these 2D simulations will be compared against the experimental data obtained by Ikeda et al. [14] in the same way as reported by Jaouen et al. [18]. The data provided by Ikeda et al. [14] was obtained by performing a forced oscillation experiment of a rectangular box. This experiment was performed with a free water surface. Jaouen et al. [18] simulated a fully submerged forced oscillation using a CFD code called ReFresco. Because this simulation was fully submerged, the component of the reaction moment caused by the free water surface was estimated using a potential flow solver. The results from this estimation were subtracted from the reaction moment found by Ikeda et al. [14] to be able to compare the fully submerged CFD simulation with the data from Ikeda et al. [14].

To validate the 2D forced oscillation simulation in this research, the same case set-up as used by Jaouen et al. [18] was simulated with the OpenFOAM model used in this research. Only, in this research, a different turbulence model was chosen. Instead of the $k - \omega$ SST model (Section 3.2.1), the $k - kl - \omega$ model (Section 3.2.2) was used. This different approach was chosen because this way, the same turbulence model used for the 3D simulations is used for the 2D simulations. Another difference with the simulation of Jaouen et al. [18] is that, in this simulation, the VoF-method was used, where Jaouen et al. [18] use a single phase flow. However, effectively the domain of the 2D fully submerged simulation performed during this research, was always completely filled with water. This is because the domain was initialised with water in the complete domain and because both fluids had the same properties, i.e. the properties of water. This cumbersome approach was used in order to keep as many settings the same between the 2D and 3D simulations.

5.2. Geometry of the hull shape

The hull shape for the validation of the 2D simulation is a rectangular shaped box shown in Figure 5.1. OpenFOAM is not capable of performing true 2D simulations. Because of this, the cell in the lengthwise direction of the hull has to have a thickness. This thickness is chosen as 0.1 meters, the same as used by Jaouen et al.

[18]. The black dot in Figure 5.1 is the centre of rotation for the forced oscillatory roll motion. The geometry given in this figure is just the bottom half of the structure. The dashed line is the mirroring plane.

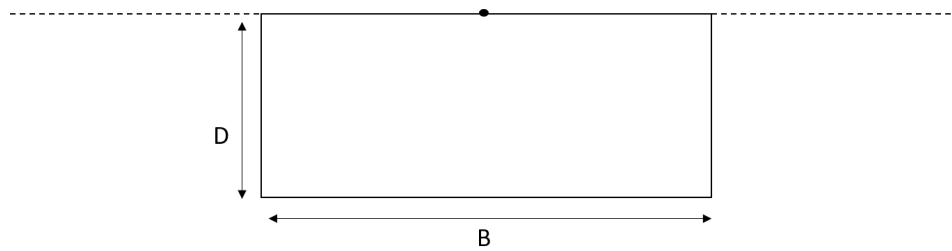


Figure 5.1: 2D hull section under investigation, $B = 0.28\text{m}$, $D = 0.112\text{m}$

5.3. Numerical domain

The numerical domain is made in the same way as done by Jaouen et al. [18]. A circular domain is created, which is shown in Figure 5.2.

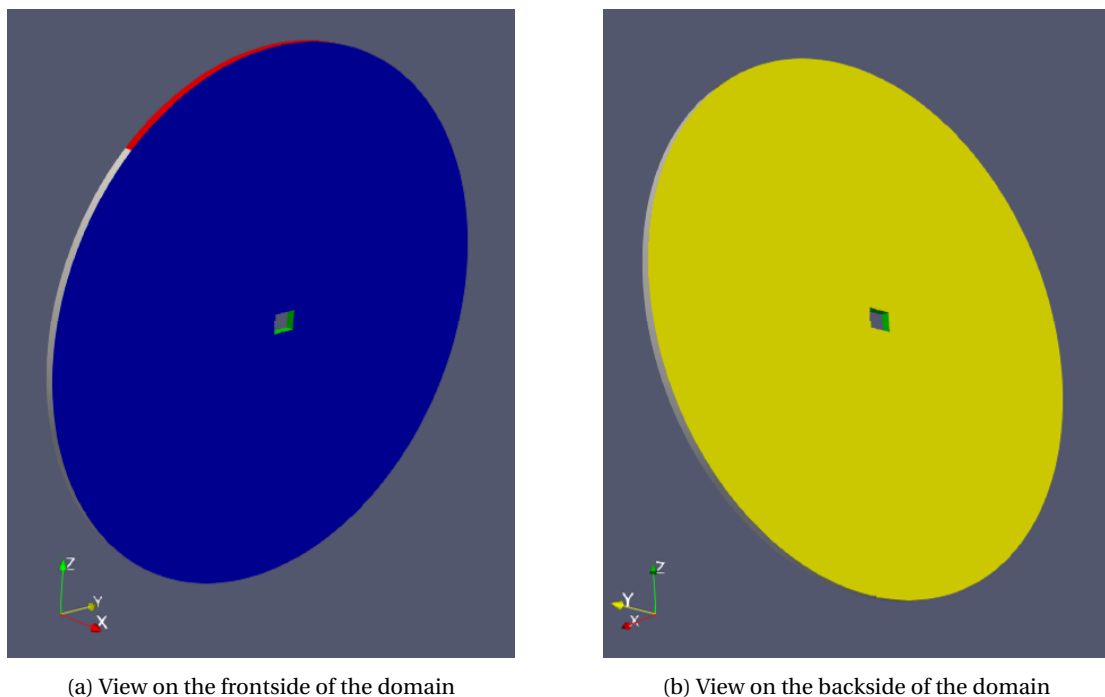


Figure 5.2: Circular domain for 2D simulations

In Figure 5.2, the different colours stand for different boundaries: Blue is the front, red is the atmosphere, grey are the stationaryWalls, yellow is the back and green is the ship. These boundaries are explained in Appendix A.1.

5.4. Mesh Convergence Study

In order to investigate the mesh dependency of the results, a mesh convergence study is performed. Three meshes with different levels of refinement have been generated. In Figure 5.3, the three different refinement levels for the mesh are shown. In Table 5.1, the corresponding number of cells per mesh and the computation time are given. All calculations regarding the 2D model have been performed on 10 cores of the high-performance cluster of which the details are given in Appendix D.

The difference in reaction moment for oscillation 10 to 13 is shown in Figure 5.4. These simulations were done with the $k-kl-\omega$ turbulence model with initial conditions set to zero. The period is 1.5 seconds and the

amplitude 0.1 radians. There is a significant difference between the coarse mesh and the other two meshes. However, the medium and fine mesh show little deviation. For this reason, and because there is a big difference in computation time, see Table 5.1, further calculations were performed on the medium mesh or meshes with an equal level of refinement as the medium mesh.

Table 5.1: Overview of different mesh sizes

Mesh	Total number of cells	Computation time [h]
Coarse	40k	2
Medium	160k	9
Fine	699k	39

5.5. Damping extraction methods

In order to compare the damping, the reaction moment obtained through the simulation should be translated to a damping coefficient. There are several methods to do this. The method used by Jaouen et al. [18] will be used in this case because this is the most logical approach to compare the results of their simulations to the results of the simulations performed during this research. This method will be briefly explained below.

Equation (5.1) shows that the hydrodynamic moment M_h is a superposition of the added mass moment, the added damping moment and the restoring moment.

$$M_h = M_a(\ddot{\phi}) + M_b(\dot{\phi}) + M_c(\phi) \quad (5.1)$$

5.5.1. Linearised equivalent damping

According to Himeno [8] and Ikeda et al. [13] Equation (5.1) is a non-linear equation. This non-linearity is expected to originate from the added damping component. In Equation (5.2), Equation (5.1) is linearised.

$$M_h = m_a\ddot{\phi} + b_{eq}\dot{\phi} + c\phi \quad (5.2)$$

Where m_a is the added mass coefficient, b_{eq} the equivalent damping coefficient of the linear and non-linear damping coefficient and c is the restoring coefficient.

Because the forced oscillation has a sinusoidal form (Equation (5.3)), it can be assumed that the reaction moment also has a sinusoidal form (Equation (5.4)).

$$\phi = \phi_a \sin(\omega t) \quad (5.3)$$

$$M_h = M_0 \sin(\omega t + \varepsilon) \quad (5.4)$$

Where ω is the frequency, ϕ_a is the amplitude of the forced oscillation, M_0 is the amplitude of the hydrodynamic moment and ε is the phase shift between the forced motion and the reaction moment.

By fitting a sine function through the reaction moment extracted from OpenFOAM, M_0 and ε can be determined.

Substituting Equations (5.3) and (5.4) in Equation (5.2) gives Equation (5.5).

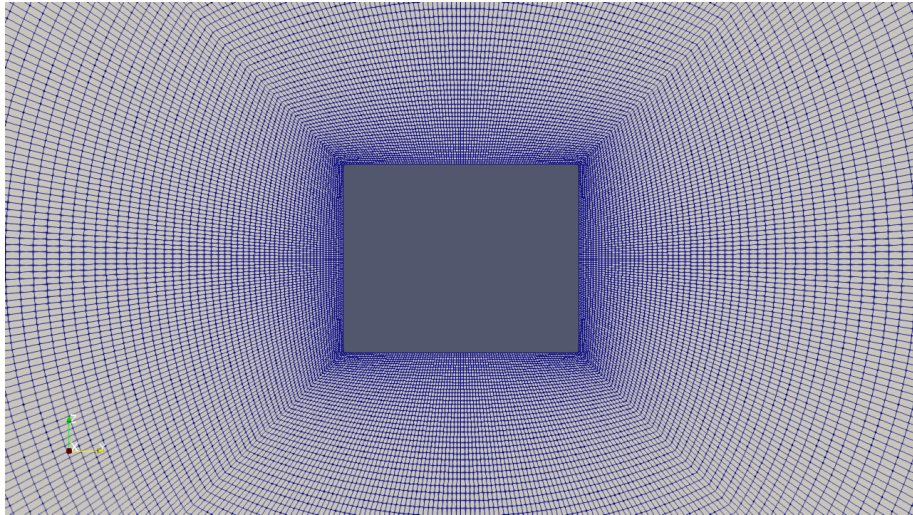
$$M_0 \sin(\omega t) \cos(\varepsilon) + M_0 \cos(\omega t) \sin(\varepsilon) = -\omega^2 \phi_a m_a \sin(\omega t) + \omega \phi_a b_{eq} \cos(\omega t) + \phi_a c \sin(\omega t) \quad (5.5)$$

From Equation (5.5) and with the extracted M_0 and ε , it is possible to obtain the equivalent damping coefficient b_{eq} , see Equation (5.6).

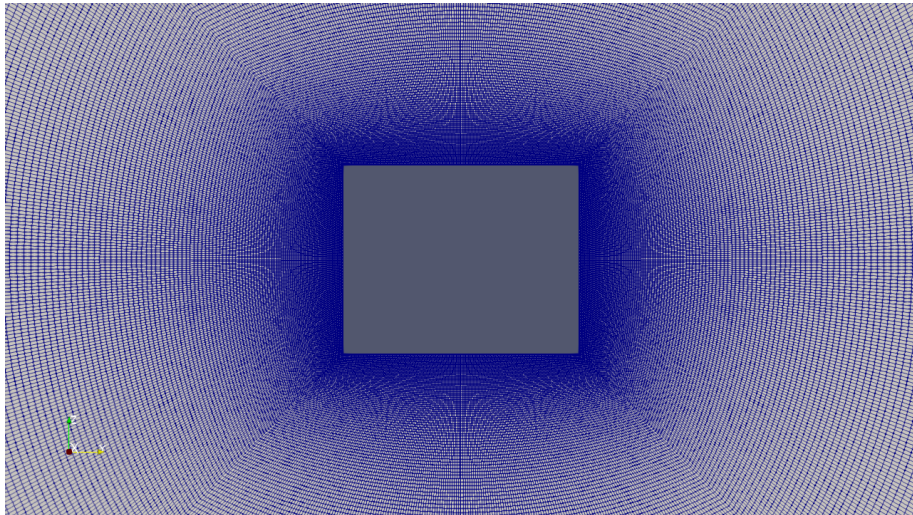
$$b_{eq} = \frac{M_0 \sin(\varepsilon)}{\phi_a \omega} \quad (5.6)$$

5.5.2. Non-linear damping

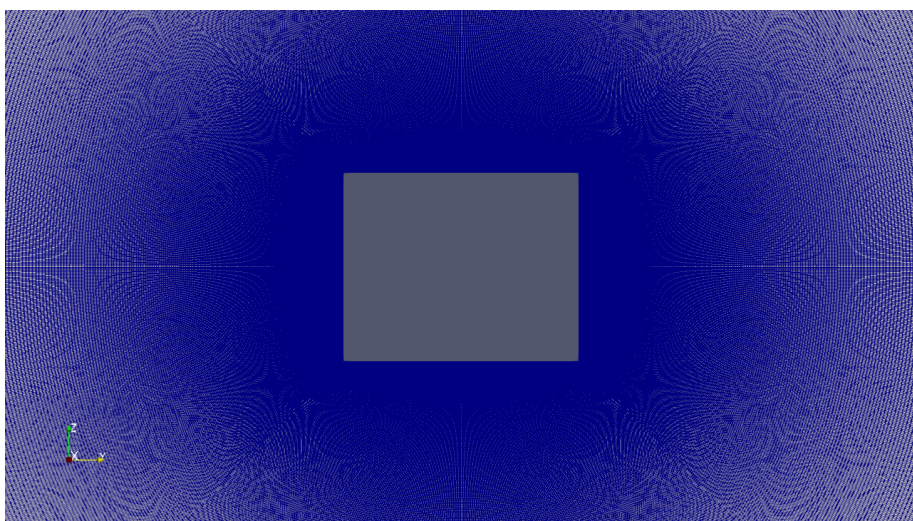
With the linearised equivalent damping, it is also possible to extract the linear and non-linear component of the damping, when multiple simulations with the same frequency but different amplitudes are performed. The total damping moment can be expressed as a series expansion of $\dot{\phi}$ and $|\dot{\phi}|$ as given in Equation (5.7)



(a) Coarse mesh

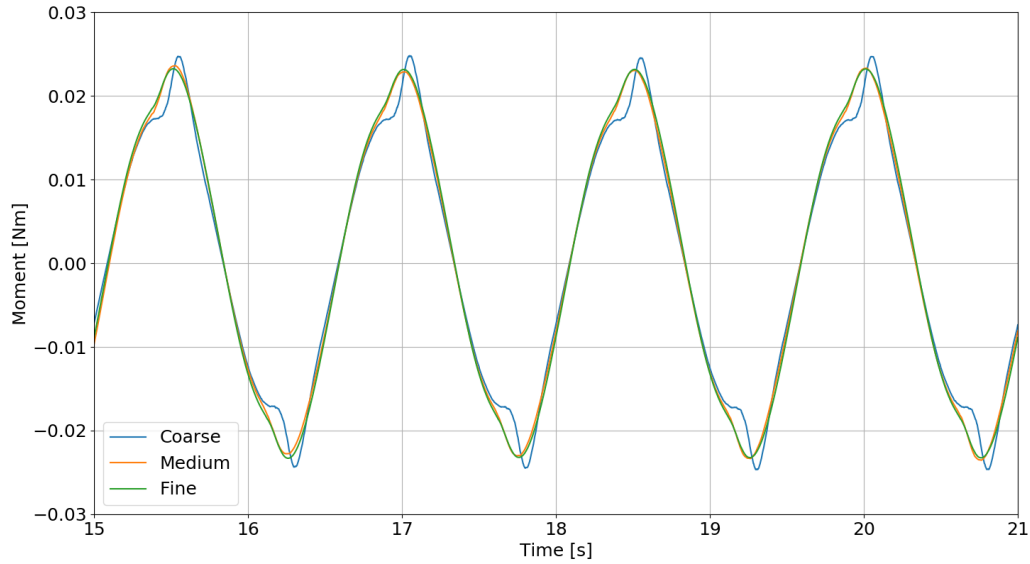


(b) Medium mesh

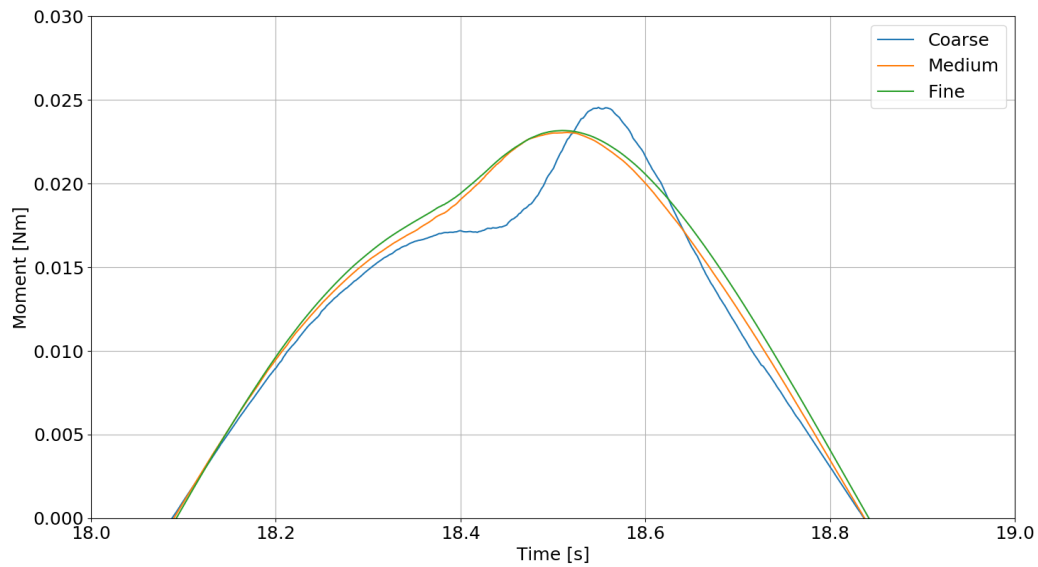


(c) Fine mesh

Figure 5.3: Three different refinement levels for the mesh



(a) Four succeeding oscillations ranging from oscillation 10 to 13



(b) Close-up of 12th oscillation

Figure 5.4: Difference in reaction moment between the three different refinement levels for the mesh and close-up

$$M_b(\dot{\phi}) = b_1\dot{\phi} + b_2\dot{\phi}|\dot{\phi}| + b_3\dot{\phi}^3 + \dots + b_n\dot{\phi}^n \quad (5.7)$$

Where b_1, b_2, b_3 etc. are respectively the first, second, third and higher-order damping coefficient. b_1 and b_2 are equal to b_l and b_q mentioned in Section 4.7. Within this research, the third and higher-order damping coefficient are not taken into account as they are very small compared to the first and second-order damping coefficient. Assuming that Equation (5.7) can be linearised and not taking third or higher-order damping into account gives Equation (5.8).

$$b_{eq}\dot{\phi} = b_1\dot{\phi} + b_2\dot{\phi}|\dot{\phi}| \quad (5.8)$$

By applying a Fourier transform, it is possible to determine a formula to calculate the linear and non-linear damping coefficient.

$$\frac{1}{T} \int_0^T b_{eq}\dot{\phi} \cos(\omega t) dt = \frac{1}{T} \int_0^T b_1\dot{\phi} + b_2\dot{\phi}|\dot{\phi}| \cos(\omega t) dt \quad (5.9)$$

$$\begin{aligned} \frac{1}{T} \int_0^T b_{eq}\dot{\phi} \cos(\omega t) dt &= \frac{1}{T} \int_0^T b_1\phi_a\omega \cos(\omega t) \cos(\omega t) dt \\ &+ \frac{1}{T} \int_0^T b_2\phi_a\omega \cos(\omega t) |\phi_a\omega \cos(\omega t)| \cos(\omega t) dt \end{aligned} \quad (5.10)$$

$$b_{eq}\phi_a\omega = b_1\phi_a\omega + \phi_a\omega \left(b_2\phi_a\omega \frac{8}{3\pi} \right) \quad (5.11)$$

$$b_{eq} = b_1 + b_2\omega\phi_a \frac{8}{3\pi} \quad (5.12)$$

By plotting multiple equivalent damping coefficients with their corresponding amplitudes and fitting the first-order polynomial through these points it is possible to extract a linear and non-linear damping coefficient using Equation (5.12).

5.6. Results of the fully submerged simulations

Because Jaouen et al. [18] use the $k-\omega$ SST turbulence model and the $k-kl-\omega$ model is used during this research, a difference in turbulence is to be expected. The vorticity of the OpenFOAM simulation is shown side by side the vorticity of the simulation performed by Jaouen et al. [18] in Figure 5.5. The expected difference in turbulence is visible. On the left, the results of Jaouen et al. [18] are shown, on the right, the results of this research are shown. The difference in vorticity also leads to a difference in pressure distribution along the hull, which is shown in Figure 5.6.

To confirm that this difference in vorticity is due to the turbulence model, the $k-\omega$ SST turbulence model is incorporated in the simulation of this research. All other settings have remained the same. All differences should thus be due to the turbulence model. The vorticity is again compared against the simulation of Jaouen et al. [18] in Figure 5.7. The results are in excellent agreement with each other. It can thus be concluded that the difference, visible in Figure 5.5, is due to the selected turbulence model.

These small differences in pressure and vorticity between the $k-\omega$ SST turbulence model and the $k-kl-\omega$ model have little impact on the damping. Using the equations given in Section 5.5, the damping is determined from the reaction moment. The normalised equivalent damping, according to Ikeda et al. [14], Jaouen et al. [18] and this research, are plotted against the forced motion amplitude in Figure 5.8. As can be seen, the results from this research are in good agreement with both Ikeda et al. [14] and Jaouen et al. [18]. The exact values of the plotted data in Figure 5.8 are given in the column $b'_{eq,viscous}$ of Table 5.2 and Table 5.3.

5.7. Results of the simulations with free water surface

In order to be able to make a fair comparison between the 3D simulation and the 2D simulation, the free water surface had to be included in the 2D simulations as well. For both the 3D simulation as for the experiment performed by Ikeda et al. [14], a free water surface was present.

The same approach as with the fully submerged simulation is used. In order to be able to validate the results, they are compared with the total normalised damping coefficient from Ikeda et al. [14] given in column $b'_{eq,total}$ of Table 5.2. The comparison of the normalised total damping coefficient is given in Figure 5.9, the values are given in Table 5.4.

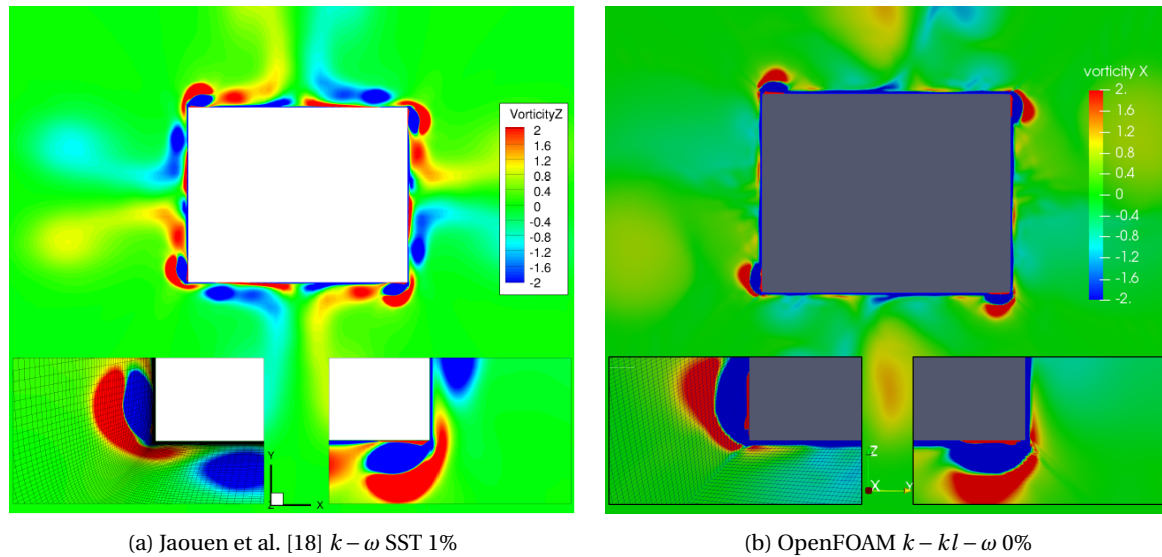


Figure 5.5: Vorticity compared between the results from Jaouen et al. [18] and OpenFOAM at the 13th oscillation, $t = 19.5s$, $\phi_a = 0.1rad$ $T = 1.5s$. Vorticity is given in $[1/s]$. The percentage is the amount of initial turbulence values.

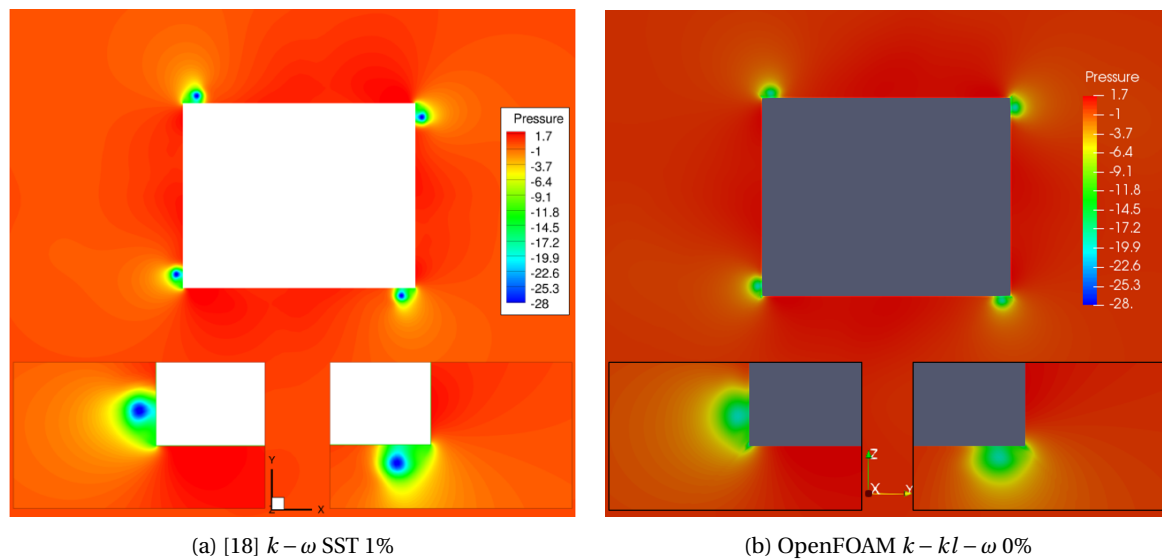


Figure 5.6: Pressure distribution comparison between the results from Jaouen et al. [18] and OpenFOAM at the 13th oscillation, $t = 19.5s$, $\phi_a = 0.1rad$ $T = 1.5s$. Pressure is given in $[m^2/s^2]$. The percentage is the amount of initial turbulence values.

Table 5.2: Normalised damping coefficient measured by Ikeda et al. [14] per category

Ikeda et al. [14]			
ϕ_a [rad]	$b'_{eq,total}$ [-]	$b'_{eq,potential}$ [-]	$b'_{eq,viscous}$ [-]
0.085	0.0104	0.000739	0.00966
0.102	0.0128	0.000739	0.0121
0.117	0.0137	0.000739	0.013
0.132	0.0149	0.000739	0.0142
0.143	0.0184	0.000739	0.0177
0.153	0.0216	0.000739	0.0209
0.165	0.0193	0.000739	0.0186
0.177	0.0239	0.000739	0.0232
0.204	0.0275	0.000739	0.0268
0.232	0.0303	0.000739	0.0296

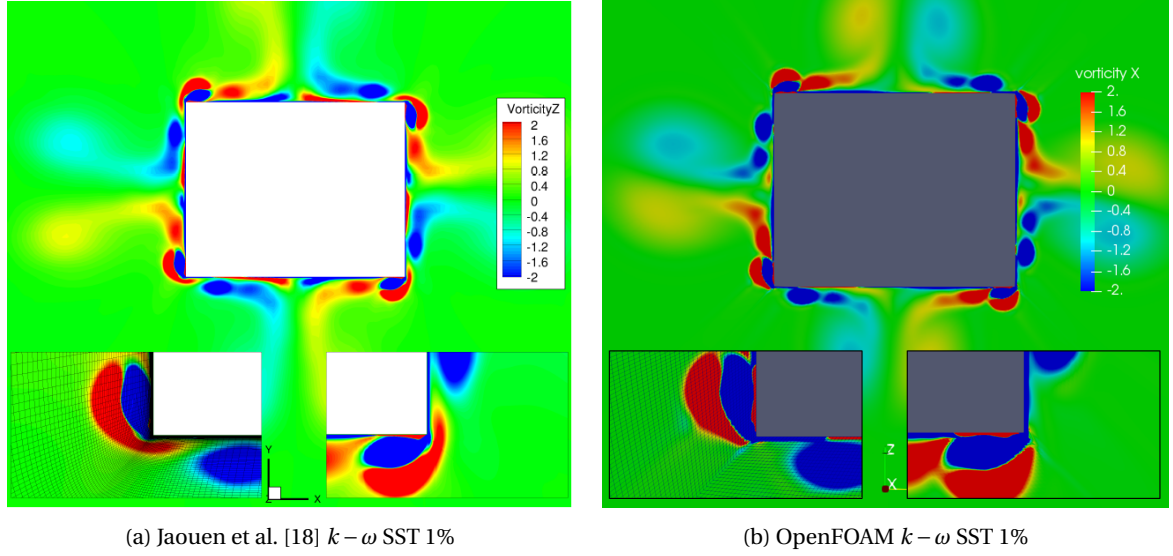


Figure 5.7: Vorticity comparison between the results from Jaouen et al. [18] and OpenFOAM with $k-\omega$ SST turbulence model at the 13th oscillation, $t = 19.5s$, $\phi_a = 0.1rad$ $T = 1.5s$. Vorticity is given in $[1/s]$. The percentage is the amount of initial turbulence values.

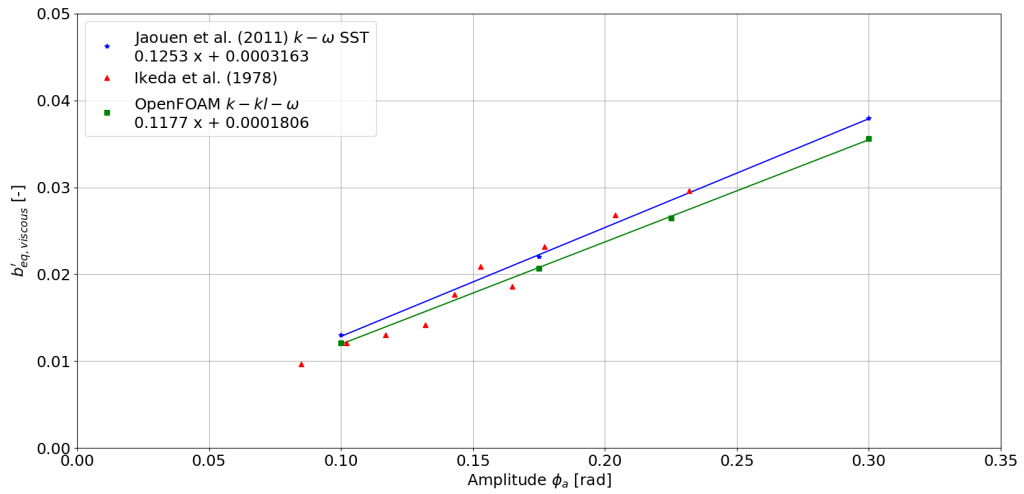


Figure 5.8: Viscous damping compared to experimental data from Ikeda et al. [14] corrected for absence of free water surface, $T = 1.5s$

Table 5.3: Normalised viscous damping coefficient found by Jaouen et al. [18] and OpenFOAM

	Jaouen et al. [18]	OpenFOAM
	$k-\omega$ SST	$k-kl-\omega$
ϕ_0 [rad]	$b'_{eq,viscous}$ [-]	
0.100	0.013	0.0121
0.175	0.022	0.0207
0.225		0.0265
0.300	0.038	0.0356

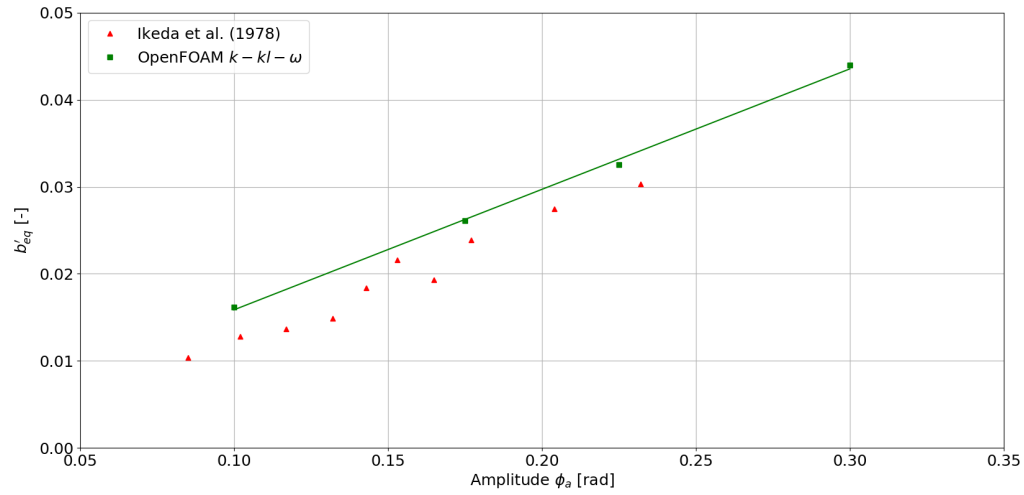
Figure 5.9: Damping compared to experimental data from Ikeda et al. [14], $T = 1.5s$

Table 5.4: Normalized equivalent damping coefficient calculated from OpenFOAM simulation

	OpenFOAM
	$k - kl - \omega$
ϕ_0 [rad]	b'_{eq} [-]
0.100	0.0162
0.175	0.0261
0.225	0.0325
0.300	0.0440

As can be seen, the results from the simulation overestimate the damping found by Ikeda et al. [14]. In the fully submerged case, the simulation data was in excellent agreement with both the data from the experiment from Ikeda et al. [14] and with the simulation data from Jaouen et al. [18]. This suggests that the difference in damping between experimental data and the simulation with the free water surface, is unlikely to result from the experimental data. The only difference between the simulation with free water surface and the fully submerged case is the presence of the free water surface. In Figure 5.10 the vorticity at $t = 19.5$ s is shown. If this is compared to Figure 5.1, it can be seen that there is severely more vorticity in the simulation with the free water surface. It is also noteworthy that this excess vorticity mainly occurs at the free water surface.

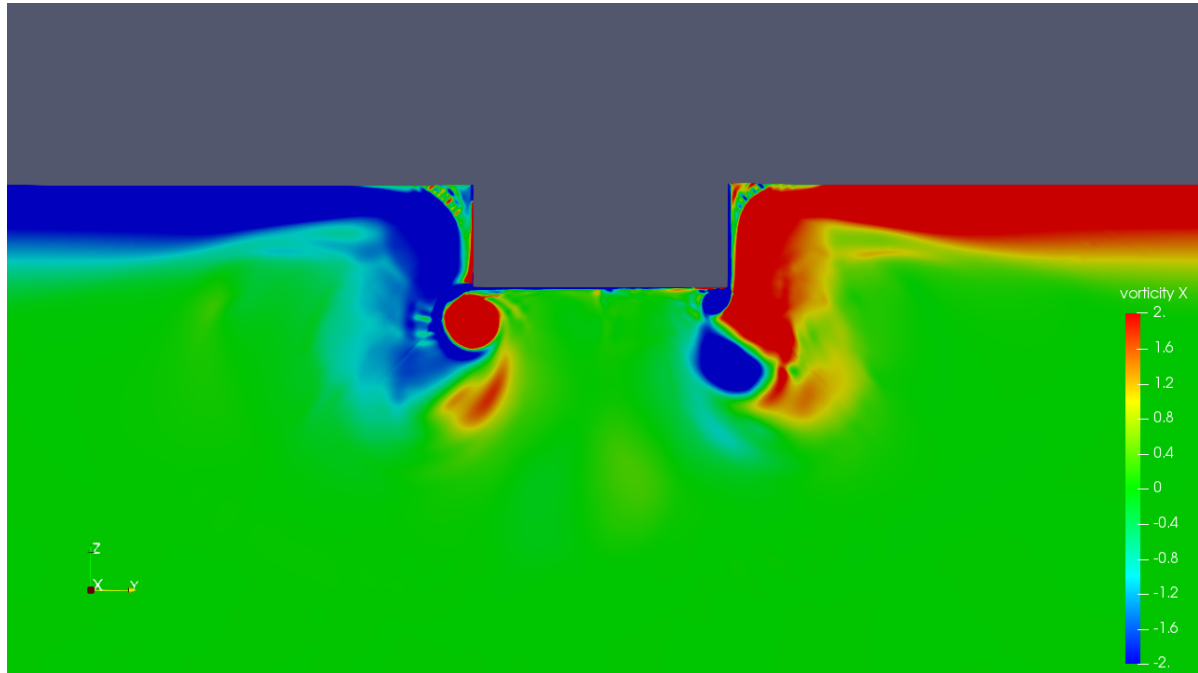


Figure 5.10: Vorticity, given in $[1/s]$, at the 13th oscillation for free water surface simulation in OpenFOAM, $t = 19.5$ s $\phi_a = 0.1$ rad
 $T = 1.5$ s

5.8. Conclusion

The fully submerged 2D simulation produced outstanding results. These results were in excellent agreement with both experimental data and a comparable CFD simulation. For these reasons, this model is considered to be fully validated.

The 2D simulation with free water surface gave less satisfactory results. The VoF-method seems to cause nonphysical vorticity at the free water surface, which impairs the results.

OpenFOAM is capable of simulating forced oscillations to determine the roll damping coefficients. However, the VoF-method as incorporated in this research, needs further development in order to use it in simulations with the free water surface.

6

2D CFD section method

In this chapter, the validated 2D simulation model, described in Chapter 5, will be used to determine the damping coefficient of the complete ship. The damping moment of multiple longitudinal sections will be determined and these results will be combined to create the total damping moment of the ship. From this damping moment, the damping coefficients will be determined and these will be compared to the experimental results from Marin. First, the fully validated 2D submerged model will be used in combination with the diffraction analysis method AQWA and secondly, the 2D model with a free water surface will be used. This is done in order to answer the third sub-question.

Is it possible to combine the results of multiple 2D CFD simulations, to obtain roll damping coefficients, which are in accordance with 3D experimental data?

All calculations in this chapter are performed on 10 cores of the high-performance cluster of which the details are given in Appendix D.

6.1. Method to combine multiple 2D results

In order to be able to compare the results from the 2D simulations to the 3D experimental data, the results from the 2D simulations will have to be extrapolated to correspond for a certain part of the ship and thereafter have to be combined to account for the complete ship. During this research, the ship is divided into three longitudinal sections. In Figure 6.1, the ship is shown. In Figure 6.2, it is shown how the ship is divided into three sections; a backsection, a midsection and a frontsection. The cuts were made in such a way that the midsection has a uniform cross-section over almost the entire length of the longitudinal section.

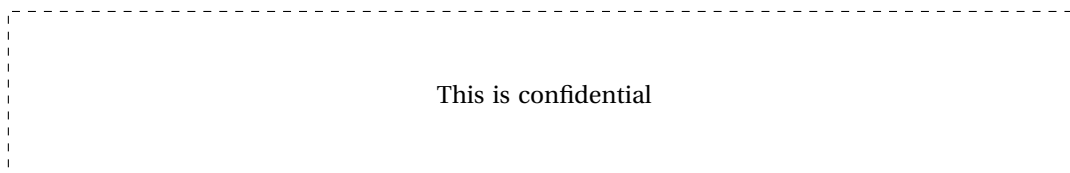


Figure 6.1: Side view of the ship under consideration

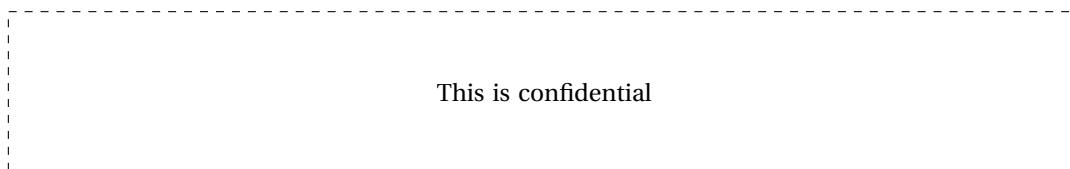


Figure 6.2: Side view of the different ship sections

From all three longitudinal sections, a cross-section is taken. These cross-sections are taken at locations

within the longitudinal section, where they should capture the averaged behaviour of that section. For the midsection, this is straight forward as the midsection is almost completely uniform. The resulting cross-sections are given in Figure 6.3.

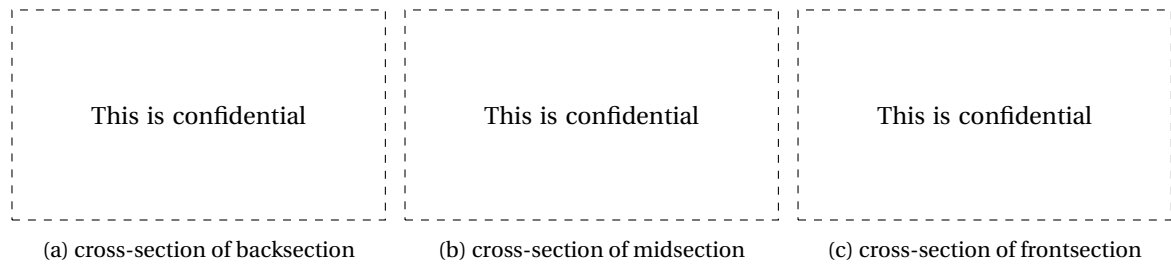


Figure 6.3: Cross-sections of the back-, mid- and frontsection

Next all cross-sections are simulated with four different motion amplitudes ($\phi_a = [1.23^\circ, 2.56^\circ, 3.82^\circ, 4.81^\circ]$). These amplitudes are chosen in such a way that they coincide with peaks in the free decay curve from the experimental data of Marin shown in Figure 4.5. Per simulation, a reaction moment is determined using the same approach as mentioned in Chapter 5. This reaction moment is linearly extrapolated to account for the complete longitudinal section. The length of the cross used during the simulation in the direction of the length of the ship is 0.05 meter for every simulation. To get the complete moment for a longitudinal section, the reaction moment obtained from the simulation has to be multiplied by the length of that section divided by the length of the cross-section during the simulation. This is called the multiplication factor. The lengths of the different longitudinal sections are given in Table 6.1 as well as the corresponding multiplication factor.

Table 6.1: Length per longitudinal section and corresponding multiplication factor for the reaction moment based on a cross-section length of 0.05 meter

Longitudinal section	Length [m]	Multiplication factor [-]
Backsection	Confidential	Confidential
Midsection	Confidential	Confidential
Frontsection	Confidential	Confidential

According to Himeno [8] and Ikeda et al. [14], the separate damping moments per longitudinal section can be added together to obtain the damping moment of the complete ship, if linearity is assumed. With this total moment, the linear and non-linear damping coefficient are determined using the same method as described in Chapter 5.

6.2. Results of the fully submerged simulations

As described by Himeno [8] and Ikeda et al. [14], the damping can be decomposed into several terms, if linearity is assumed. As these simulations will be carried out without the free water surface, the damping due to the free water surface has to be determined separately in order to compare the simulation results with the experimental results from Marin. To estimate this damping due to the free water surface, a diffraction analysis is performed using ANSYS AQWA, a commercial code. This analysis found a damping moment of $37.8[Nm]$. This value will be added to the combined damping moments of the different longitudinal sections to get the total damping of the complete ship.

For the fully submerged simulations, the cross-sections have to be mirrored on the waterline. The resulting sections are shown in Figure 6.4.

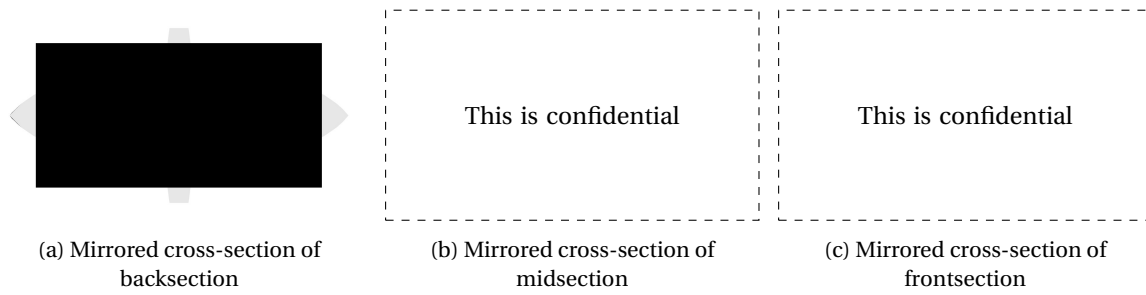


Figure 6.4: Mirrored cross-sections of the back-, mid- and frontsection. Part of the cross-section is blacked out because of confidentiality.

Due to the mirroring, some sharp corners are introduced at the backsection and the frontsection. This is undesirable as it is highly probable that vortices will originate from these sharp corners. However, with the current method, this problem could not be resolved without corrupting other parameters, e.g. correct draft or ship geometry. This issue should be resolved in future research to obtain more accurate results.

The cross-sections are meshed in a circular domain in the same manner as mentioned in Section 5.3. A close-up of the cross-sections within the mesh is shown in Figure 6.5. The mesh was refined to the same level as the medium mesh in Chapter 5. The mesh size for all three cross-sections was approximately 160k cells and the total simulation time, i.e. the time it took to run every cross-section at four different amplitudes, was approximately 70 hours. This is half the time it took to run the 3D simulation.

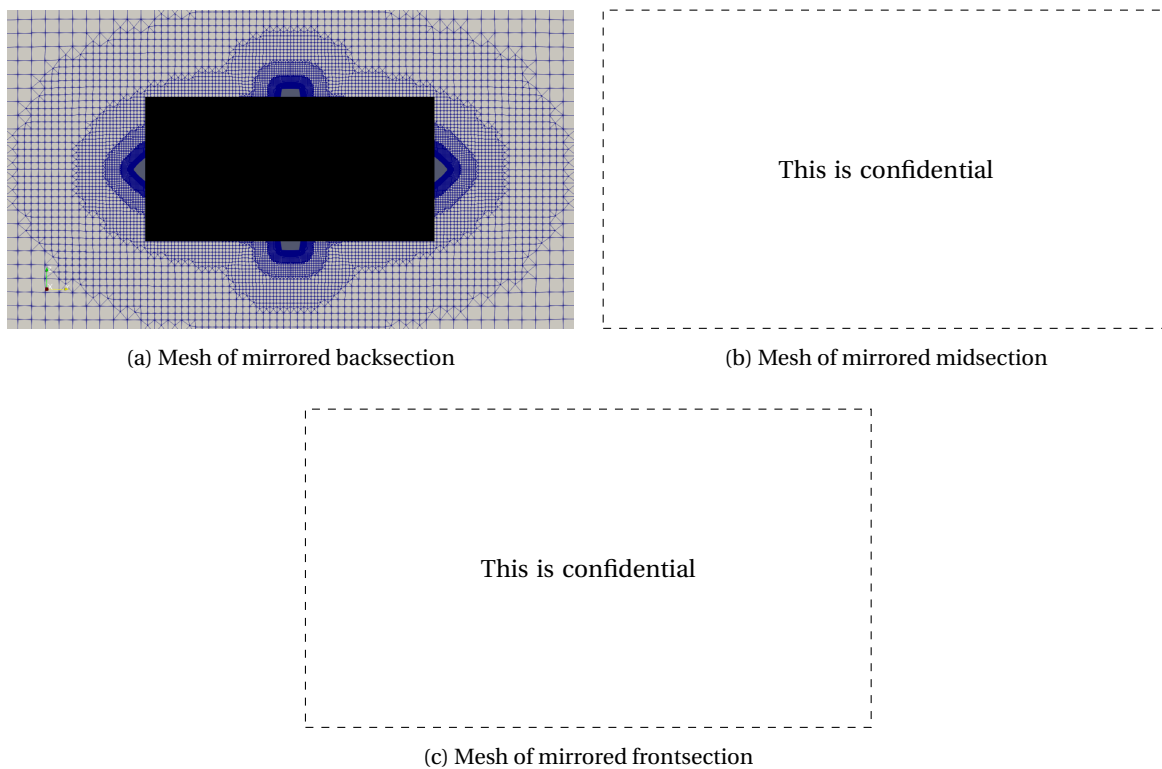


Figure 6.5: Meshes of the cross-sections. Part of the cross-section is blacked out because of confidentiality.

The amplitude of the viscous damping moment for four different motion amplitudes is plotted in Figure 6.6. The midsection has a minimal non-linear damping component. This was expected as the bilges are rounded and cause for little vorticity. Although the frontsection is even more circular shaped than the midsection, the non-linear component is higher than with the midsection. This is the result of the sharp corners created by the mirroring, as was expected. The backsection has a strong non-linear component compared to the mid- and frontsection. This is partly due to the sharp corners introduced by the mirroring and partly due to the vorticity created by the skeg. In Figure 6.7 the vorticity for the three cross-sections at the 13th

oscillation is shown.

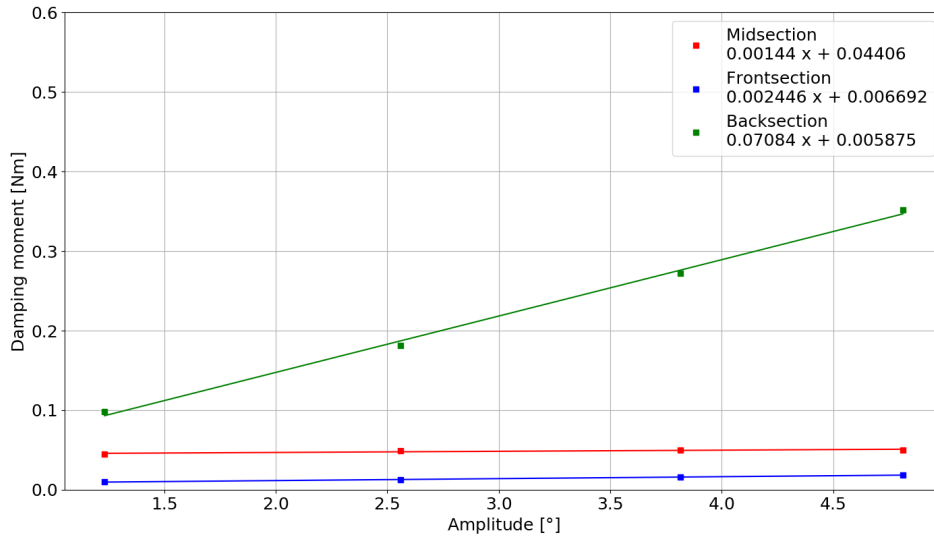


Figure 6.6: Viscous damping moment as calculated by OpenFOAM on 2D simulations with thickness 0.05 m

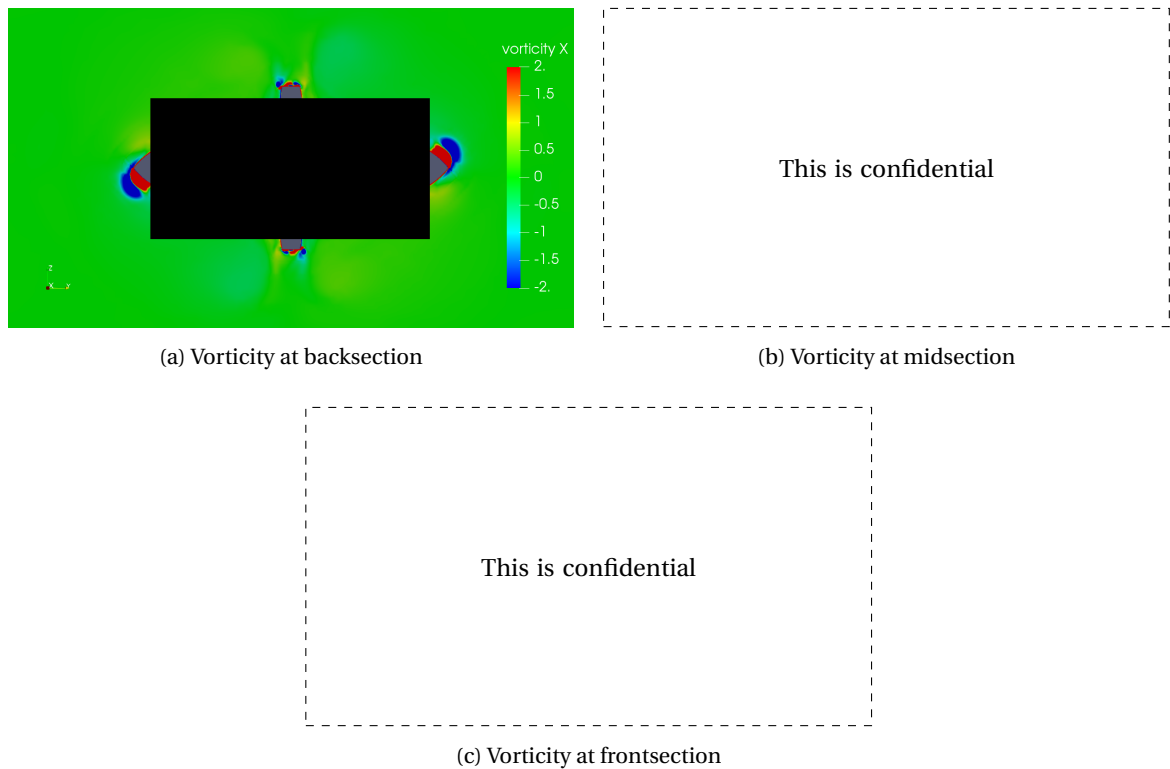


Figure 6.7: Vorticity, given in $[1/s]$, at the three cross-sections at 13th oscillation, $t = 19.197$ s, $\phi_a = 4.81^\circ$, $T = T_{nat} = 1.422$ s. Part of the cross-section is blacked out because of confidentiality.

When multiplying the results shown in Figure 6.6 with the multiplication factor given in Table 6.1, the viscous damping moment of the three longitudinal sections is obtained. This is shown in Figure 6.8. The contribution to the total damping moment per longitudinal section can be examined here. The frontsection accounts for very little of the total damping moment, as was expected due to its round shape overall. The

backsection accounts for a big part of the total damping, especially when roll angles start to increase. This is mainly due to the skeg. However, it should also be noted that the damping moment for the back and frontsection given here is overestimated due to the vorticity created by the sharp corners at the mirror plane. The amount of damping due to the midsection is fairly large mainly due to the fact that it accounts for the largest part of the ship, i.e. 3.238 out of the 5.021 meter in total.

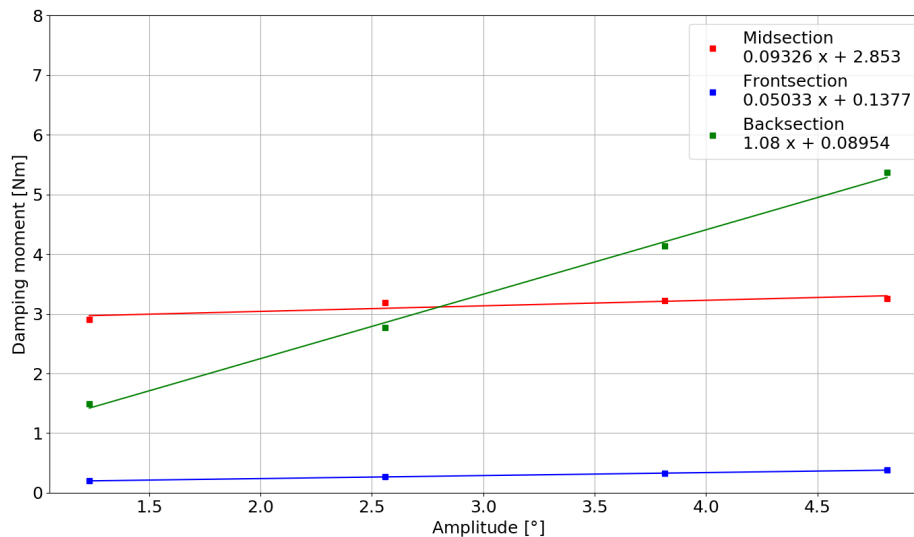


Figure 6.8: Viscous damping moment amplitude per section

The viscous damping of the three longitudinal sections and the combined viscous damping with the damping due to the free water surface added are given in Figure 6.9. The latter, the black line in Figure 6.9, is the total damping moment as determined by this method. The averaged damping moment determined by Marin through three free decay tests is also given in Figure 6.9. The corresponding damping coefficients of the 2D section method are given in Table 6.2. These are obtained by fitting a first-order line through the reaction moment amplitudes. Using Equation (5.12) these can be translated in a linear and quadratic damping coefficient.

In Table 6.3 the damping coefficients resulting from the free decay tests performed by Marin are given.

Table 6.2: The summation of the different linear and quadratic damping coefficients into the total damping coefficients as determined by the 2D section method

Damping component	b_l [$Nm/(\circ/s)$]	b_q [$Nm/(\circ/s^2)$]	
Backsection	0.0895	0.2878	
Midsection	2.8533	0.0249	
Frontsection	0.1377	0.0134	
Total ship viscous	3.0806	0.3261	+
Damping due to FWS	37.8000	0.000	+
Total ship	40.8806	0.3261	

Table 6.3: The linear and quadratic damping coefficient per free decay test and the average result from Marin

Experimental data	b_l [$Nm/(\circ/s)$]	b_q [$Nm/(\circ/s^2)$]
Marin 1	34.065	0.3516
Marin 2	35.426	0.0000
Marin 3	35.532	0.1064
Marin averaged	35.008	0.1526

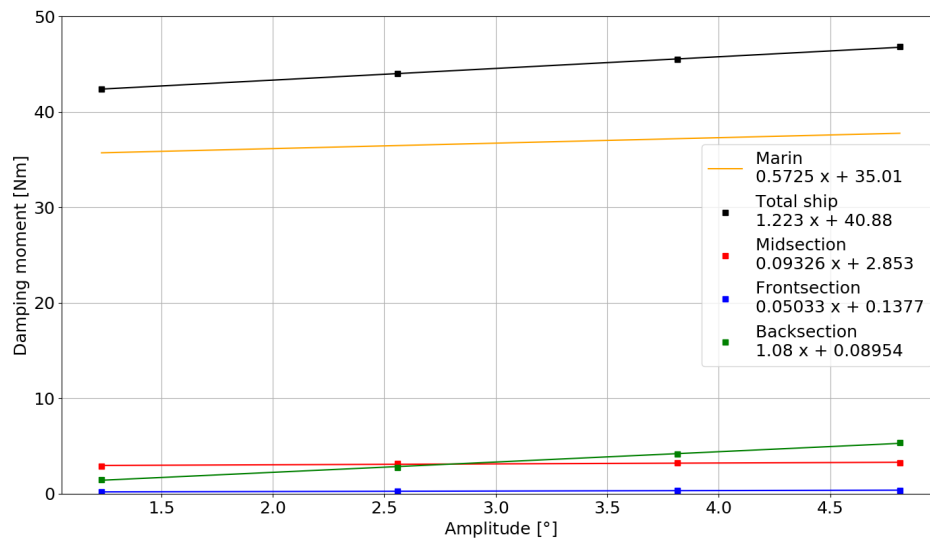


Figure 6.9: Damping moment amplitude following from free decay experiments of Marin, damping moment per section and damping moment of total ship including the potential damping

When comparing the averaged results of Marin against the results of the 2D section method it is clear that both the linear and the quadratic damping are overestimated by the 2D section method. The reason for the overestimation of the quadratic part of the damping is the extra vorticity created at the mirror plane of the back and frontsection. The overestimation for the linear part of the damping is harder to explain. As can be seen in Table 6.2, the damping due to the free water surface is already higher than the linear damping component determined by Marin. This could be due to inaccuracies in the model tests performed by Marin or errors in the diffraction analysis. Another possibility is that the chosen lengths of the different longitudinal sections are not chosen properly. This could cause an overall increase in damping as a section in this method is overrepresenting the damping of that part of the ship. One last possibility is that the summation method as mentioned by Himeno [8] and Ikeda et al. [14] does not hold for this case. This would mean that the damping due to the free water surface cannot simply be added to the viscous damping to obtain the total damping. A reason for this could be that due to vorticity the boundary layer at the ship hull is broken up which causes a drop in friction force on the hull of the ship, which then reduces the damping moment (Munson et al. [26]). The diffraction analysis can not capture this effect, as this is a potential flow solver and does not take viscosity into account. This would cause the total linear damping to be overestimated by the 2D section method.

6.3. Results of the simulations with free water surface

Although it was already noticed in Chapter 5 that the simulation with the free water surface has unrealistic high vorticity at the free water surface, the 2D section method is also tried with the free water surface. The simulation set-up is completely the same as for the simulation without free water surface with one difference: the presence of a free water surface.

The same sections, as shown in Figure 6.3, are used. The meshes of the different cross-sections are shown in Figure 6.10. The water level is also shown. Alpha in the figure corresponds to α_{water} as mentioned in Section 3.3. Where $\alpha_{water} = 1$, there is water (red), and where $\alpha_{water} = 0$, there is air (blue).

In Figure 6.11, the amplitude of the damping moment for the same four motion amplitudes as given in Section 6.2, are plotted. When comparing Figure 6.6 with Figure 6.11, it can be seen that the absolute values are approximately 10 times as high. It is also noteworthy to mention that the non-linear damping is significantly less in the simulation with the free water surface. This is due to the fact that there are no sharp corners due to mirroring in the simulation with free water surface. The only corners which cause vorticity are the corners of the skeg. In Figure 6.11, the damping moment of the cross-section in the backsection is still the largest and has the largest non-linear damping. This is expected due to the presence of the skeg.

In Figure 6.12, the damping moment from the three sections is multiplied with the multiplication factor

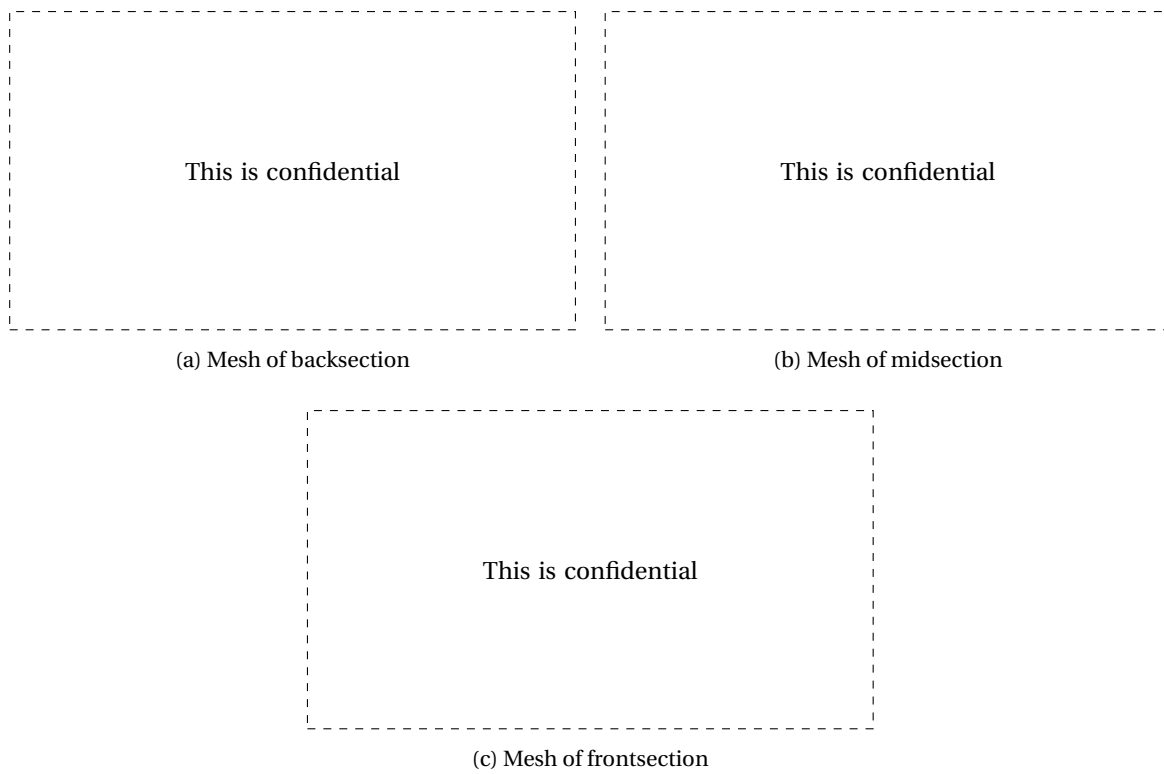


Figure 6.10: Meshes of the three sections with free water surface where red corresponds to water and blue to air

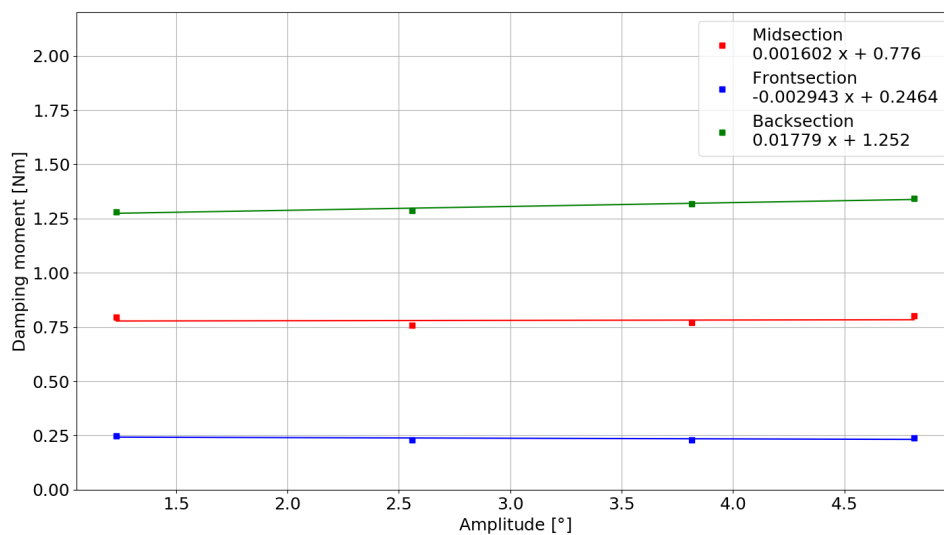


Figure 6.11: Damping moment as calculated by OpenFOAM on 2D simulations with free water surface with thickness 0.05 m

given in Table 6.1, to obtain the damping moment per longitudinal section.

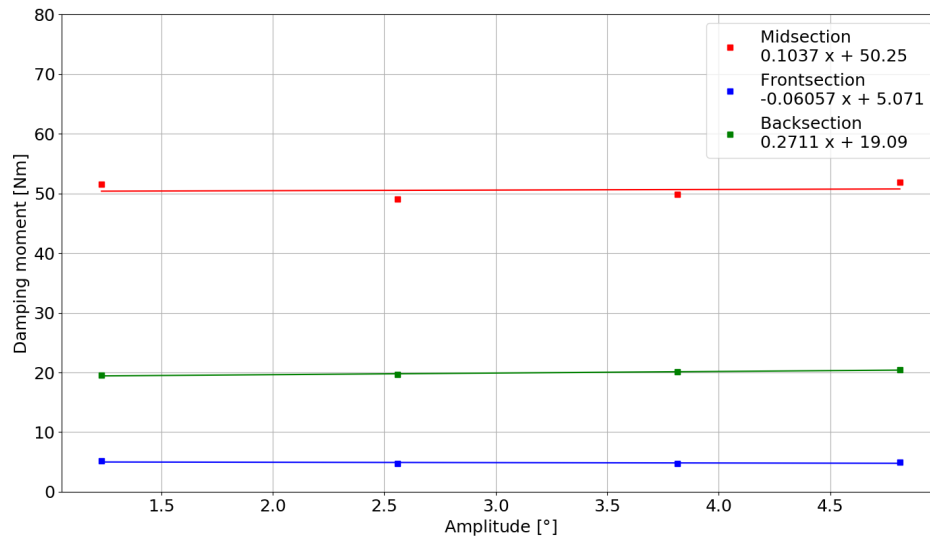


Figure 6.12: Damping moment amplitude per section with free water surface

By using the same summation method as with the simulation without free water surface, we obtain the damping values as presented in Table 6.4. In Figure 6.13, the total damping as determined by the 2D section method with free water surface is plotted along with the damping of the three longitudinal sections and the averaged damping of the three free decay tests performed by Marin. It is clear that the 2D section method with free water surface highly overestimates the damping. A likely reason for this overestimation is the unrealistic vorticity occurring at the free water surface, mentioned in Section 5.7, which is shown in Figure 6.14.

Table 6.4: The summation of the different linear and quadratic damping coefficients into the total damping coefficients as determined by the 2D section method with free water surface

Damping component	b_l [$Nm/(\circ/s)$]	b_q [$Nm/(\circ/s^2)$]
Backsection	19.0862	0.0723
Midsection	50.2514	0.0276
Frontsection	5.0715	-0.0162
Total ship	74.4090	0.0838

6.4. Conclusion

The fully submerged 2D section method with added damping due to free water surface gives promising results. The reduction in computation time in comparison with full 3D simulations is remarkable. However, both the linear and non-linear damping coefficients are overestimated. Especially the non-linear damping coefficient is overestimated due to the sharp corners introduced by mirroring the sections in the water plane. Keeping in mind that the 2D CFD model, discussed in chapter 5, had an excellent agreement with experimental data, it could be argued that the method is better suitable for hard chine bilges. It is therefore recommended that in future research, ships with different bilge configurations are investigated.

The 2D section method with free water surface incorporated, highly overestimated the linear damping coefficient. The non-linear damping coefficient was slightly underestimated but within the range of the results from the free decay tests performed by Marin. The overestimation of the linear damping coefficient is driven by the nonphysical vorticity occurring at the free water surface.

The 2D section method shows promising results, but more research is necessary to be able to tell whether it can reproduce roll damping coefficients in accordance with experimental data.

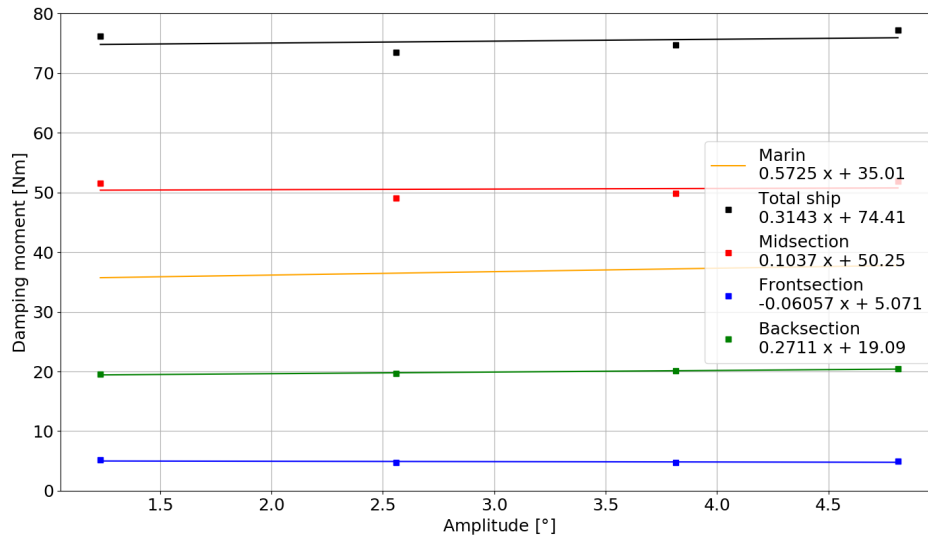


Figure 6.13: Damping moment amplitude following from free decay experiments of Marin, damping moment per section with free water surface and damping moment of total ship

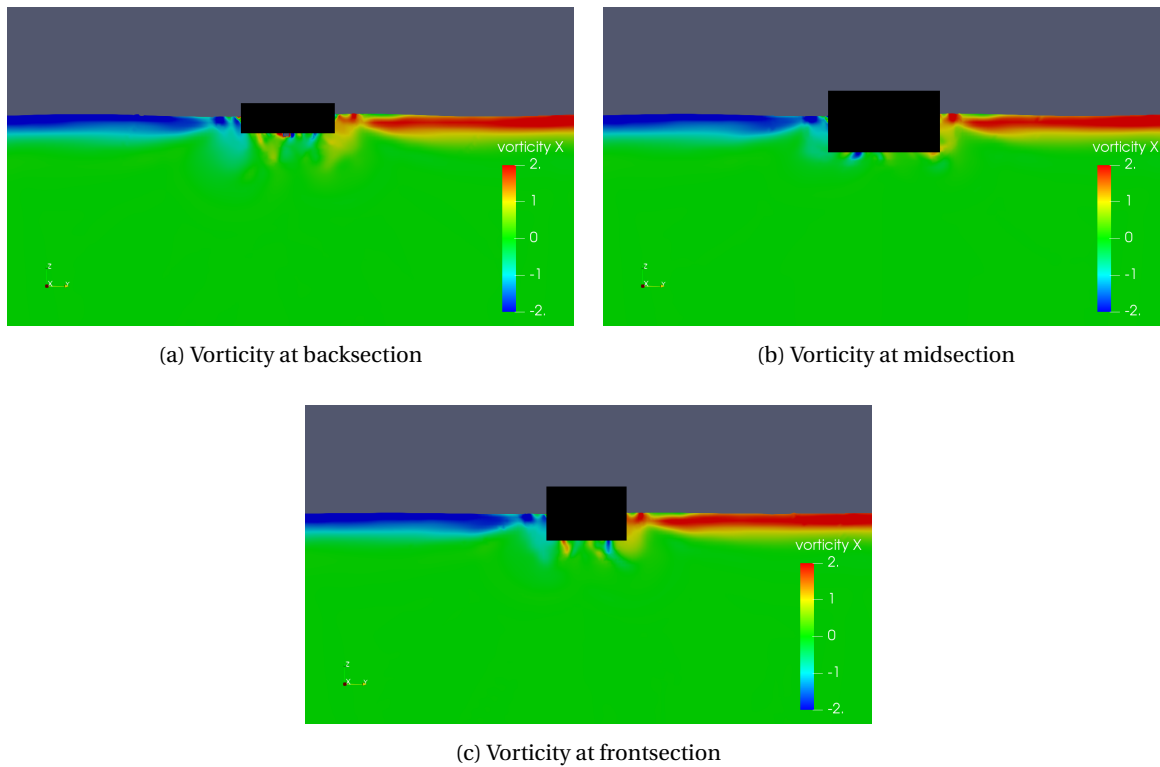


Figure 6.14: Vorticity, given in [1/s], at the three cross-sections at 13th oscillation, $t = 19.197$ s, $\phi_a = 4.81^\circ$, $T = T_{nat} = 1.422$ s. The ship hull is blacked out because of confidentiality.

Conclusion & Recommendations

The conclusion and recommendations are presented in this chapter.

7.1. Conclusion

The aim of this research was to investigate whether a 2D section method, based on multiple 2D CFD simulations, could predict the roll damping coefficient of a ship. Two types of CFD simulations have been used to achieve this.

A 3D free roll decay simulation is performed using OpenFOAM and the results were compared with experimental data. A comparison was made for the linear and quadratic damping coefficient. The experimental data consists of three of the same free roll decay tests performed by Marin. The results from these three tests are consistent regarding the linear damping coefficient, but the quadratic damping coefficient deviates significantly between the three tests. The linear damping coefficient resulting from the CFD simulation was 17% lower than the averaged linear damping coefficient from the experimental data. The quadratic damping coefficient resulting from the CFD simulation was 60% lower. However, the quadratic damping coefficient predicted by the simulation using OpenFOAM is within the range of the different values obtained through the model tests. The presumed cause of the deviation in the results is likely to find its origin in the initial turbulence difference between simulation and experiments. During the model tests, the water in which the ship was tested was not entirely still, i.e. there was an unknown amount of turbulence in the water present at the start. This turbulence was not measured during the tests and thus, no values were known to initiate the simulation with. After performing a study regarding initial turbulence values, it was found that the damping is highly influenced by the initial turbulence values. As it was not within the scope of this research to determine these initial values through simulations, a turbulence model, with the possibility to initiate a simulation with initial turbulence values set to zero, was chosen. Another possible cause for the deviation in results between the model tests and the simulations is that the radii of inertia of the ship were measured in dry conditions. Once the ship was laid in the water, the weight distribution was altered to obtain the correct metacentric height. This new weight distribution was not known. Although the change was minor, this resulted in different weight distribution between the ship used for the simulation and the ship used for the model tests.

A 2D forced oscillation simulation is performed using OpenFOAM and the resulting linear and quadratic damping coefficients were compared with experimental data. The experimental data of forced oscillation tests performed by Ikeda et al. [14] was used. The results were also compared with a CFD simulation performed by Jaouen et al. [18]. The CFD simulation used in this research was performed with and without a free water surface. The linear and quadratic damping coefficients resulting from the submerged simulation are almost an exact match with the experimental data. The results were also a good match with the CFD simulation from Jaouen et al. [18] regarding both linear and quadratic damping coefficient. The minor differences between the two CFD simulations can be explained by the difference in turbulence models used. This has been confirmed by running the CFD simulation used in this research, with the same turbulence model and settings used by Jaouen et al. [18]. With the same turbulence model, the simulation performed by OpenFOAM matches the simulation performed by Jaouen et al. [18]. It can be concluded that the 2D CFD simulation without free water surface is fully validated. However, it should be noted that this validation is based on one set

of experimental data and one other CFD simulation. The results of the simulation with free water surface did not match as good as the results from the simulation without free water surface. The two simulations only differed in the presence of the free water surface. Because of this, the presence of the free water surface is seen as the leading cause for the difference in agreement with the experimental data. By checking the vorticity field, it was noticed that nonphysical vorticity exists at the free water surface. This confirms the hypothesis that the Volume of Fluid method causes nonphysical behaviour.

Because the fully submerged model proved to be a better predictor of the roll damping coefficient than the model with free water surface, the submerged model is used for the 2D section method. The 2D section method uses 2D CFD simulations of multiple cross-sections of the ship, which represent different parts of the ship, to predict the roll damping of the complete ship. Because the simulations are performed without the free water surface, the cross-sections are mirrored at the water plane. The results of this method are promising but not an exact match with the experimental data of the 3D tests. Both the linear and quadratic coefficient are overestimated by the 2D section method. The linear damping coefficient is overestimated by 17% and the quadratic damping coefficient is overestimated by 111%. The reason for the overestimation of the quadratic damping coefficient is the extra vorticity created at the back and frontsection due to the sharp corners introduced at the mirroring plane. The overestimation for the linear damping coefficient can have multiple causes. For one, the damping due to the free water surface as determined by a diffraction analysis is already higher than the linear damping coefficient following from experimental data. This could be due to inaccuracies in the experimental data or errors in the diffraction analysis. Another possibility is that the lengths of the different longitudinal sections are not chosen properly. This could cause an overall increase in damping, as a section is overrepresenting the damping of that part of the ship. One last possibility is that the summation method for the roll damping is not valid for all cases. This would mean that the roll damping caused by the free water surface cannot simply be added to the viscous roll damping to obtain the total roll damping. One reason for this could be that the boundary layer at the ship hull is broken up by turbulence which causes a drop in friction force on the hull of the ship, which would reduce the damping moment. This effect cannot be captured by the diffraction analysis as this is a potential flow solver and does not take viscosity into account. This would cause the total linear damping to be overestimated by the 2D section method. Because the mirroring causes a large overestimation of the quadratic damping coefficient, the 2D section method is also tried with the 2D CFD simulations with the presence of the free water surface. The results from these simulations overestimated the linear damping coefficient by 112% and underestimated the quadratic damping coefficient by 45%. The Volume of Fluid method caused nonphysical behaviour at the free water surface regarding vorticity, which is likely the main cause for the overestimation of the linear damping coefficient. The quadratic damping coefficient determined by the 2D section method is underestimated when compared to the averaged quadratic damping coefficient from the experimental data. However, the coefficient determined by the 2D section method is within the range of coefficients found in the separate model tests.

By having answered the sub-questions it is now possible to answer the main research question:

Is it possible to determine the roll damping coefficients of a ship by combining the results of 2D OpenFOAM CFD simulations of multiple cross-sections of the ship?

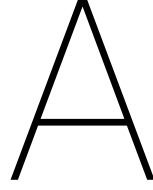
By combining 2D OpenFOAM CFD simulations of multiple cross-sections of a ship, the linear and quadratic roll damping coefficient have been determined. Unfortunately, this method did not yet succeed in determining these coefficients to an acceptable level of accuracy. However, the 2D section method using the fully submerged simulations shows promising results. Further research is necessary to determine whether this method can determine the roll damping coefficients more accurately than it has done up until now.

7.2. Recommendations

The recommendations for future research, which emerged during this research, are presented here.

- During this research, the 3D simulations were compared to experimental data from experiments commissioned by Van Oord at Marin. This experimental data was created to determine the roll damping coefficient of a ship of Van Oord. When performing these experiments, it was not yet known that the data would be used to validate CFD simulations. Because of this, the experiments were not performed at a level usable for scientific research. For future work or research on this topic, experimental data which does meet these requirements should be used to validate the CFD simulations.

- At the free water surface, nonphysical behaviour occurred during the 2D CFD simulations. High vorticity occurred at the free water surface. It is highly likely that this behaviour is due to the Volume of Fluid method used during this research. In order to prevent this behaviour during future research, an alternative Volume of Fluid method should be used, or adjustments to this Volume of Fluid method should be made.
- The best results were achieved with the 2D CFD simulations without the free water surface incorporated. For these simulations, the sections were mirrored in the water plane. The mirroring created sharp corners at the back and frontsection. These edges caused extra vorticity, which impaired the results. In future research, the adverse effects of mirroring the sections should be looked into and resolved.
- One of the reasons which may have led to the difference in experimental data and the 2D section method is that it was falsely assumed that the damping moment over the simulated cross-section, can be linearly extrapolated over the length of the entire longitudinal section. To confirm that this is a valid assumption, research should be done regarding this topic.
- Another reason which might have caused the difference in results is the chosen length of the three different longitudinal sections. During this research, the ship was divided into three sections. The length of these sections was based on the part of the ship with a uniform cross-section. This method was chosen because then, the cross-section of the midsection would be an excellent representation of the entire length of the midsection. However, it can also be argued that one cross-section for both the back- and frontsection is not enough to capture the complex geometries of these parts of the ship. Because of this, it should be investigated whether more longitudinal sections are necessary in order to obtain more accurate results with the 2D section method.
- One last recommendation is made regarding the experimental data. During this research, it was only possible to test the model against one set of experimental data. In order to get a better understanding of how well the 2D section method works, other experimental data should be used as well. There was quite a significant focus on the non-linear damping during this research. However, the ship which was used for the model tests has minimal non-linear damping characteristics. This small amount of non-linear damping makes it hard to conclude how well the 2D section method describes the non-linear damping behaviour. It is therefore recommended to use, not only more experimental data, but also experimental data of ships with more non-linear effects.



Boundary and initial conditions

A.1. Boundary conditions

A.1.1. 3D boundary conditions

In Tables A.1 and A.2 the implemented boundary conditions for the 3D case are given. The boundary stationaryWalls consist of the four walls which enclose the domain and the bottom. The atmosphere is the top of the domain, the ship is the ship and overset is a dummy patch which OpenFOAM needs to trigger the overset mesh method.

Boundary	α	k_l	k_t	\mathbf{v}_t	ω
overset	overset	overset	overset	overset	overset
stationaryWalls	zeroGradient	zeroGradient	zeroGradient	nutkWallFunction	zeroGradient
atmosphere	inletOutlet	inletOutlet	inletOutlet	calculated	inletOutlet
ship	zeroGradient	zeroGradient	zeroGradient	nutkWallFunction	zeroGradient

Table A.1: Boundary conditions for the 3D simulation using the $k - k_l - \omega$ turbulence model (part 1)

Boundary	p_{rgh}	pointDisplacement	\mathbf{U}	zoneID
overset	overset	overset	overset	overset
stationaryWalls	fixedFluxPressure	fixedValue	fixedValue	zeroGradient
atmosphere	totalPressure	fixedvalue	pressureInletOutletVelocity	zeroGradient
ship	fixedFluxPressure	calculated	movingWallVelocity	zeroGradient

Table A.2: Boundary conditions for the 3D simulation using the $k - k_l - \omega$ turbulence model (part 2)

A.1.2. 2D boundary conditions

In Tables A.3 and A.4 the implemented boundary conditions for the 2D case are given. The boundary stationaryWalls consist of the circular wall which encloses the domain in y-direction. The atmosphere is the top of the domain, front is the wall at the positive x-side, back is the wall at the negative x-side and ship is the ship.

Boundary	α	k_l	k_t	\mathbf{v}_t
stationaryWalls	zeroGradient	zeroGradient	zeroGradient	zeroGradient
atmosphere	inletOutlet	inletOutlet	inletOutlet	calculated
ship	zeroGradient	zeroGradient	zeroGradient	nutLowReWallFunction
front	empty	empty	empty	empty
back	empty	empty	empty	empty

Table A.3: Boundary conditions for the 2D simulation using the $k - k_l - \omega$ turbulence model (part 1)

Boundary	ω	p_{rgh}	pointDisplacement	U
stationaryWalls	zeroGradient	fixedFluxPressure	fixedValue	slip
atmosphere	inletOutlet	totalPressure	fixedvalue	pressureInletOutletVelocity
ship	zeroGradient	fixedFluxPressure	calculated	movingWallVelocity
front	empty	empty	empty	empty
back	empty	empty	empty	empty

Table A.4: Boundary conditions for the 2D simulation using the $k - kl - \omega$ turbulence model (part 2)

Meaning of different boundary conditions

The definitions given below are given by The OpenFOAM Foundation [28].

overset

The overset boundary condition is a dummy boundary condition which triggers the overset interpolation.

fixedValue

fixedValue is a Dirichlet boundary condition and provides a fixed value constraint at the defined boundary.

totalPressure

The totalPressure boundary condition sets the static pressure at the boundary at a certain value based on the specified total pressure.

pressureInletOutletVelocity

This boundary condition assigns a zeroGradient condition to flow out of the domain and assigns a velocity based on the flux in the boundary normal condition to the flow into the domain.

zeroGradient

The zeroGradient assigns a zero gradient condition from the internal field to the boundary. For the pressure this is not an actual boundary condition, but results from the Navier-Stokes equations at the boundary for a specified fixed value velocity boundary condition.

fixedFluxPressure

The fixedFluxPressure is similar to the zeroGradient condition apart from the fact that the pressure gradient is calculated based on the velocity specified by the according boundary condition.

movingWallVelocity

The movingWallVelocity sets the velocity to the desired value for moving walls when employed in moving mesh cases.

inletOutlet

The inletOutlet boundary condition assigns a user-specified fixed value for reverse flow to the boundary and treats the outflow as a zeroGradient boundary condition.

calculated

The calculated boundary condition states that the results will follow from solving the system of equations.

nutLowReWallFunction

The nutLowReWallFunction is a wall function that is used for cases with low Reynold number flows.

slip

The slip boundary condition only allows for tangential velocities at the boundary but not for normal velocities.

empty

OpenFOAM has no 2D or 1D option, thus every case is solved in 3D. This means that for 2D cases 1 direction only exists out of 1 cell. The empty condition is applied to the boundary in the direction which is not solved.

A.2. Initial conditions

Some boundary values need initial conditions. These initial values are given below.

A.2.1. Initial conditions of the 3D simulations

$k_l [m^2/s^2]$	$k_t [m^2/s^2]$	$\mathbf{v}_t [m^2/s]$	$\omega [1/s]$	$p_{rgh} [Pa]$	$\mathbf{U} [m/s]$
0	0	0	0	0	0

Table A.5

A.2.2. Initial conditions of the 2D simulations

$k_l [m^2/s^2]$	$k_t [m^2/s^2]$	$\mathbf{v}_t [m^2/s]$	$\omega [1/s]$	$p_{rgh} [Pa]$	$\mathbf{U} [m/s]$
0	0	0	0	0	0

Table A.6

B

Numerical schemes

B.1. Numerical schemes 3D

ddtSchemes	gradSchemes	div(rhoPhi,U)
Euler	cellLimited Gauss linear 1	Gauss linearUpwind grad(U)
div(phi,alpha)	div(phirb,alpha)	div(((rho*nuEff)*dev2(T(grad(U)))))
Gauss vanLeer	Gauss interfaceCompression	Gauss linear
div(phi,kt)	div(phi,kl)	div(phi,omega)
Gauss linearUpwind grad(kt)	Gauss linearUpwind grad(kl)	Gauss linearUpwind grad(omega)
laplacianSchemes	interpolationSchemes	snGradSchemes
Gauss linear corrected	linear	corrected
oversetInterpolation		
inverseDistance		

Table B.1: Numerical schemes used for 3D simulations

B.2. Numerical schemes 2D

ddtSchemes	gradSchemes	div(rhoPhi,U)
Euler	cellLimited Gauss linear 1	Gauss linearUpwind grad(U)
div(phi,alpha)	div(phirb,alpha)	div(((rho*nuEff)*dev2(T(grad(U)))))
Gauss vanLeer	Gauss interfaceCompression	Gauss linear
div(phi,kt)	div(phi,kl)	div(phi,omega)
Gauss linearUpwind grad(kt)	Gauss linearUpwind grad(kl)	Gauss linearUpwind grad(omega)
laplacianSchemes	interpolationSchemes	snGradSchemes
Gauss linear corrected	linear	corrected

Table B.2: Numerical schemes used for 2D simulations

C

Ship details

This is confidential

D

Details of the high-performance cluster

In Table D.1 information about the high-performance cluster which is used for the OpenFOAM simulations is used.

Architecture	x86_64
CPU op-mode(s)	32-bit, 64-bit
Byte Order	Little Endian
CPU(s)	40
On-line CPU(s) list	0-39
Thread(s) per core	1
Core(s) per socket	10
Socket(s)	4
NUMA node(s)	4
Vendor ID	GenuineIntel
CPU family	6
Model	79
Model name	Intel(R) Xeon(R) CPU E5-4627 v4 @ 2.60GHz
Stepping	1
CPU MHz	2596.992
BogoMIPS	5193.98
Hypervisor vendor	VMware
Virtualization type	full
L1d cache	32K
L1i cache	32K
L2 cache	256K
L3 cache	25600K
NUMA node0 CPU(s)	0-9
NUMA node1 CPU(s)	10-19
NUMA node2 CPU(s)	20-29
NUMA node3 CPU(s)	30-39

Table D.1: Information about the computer which was used for the OpenFOAM simulations

Bibliography

- [1] L. Bonfiglio, S. Brizzolara, and C. Chrysosostomidis. Added mass and damping of oscillating bodies: a fully viscous numerical approach. *Recent Advances in Fluid Mechanics, Heat & Mass Transfer and Biology*, 2011.
- [2] L. Chen, L. Sun, J. Zang, A. J. Hillis, and A. R. Plummer. Numerical study of roll motion of a 2-d floating structure in viscous flow. *Journal of Hydrodynamics*, 28:544–563, 08 2016. doi: 10.1016/S1001-6058(16)60659-5.
- [3] J. Falzarano, A. Somayajula, and R. Seah. An overview of the prediction methods for roll damping of ships. *Ocean Systems Engineering*, 5:55–76, 05 2015. doi: 10.12989/ose.2015.5.2.055.
- [4] J. Fürst. Numerical simulation of transitional flows with laminar kinetic energy. *Engineering Mechanics*, 20:379–388, 01 2013.
- [5] M. K. Gokce and O. K. Kinaci. Numerical simulations of free roll decay of DTMB 5415. *Ocean Engineering*, 01 2018. doi: 10.1016/j.oceaneng.2017.12.067.
- [6] M. Gu, J. Lu, S. Bu, C. Wu, and G Qiu. Numerical simulation of the ship roll damping. *Proceedings of the 12th International Conference on the stability of Ships and Ocean Vehicles*, 12, 2015.
- [7] M. Gu, J. Lu, S. Bu, C. Wu, G Qiu, and K. Zeng. Validation of cfd simulation for ship roll damping using one pure car carrier and one standard model. *Proceedings of the 15th International Ship Stability Workshop*, 15, 2016.
- [8] Y. Himeno. Prediction of ship roll damping. a state of the art. *University of Michigan Department of Naval Architecture and Marine Engineering, (Report)*, page 87, 09 1981.
- [9] C. W. Hirt and B. D. Nichols. Volume of fluid (VOF) method for the dynamics of free boundaries. *Journal of Computational Physics*, 39:201–225, 1981.
- [10] T. Holzmann. *Mathematics, Numerics, Derivations and OpenFOAM*. Leoben, 4th edition, 2017.
- [11] Y. Ikeda, Y. Himeno, and N. Tanaka. On roll damping force of ship - effect of friction of hull and normal force of bilge keels. *Journal of the Kansai Society of Naval Architects*, 161, 1976.
- [12] Y. Ikeda, Y. Himeno, and N. Tanaka. On eddy making component of roll damping force on naked hull. *Journal of the Society of Naval Architects of Japan*, 1977:54–64, 01 1977. doi: 10.2534/jjasnaoe1968.1977.142_54.
- [13] Y Ikeda, K Komatsu, Y Himeno, and N Tanaka. On roll damping force of ship - effects of hull surface pressure created by bilge keels. *Journal of Kansai Society of Naval Architects*, 165:31–40, 01 1977.
- [14] Y. Ikeda, Y. Himeno, and N. Tanaka. Components of roll damping of ship at forward speed. *Journal of the Society of Naval Architects of Japan*, 143:121–133, 01 1978. doi: 10.2534/jjasnaoe1968.1978.113.
- [15] Y. Ikeda, Y. Himeno, and N. Tanaka. A prediction method for ship roll damping. *Journal of the Kansai Society of Naval Architects*, 1978.
- [16] International Towing Tank Conference. Numerical estimation of roll damping, 2011.
- [17] M. A. R. Iral, S. Nallayarasu, and S. K. Bhattacharyya. CFD approach to roll damping of ship with bilge keel with experimental validation. *Applied Ocean Research*, 55:1–17, 02 2016. doi: 10.1016/j.apor.2015.11.008.

- [18] F. Jaouen, A. H. Koop, and G. Vaz. Predicting roll added mass and damping of a ship hull section using cfd. *Proceedings of the International Conference on Offshore Mechanics and Arctic Engineering - OMAE*, 7, 01 2011. doi: 10.1115/OMAE2011-49085.
- [19] F. Jaouen, A. H. Koop, G. Vaz, and G. Crepier. RANS predictions of roll viscous damping of ship hull sections. *V International Conference on Computational Methods in Marine Engineering, MARINE 2011*, 2011.
- [20] H. Jasak. *Error Analysis and Estimation for the Finite Volume Method with Applications to Fluid Flows*. Phd thesis, University of London, 1996.
- [21] Y. Jiang, R. Zhu, G. Miao, L. Hong, and C Ma. Study on ship roll damping. *The Second Conference of Global Chinese Scholars on Hydrodynamics*, 2016.
- [22] N. Karagiannis, A. Stampoulzoglou, and P. Prinos. Numerical simulation of swash flow using OpenFOAM. *IAHR*, 2015.
- [23] T. Katayama, B. Yildiz, and J. Umeda. Numerical estimation and validation of shallow draft effect on roll damping. *The 14th International Ship Stability Workshop (ISSW)*, 14, 2014.
- [24] Y. Kawahara, K. Maekawa, and Y. Ikeda. A simple prediction formula of roll damping of conventional cargo ships on the basis of ikeda's method and its limitation. *Journal of Shipping and Ocean Engineering*, 2, 05 2011. doi: 10.1007/978-94-007-1482-3_26.
- [25] G. Malara, P.D. Spanos, and F. Arena. Maximum roll angle estimation of a ship in confused sea waves via a quasi-deterministic approach. *Probabilistic Engineering Mechanics*, 35:75–81, 08 2013. doi: 10.1016/j.pro bengmech.2013.08.001.
- [26] B. R. Munson, T. H. Okiishi, W. W. Huebsch, and A. P. Rothmayer. *Fundamentals of Fluid Mechanics*. Wiley, 7th edition, 2013. ISBN 978-1-118-11613-5.
- [27] Z Shen, D. Wan, and P. M. Carrica. Dynamic overset grids in OpenFOAM with application to kcs self-propulsion and maneuvering. *Ocean Engineering*, 108:287–306, 11 2015. doi: 10.1016/j.oceaneng.2015.07.035.
- [28] The OpenFOAM Foundation. *OpenFOAM v6 User Guide*. The OpenFOAM Foundation, 6th edition, 2017. URL <https://cfd.direct/openfoam/user-guide>.
- [29] D. C. Wilcox. *Turbulence Modeling for CFD*. DCW industries Inc., 3rd edition, 2006. ISBN 978-1-928729-08-2.
- [30] B. Yang, Z. Wang, and M. Wu. Numerical simulation of naval ship's roll damping based on cfd. *Procedia Engineering*, 37:287–293, 12 2012. doi: 10.1016/j.proeng.2012.04.241.
- [31] C. Yang, R. Zhu, G. Miao, and J. Fan. Numerical simulation of rolling for 3-d ship with forward speed and nonlinear damping analysis. *Journal of Hydrodynamics, Ser. B*, 25:148–155, 02 2013. doi: 10.1016/S1001-6058(13)60348-0.
- [32] B. Yildiz, F. Çakici, T. Katayama, and H. Yilmaz. URANS prediction of roll damping for a ship hull section at shallow draft. *Journal of Marine Science and Technology*, 21, 07 2015. doi: 10.1007/s00773-015-0331-4.